# PHOTO-FENTON CATALYSTS SUPPORTED ON MICROPOROUS MATERIALS FOR INDUSTRIAL POLLUTANT OXIDATION

---

A thesis submitted in fulfilment of the requirements for the Degree of

Doctor of Philosophy in Chemical and Process Engineering in the

University of Canterbury

2017

---

Matthew MacDonald

Thesis Supervisors:

Dr Alex Yip

Dr Aaron Marshall

# ACKNOWLEDGEMENTS

First and foremost I would like to thank my supervisor, Dr Alex Yip for his patience, support, and guidance throughout the project.

I would also like to thank:

- My co-supervisor Dr Aaron Marshall, and all of the academic staff in CAPE for creating an intellectually stimulating environment.
- Ranee Hearst, Leigh Richardson, Stephen Hood, Frank Weerts, Stephen Beuzenberg, Tim Moore, Michael Sandridge, Tony Allen, Graham Furniss, Glenn Wilson and any other CAPE technical staff. Thanks for keeping everything running so that we can focus on research.
- My groupmates, Iman Hashemi, Wasim Khan, Vincent Jia, and Yin Hang for your support in the lab, and for keeping my spirits up in the office.
- Kat for keeping the home fire burning, and your love and support through all of this.
- Finally, I'd like to thank my parents, Alison and Grant, for their generous encouragement and support throughout my life and especially my academic career.

# ABSTRACT

Industrial pollution remains an issue in many parts of the world. While the problem is localised to certain areas with high densities of heavy industries, the worldwide demand for the products produced means that there is a worldwide responsibility for dealing with the pollution. As some compounds in the wastewater are difficult to treat with traditional methods, new processes must be developed to remove or degrade these pollutants. Advanced Oxidation Processes (AOPs) are a promising method of wastewater treatment that utilize in situ generation of the powerful hydroxyl radical to oxidize pollutants with little to no secondary waste. A significant disadvantage to AOPs is cost, which is compounded by the need for specific reaction conditions, especially pH. Therefore, any catalyst that can widen the range of reaction conditions will help to reduce the cost and improve adoption of AOPs for recalcitrant wastewater treatment.

In this work, a novel heterogenous photocatalyst was synthesized by the loading of iron onto the metal-organic framework MIL-47 to create Fe/MIL-47. An iron-zeolite Y catalyst was also synthesized following methods previously reported. These catalysts were then tested for the photo-oxidation of methylene blue, a common model pollutant dye, under UV irradiation. The Fe/MIL-47 catalyst was found to be very effective for both the decolourisation and total organic carbon (TOC) removal at low pH when compared with the iron-zeolite catalyst, with 94% colour removal and 52% TOC removal after 180 minutes for the Fe/MIL-47 catalyst and only 74% colour removal and 8% TOC removal for the Fe-zeolite Y catalyst at the same catalyst loading. The base MIL-47(V) catalyst was also tested and was found to be active for the decolourisation of methylene blue, a result in agreement with previous research that found that other metal-carboxylate frameworks were also photocatalytically active. The Fe/MIL-47 catalyst was found to only be effective over a limited pH range, and therefore a copper MIL-47 catalyst was also synthesized, with a goal of possibly creating a bimetallic catalyst with a wide effective pH range. While the Cu/MIL-47 was indeed found to be active at the higher pH that the Fe/MIL-47 was less active at, the stability of the MIL-47 support was determined to be less than what was necessary for a durable catalyst, and therefore the focus of the remaining studies was shifted to the zeolite based catalyst.

While iron-zeolite Y catalysts have been used as heterogenous photocatalysts before, the potential effect of the Brønsted acid sites on the reaction rate has not been researched. In this section of work, the effect of $NH_4^+$, $Na^+$ and $H^+$ in zeolite Y on photo-Fenton oxidation of formaldehyde in a batch reactor was examined. The model pollutant was changed to formaldehyde,

as unlike methylene blue, formaldehyde can diffuse within the pore structure of the zeolite, helping to illuminate any effect on the oxidation reaction by the internal pore environment The catalysts were prepared by partial exchange of $Fe^{3+}$, in the zeolite Y. The charge balancing cations were found to play a vital role in the photo-Fenton oxidation of formaldehyde, with the Fe/zeolite Y catalyst prepared with Brønsted acid sites ($H^+$) exhibiting three times the reaction rate of the $NH_4^+$ or $Na^+$ containing catalysts at pH 7 (TOF are 10.3, 2.7 and 3.4 μmol [mol Fe s]$^{-1}$, for Fe/H-Y, Fe/$NH_4$-Y and Fe/Na-Y respectively).

The results of the study into the charge balancing cations in zeolite Y, did yield an effective photocatalyst at high pH, however the effect was only observable at low catalyst loading (0.5 g $L^{-1}$), and low iron loading on the catalyst (50% exchanged), limiting the maximum concentration of pollutant that could be treated. Therefore, a bimetallic copper-iron catalyst was synthesized by incipient wetness ion impregnation of zeolite Y with iron and copper ions. This FeCu-zeolite Y catalyst was then tested for the photo-oxidation of methylene blue over a range of pHs. It was found to be effective at both low pH, with 98% colour removal and 89% TOC removal, and high pH, with 99% colour removal and 79% TOC removal. The FeCu-zeolite Y catalyst was also tested under recycle and found to remain effective after 3 runs. The XRD results also showed no loss in crystallinity, indicating the catalyst support continued to be stable throughout the recycle.

Collectively, these results present the attempt to create a pH insensitive heterogeneous photo-Fenton catalyst. The MIL-47 based catalyst unfortunately did not have the required stability to fulfil this, however the partially exchanged zeolite Y and the bimetallic zeolite Y catalysts did allow for wider pH range photo-Fenton reactions.

# TABLE OF CONTENTS

# LIST OF FIGURES

# LIST OF TABLES

# GLOSSARY

| | |
|---|---|
| Å | Angstroms |
| AOP | Advanced oxidation process |
| FA | Formaldehyde |
| FAU | Faujasite |
| MB | Methylene blue |
| MOF | Metal-organic framework |
| SEM | Scanning electron microscopy |
| TCD | Thermal conductivity detector |
| TEM | Transmission electron microscopy |
| TOC | Total organic carbon |
| TOF | Turnover frequency |
| XRD | X-ray diffraction |

# 1 INTRODUCTION

## 1.1 Introduction

Industrial wastewater remains a problem in many parts of the world [1] with pollutant streams often containing compounds that are difficult to treat with traditional methods [2]. With an increasing world population, and industrialization becoming the norm across the world, the magnitude of the pollution streams is also increasing, causing further degradation to water quality in areas where intensive industrial processes are located [3]. Many solutions have been examined to treat this waste water, including direct oxidation [4], adsorption [5], electro-coagulation [6], bioremediation [7], and Advanced Oxidation Processes (AOPs) [8]. Of these, AOPs are an especially attractive method as they operate at or near ambient temperatures and pressures [9], and are able to degrade recalcitrant compounds that other methods cannot easily remove or degrade [10], while leaving little or no secondary waste. The main drawback to AOPs is the cost of treatment which is compounded by the need for specific reaction conditions [11], therefore more research is needed into catalysts that can facilitate AOP reactions at a wider range of operating conditions.

Advanced Oxidation Processes are defined as a broad class of chemical treatments that operate primarily through the generation of hydroxyl radicals (HO• ). The Fenton reactions are a widely studied AOP based on the electron transfer between hydrogen peroxide and iron ions, shown in Equations 1.1 and 1.2 below. The iron(II) ion is oxidized by hydrogen peroxide to iron(III) (Equation 1.1), and subsequently the iron(III) ion is reduced back to iron(II) (Equation 1.2), with the net effect being a disproportionation of hydrogen peroxide to form two oxygen radical species (hydroxyl HO• and hydroperoxyl $HO_2$• ) and water (in the form of $OH^-$ + $H^+$).

$$Fe^{2+} + H_2O_2 \rightarrow Fe^{3+} + HO\bullet + OH^- \quad 1.1$$

$$Fe^{3+} + H_2O_2 \rightarrow Fe^{2+} + HO_2\bullet + H^+ \quad 1.2$$

This reaction is significantly accelerated by UV irradiation [12], commonly called the photo-Fenton reactions, which allows the reactions to proceed at lower temperatures than the dark Fenton reactions. Additionally heterogenous Fenton catalysts – where the iron ions are immobilized by a support material rather than in solution, have many advantages over traditional homogenous Fenton catalysis and have been widely studied in recent years [13]. While the Fenton reactions have been extensively researched, a common problem is that they require a low pH (around pH 3) to function [14], and industrial wastewater is known to have variable pH [15]. Therefore, the development of Fenton catalysts that operate over a wide pH range is necessary for widespread adoption into industrial practice.

The support material for heterogenous Fenton catalysts is also very important, as the ability of the iron ion to react with hydrogen peroxide is affected by the size and structure of the support [16]. Microporous materials are desirable as catalyst support materials due to their extremely high surface areas compared to bulk materials. Metal-organic frameworks are a class of microporous materials that have been of extreme interest [17] in recent years, however they are relatively untested as platforms for AOPs. Zeolites are another microporous material that have been more extensively studied as supports for AOPs, although typical zeolite Fenton catalysts have a limited pH range [18], similar to traditional Fenton catalysts.

## 1.2 Thesis scope and structure

Since existing Fenton catalysts have a limited pH range of operation, the focus of this project was on the development of a Fenton catalyst for industrial wastewater oxidation that can operate over a wide pH range. The initial focus was on developing and evaluating a MOF based catalyst, with a shift to focus on zeolite based catalysts after initial testing showed the stability of the MOF based catalyst was insufficient. Two possible methods of improving the operating pH range of zeolite based Fenton catalysts were investigated; partial exchange of acidic zeolite, and the addition of copper as a co-ion in the zeolite catalyst.

The thesis has been written in six chapters. Appendices have been numbered for the corresponding chapter and therefore the numbering starts with “Appendix 2” as there are no appendices for Chapter 1. The remaining chapters are as follows:

Chapter 2: A review of literature is presented in Chapter 2, which serves to provide the reader with the rational behind the thesis, and to set this thesis in the context of other research in the area of wastewater treatment using microporous supported photo-Fenton catalysts.

Chapter 3: This chapter describes the investigation of the metal-organic framework, MIL-47, as a support material for photo-Fenton degradation of aqueous methylene blue. Based on the relevant literature it is hypothesised that MIL-47 based catalyst will be a highly effective and robust catalyst for dye degradation. The results of the degradation experiments, and an investigation of the stability and reusability of the catalyst are presented. Early results from this study were presented at WCCE9 as “*Decolourisation of Methylene Blue Aqueous Solution By Photo-Fenton Process Over Fe/MIL-47”.*

Chapter 4: The work that was published as "*Catalytic consequences of charge-balancing cations in zeolite during photo-Fenton oxidation of formaldehyde in alkaline conditions*" in Separation and Purification Technology is presented in this chapter; an investigation into the effect of partial exchange of acidic zeolite Y with iron on the effective pH operating range of the oxidation of formaldehyde. It was hypothesised that the partial exchange of the acidic zeolite could lead to a wider effective pH range by providing a localised acidic environment within the zeolite pores.

Chapter 5: While the effective pH range of the zeolite based catalyst was successfully expanded in the experiments detailed in Chapter 4, this came at the expense of active site density. Therefore, the co-addition of copper to the iron-zeolite Y catalyst was investigated in Chapter 5, with the hypothesis that the addition of copper to the iron zeolite catalyst would expand the effective pH range without significantly decreasing the active site density of the catalyst as in Chapter 4.

Chapter 6: Conclusions drawn from the current work and recommendations for future studies are presented in Chapter 6.

## 1.3 References


1. Wang, Q. and Z. Yang, *Industrial water pollution, water environment treatment, and health risks in China.* Environmental Pollution, 2016. **218**: p. 358-365.
2. Xiong, W., et al. *The Bimetallic Synergistic Effect in Heterogeneous UV/Fenton System for the Treatment of Refractory 6-Nitryl Wastewater*. in *Advanced Materials Research*. 2014. Trans Tech Publ.
3. Kanagaraj, J., et al., *Eco-friendly waste management strategies for greener environment towards sustainable development in leather industry: a comprehensive review.* Journal of Cleaner Production, 2015. **89**: p. 1-17.
4. Oyama, T., et al., *Remediation of aquatic environments contaminated with hydrophilic and lipophilic pharmaceuticals by TiO2-photoassisted ozonation.* Journal of Environmental Chemical Engineering, 2014. **2**(1): p. 84-89.
5. Rafatullah, M., et al., *Adsorption of methylene blue on low-cost adsorbents: A review.* Journal of Hazardous Materials, 2010. **177**(1–3): p. 70-80.
6. Khandegar, V. and A.K. Saroha, *Electrocoagulation for the treatment of textile industry effluent – A review.* Journal of Environmental Management, 2013. **128**: p. 949-963.
7. Harrelkas, F., et al., *Photocatalytic and combined anaerobic–photocatalytic treatment of textile dyes.* Chemosphere, 2008. **72**(11): p. 1816-1822.
8. Yang, S., et al., *Decolorization of methylene blue by heterogeneous Fenton reaction using Fe3−xTixO4 (0 ≤ x ≤ 0.78) at neutral pH values.* Applied Catalysis B: Environmental, 2009. **89**(3–4): p. 527-535.
9. Babuponnusami, A. and K. Muthukumar, *A review on Fenton and improvements to the Fenton process for wastewater treatment.* Journal of Environmental Chemical Engineering, 2014. **2**(1): p. 557-572.
10. Ayoub, K., et al., *Application of advanced oxidation processes for TNT removal: A review.* Journal of Hazardous Materials, 2010. **178**(1–3): p. 10-28.
11. de Araú jo, K.S., et al., *Advanced oxidation processes: a review regarding the fundamentals and applications in wastewater treatment and industrial wastewater.* Ambiente e Agua-An Interdisciplinary Journal of Applied Science, 2016. **11**(2): p. 387-401.
12. Pignatello, J.J., E. Oliveros, and A. MacKay, *Advanced Oxidation Processes for Organic Contaminant Destruction Based on the Fenton Reaction and Related Chemistry.* Critical Reviews in Environmental Science and Technology, 2006. **36**(1): p. 1-84.
13. Chen, J. and L. Zhu, *Heterogeneous UV-Fenton catalytic degradation of dyestuff in water with hydroxyl-Fe pillared bentonite.* Catalysis Today, 2007. **126**(3–4): p. 463-470.
14. Lam, F.L., A.C. Yip, and X. Hu, *Copper/MCM-41 as a highly stable and pH-insensitive heterogeneous photo-Fenton-like catalytic material for the abatement of organic wastewater.* Industrial & engineering chemistry research, 2007. **46**(10): p. 3328-3333.
15. Yilmaz, B., N. Trukhan, and U. MÜLler, *Industrial Outlook on Zeolites and Metal Organic Frameworks.* Chinese Journal of Catalysis, 2012. **33**(1): p. 3-10.
16. Navalon, S., M. Alvaro, and H. Garcia, *Heterogeneous Fenton catalysts based on clays, silicas and zeolites.* Applied Catalysis B: Environmental, 2010. **99**(1–2): p. 1-26.
17. Farrusseng, D., S. Aguado, and C. Pinel, *Metal–Organic Frameworks: Opportunities for Catalysis.* Angewandte Chemie International Edition, 2009. **48**(41): p. 7502-7513.
18. Rache, M.L., et al., *Azo-dye orange II degradation by the heterogeneous Fenton-like process using a zeolite Y-Fe catalyst—Kinetics with a model based on the Fermi's equation.* Applied Catalysis B: Environmental, 2014. **146**(0): p. 192-200.

# 2 LITERATURE REVIEW

## 2.1 Industrial Wastewater

The world has an ever-increasing population [1], which coupled with increasing rates of urbanization and industrialization, means that wastewater emissions have developed into a major environmental concern in many parts of the world [2]. With climate change induced water scarcity also likely to be a worldwide issue in the near future [3], clean water will continue to be an issue of utmost importance. Increased industrial effluent has been identified as the primary cause of water pollution in developing nations [4], and as many of the effluent streams contain toxic organic compounds that are difficult to treat with traditional methods [5], new methods of wastewater treatment must be developed to ensure acceptable water quality. As a large proportion of manufacturing has shifted from developed nations, where pollution is tightly regulated, to developing nations where regulations are less strict and less strictly enforced [6], water quality has been especially degraded in developing nations where significant industrial process are extensively carried out [7]. In addition to a lack of regulation and enforcement, the industries of many developing nations are more sensitive to increases in costs, so any improvements to operating efficiencies and price of implementation will greatly improve adoption rates.

In New Zealand, as an example of a developed nation with relatively strict wastewater regulations, wastewater discharge is covered under the Resource Management Act (RMA). Under this scheme, the overall effect of the discharge is considered rather than general specified limits. Industrial wastewater is typically diluted and discharged to sewage. Biological oxidation is then used to treat both the dilute industrial effluent and domestic sewage. While this method works for a small, water rich population with a relatively limited industry, New Zealand's population is rapidly increasing, so dilution will not be a viable method of wastewater treatment in the future, as it is already not a viable method for nations with extensive heavy industry. By taking the lead in developing advanced wastewater treatment processes, New Zealand can not only prepare for the future but also help developing nations already face industrial pollution problems.

A number of compounds which cannot be easily treated by existing wastewater treatment processes have specified concentration limits in New Zealand regulations, an example of problematic organic compounds, from the Christchurch City Council Tradewaste Bylaw [8], is presented in Table 2.1. Many of these compounds are recalcitrant to biological oxidation, and as the specified limits for some compounds are too low for dilution within overall discharge volume limits, these specific compounds would require pre-discharge treatment to be within the limits. Therefore,

enhanced wastewater treatment processes already have utility in New Zealand and will be of increasing importance in the future.

Table 2.1 – Specified organic compound limits for industrial waste in Christchurch, New Zealand [8].

| Compound | Maximum Concentration [g/m$^3$] |
|---|---|
| Formaldehyde (as HCHO) | 50 |
| Phenolic compounds (as phenols) excluding chlorinated phenols | 50 |
| Chlorinated phenols | 0.02 |
| Petroleum hydrocarbons | 30 |
| Halogenated aliphatic compounds | 1 |
| Monocyclic aromatic hydrocarbons | 5 |
| Polycyclic (or polynuclear) aromatic hydrocarbons (PAHs) | 0.05 |
| Halogenated aromatic hydrocarbons (HAHs) | 0.002 |
| Polychlorinated biphenyls (PCBs) | 0.002 |
| Polybrominated biphenyls (PBBs) | 0.002 |
| Pesticides (general) | 0.2 in total |
| Organophosphate pesticides | 0.1 |

Another type of significant recalcitrant wastewater contamination not mentioned in Table 2.1 – Specified organic compound limits for industrial waste in Christchurch, New Zealand [8]. is pharmaceutical wastewater. Pharmaceutical wastewater is typically created from medicines entering sewage streams. Recalcitrant pharmacologically active compounds are especially of concern due to extraordinary harm they can do to ecology [9]. Examples include; hormonally active compounds[10], anti-biotics[11], and anti-inflammatory drugs [12]. While pharmaceutical wastewater is beyond the scope of this thesis, many of the treatment techniques discussed can also be applied to pharmaceutical wastewater, and as society looks to limit the impact on the environment, treatment methods for these problematic compounds will become a high priority.

### 2.1.1 Textile industry wastewater

Textile industry wastewater, especially that generated during the dying process, is a significant pollutant source in nations with large textile industries [13]. As shown in Figure 2.1, worldwide production of textiles has been increasing year on year, with the increase in consumption per capita also showing that the large increases in production are not merely from an increasing population but from increased demand per person. This means that as the textile industry continues to grow, the wastewater it produces will become an increasing problem.

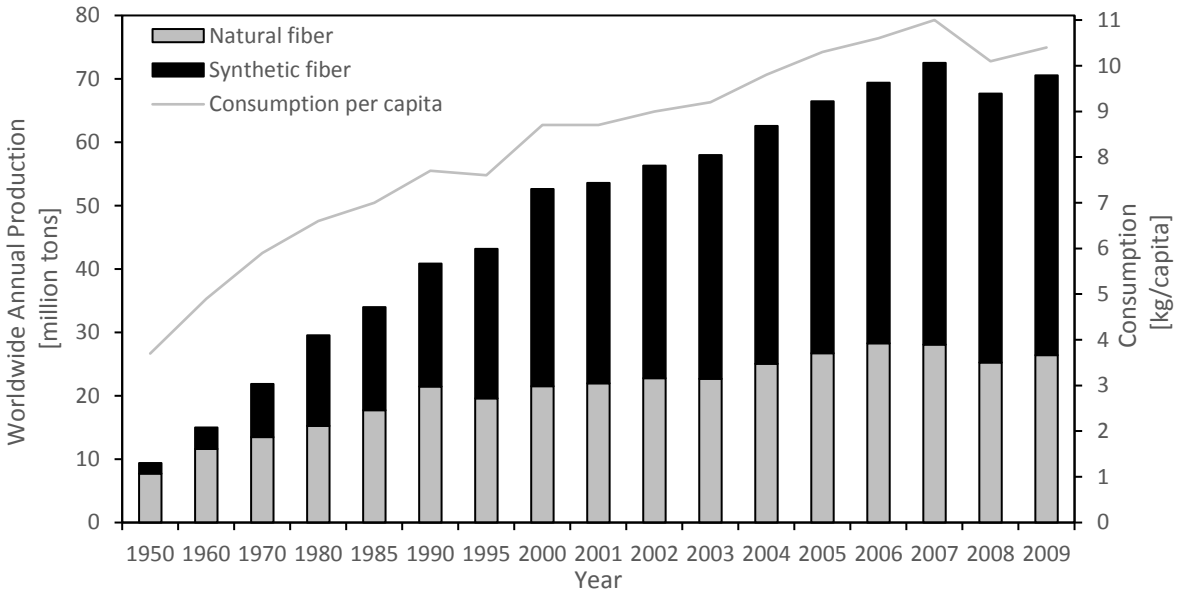


Figure 2.1 – Worldwide consumption of man-made and natural fibers between 1950 and 2009 [14].

Dyes are the most visible pollutant from the textile industry, and are also discharged from a wide variety of other industries, including; rubber, paper, leather, plastics, cosmetics, and printing. Worldwide annual production of dyes is over $7x10^5$ metric tons [15], with around half that textile dyes [16]. While 15% is a commonly cited figure [17-21] for the amount of dye discharged as wastewater, this citation appears to have originated from *Color Chemistry, 1997*[22] and does not appear to have a recent basis. While it is difficult to find contemporary estimates of dye discharge amounts, recent studies have shown that dye wastewater is of concern as it is one of the main sources of pollution in textile industry areas [13]. Additionally wastewater containing dyes can be toxic and carcinogenic [23], as well as aesthetically displeasing. High levels of dye in wastewater can also cause a lack of dissolved oxygen [15], as well as impede light penetration in treatment pans, limiting the effectiveness of traditional biological treatment methods.

Methylene blue (Figure 2.2) is a cationic dye that is used for dying cotton, wool, leather, and silk in the textile industry [17, 24], and also has medical applications [25]. Methylene blue is also widely studied as a model dye for textile industry wastewater [17, 24, 26-29]. Methylene blue has a dynamic diameter of 5.91Å x 13.82Å [30], and features a chromophoric thiazine group [31] with an amino group on either side. Methylene blue is known to form dimers at high concentrations (>$10^{-3}$ mol $L^{-1}$) [32], therefore concentrations below this should be used to avoid potential problems. Several oxidation studies have revealed that the initial step in the methylene blue oxidation is the cleavage of the sulphur-carbon [33] bond followed by further opening of the central ring structure [18].

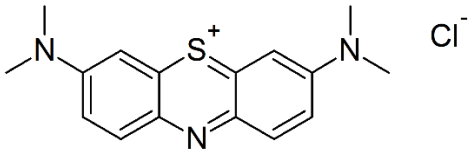


Figure 2.2 – Molecular structure of methylene blue.

The negative health effects of methylene blue, or methylene blue wastewater are often mentioned in methylene blue studies, however methylene blue is actually relatively safe for humans – it is not classified as a known carcinogen to humans, IARC Class 3 [34], and indeed is prescribed as a medicine [25] with few side effects listed. While the typical claimed effects; burns to the eyes, nausea, and diarrhoea [23, 35] are unlikely to manifest from industrial discharge, methylene blue has been shown to be toxic to neonates, at a dosage 20mg/kg administered directly into the babies bloodstream [36]. Obviously this dosage is extremely large, and is unlikely to occur from polluted water for either neonates or adults. Although the estimates of methylene blue toxicity to humans given in contemporary research do not have a basis in reality, even small amounts of dye in wastewater streams can give the perception of a more significant problem due to the visible colour even at low concentrations. Therefore, research into both the decolourisation and mineralization is justified to treat this pollution.

### 2.1.2 Formaldehyde

Formaldehyde (Figure 2.3) is used in many industries, including; pharmacy, perfumery and cosmetics, organic synthesis, resin and colour manufacturing [37]. It is also widely used in hospitals at high concentrations as embalming fluid, and in developing nations, the batch discharge of large volumes of such formaldehyde wastewater can cause a shock load of high toxicity to the

microorganisms in biological wastewater treatment systems [38]. While the health risks to humans of methylene blue has often been over stated in academic discourse, this is not the case with formaldehyde, which is an IARC Class 1 chemical [39], meaning it is known to have carcinogenic effects in humans. Exposure to formaldehyde in industrial effluents, for example wastewater discharged from the phenol–formaldehyde resin manufacturing industry, wood processing industry and paper industry [27,28], has been shown to give many acute and chronic adverse health effects [40]. It is therefore important to find effective and robust methods of treating aqueous formaldehyde wastewater.

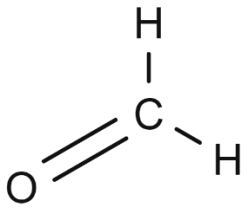


Figure 2.3 – Molecular structure of formaldehyde.

While FA is relatively simple model pollutant, in many nations, formaldehyde discharge streams are tightly regulated, so the treatment of FA wastewater does have real world applications. The maximum discharge amount in NZ is 50 mg $L^{-1}$ [8]. While dilution may be used to decrease the concentration within this limit, this method of waste treatment may be cost prohibitive in the future, as water becomes more scarce. Additionally, a large proportion of the industry which creates FA wastewater has moved into developing nations, which have more relaxed regulations and enforcement [37]. The treatment of FA contaminated wastewater has been studied for a number of methods. These include adsorption onto low cost materials such as clays [41] or activated carbon [42]; and Advanced Oxidation Processes [43] including; homogenous photo-Fenton [38, 44, 45], homogenous Fenton [46], mixed oxide catalysts [47], and titania based photocatalysts[48].

### 2.1.3 Methods of wastewater pollution measurement

Wastewater pollution levels are typically measured using a Biological Oxygen Demand (BOD) test [8], as the most common primary treatment method is biological oxidation. $BOD_5$ is the standard BOD test, which measures the amount of oxygen consumed by bacteria to digest a sample of wastewater over five days. The similar Chemical Oxygen Demand (COD), uses direct chemical oxidation of the wastewater sample, and has the advantage of not requiring five days to complete; and is viable for biologically toxic compounds. $BOD_5$ and COD are equivalent measures given a non-toxic compound, therefore the ratio of $BOD_5$:COD is used as a measure of how treatable wastewater is by biological methods [49]. Total Organic Carbon (TOC) is another method that is frequently used to quantify wastewater pollution levels. This method has a good correlation with COD for organic pollutants, as the organic carbon makes up a significant portion of the chemical oxygen demand of the compound, although it will not account for un-oxidised non-carbon species in solution. While empirical correlations can be found for BOD:COD:TOC for effluent streams [50], these correlations are not necessarily valid for individual compounds, and should not be used without validation for an individual compound.

The removal efficiency of a wastewater treatment process is defined as:

$$\text{Removal efficiency} = \frac{[C_0]\text{-}[C_t]}{[C_0]} \qquad 2.1$$

Where $[C_0]$ is the initial concentration, and $[C_t]$ is the concentration at time *t.* TOC, BOD, or COD may be used here instead of a chemical concentration as they represent a general pollution concentration of the solution. The removal efficiency of visual pollution is also defined using Equation 2.1, where $C_0$ is the initial concentration of the colour contributing compound, and $C_t$ is the concentration at time *t*. This concentration is typically determined by measuring the absorbance of the solution over visual light wavelengths. The absorbance of a given concentration of a compound, at low concentrations, is given by Beers Law:

$$\text{Absorbance} = \varepsilon \, \text{L} \, \text{C} \qquad 2.2$$

where ε is the molar absorptivity, *L* is the path length, and *C* is the concentration. At low concentrations of colour contributing compounds, the relationship between abs and concentration is linear, and therefore absorbance may be used directly:

$$\text{Removal efficiency} = \frac{Abs_0\text{-}Abs_t}{Abs_0} \qquad 2.3$$

## 2.2 Wastewater treatment methods

The most common bulk method of wastewater treatment is biological oxidation [51]. While bio-oxidation is extremely low cost and effective for most wastewater [52], it requires significantly more time than other methods [53], and is typically of limited use for recalcitrant compounds such as those listed in Table 2.1. Recent research has discovered bacteria and conditions suitable to treat problematic compounds, such as the use of formaldehyde resistant bacteria [54, 55] from seawater to treat formaldehyde wastewater, or anaerobic digestion of methylene blue [56]. However, these specific compound methods increase the cost of treatment and still produce secondary waste streams.

Another commonly studied method of treating wastewater that contains recalcitrant compounds is adsorption, typically onto a low cost solid [57]. Some examples of low cost adsorbents reported for the removal of methylene blue from wastewater are; oak sawdust [58], red mud, an aluminium industry by-product [24], and oil palm fibre activated carbon [35]. Other adsorbents, not described as low-cost, such as metal-organic frameworks [23, 59, 60], have also been reported for the treatment of dye wastewater. Adsorption can be an excellent treatment method, especially with regard to cost, however, the pollutant is not destroyed and therefore dangerous compounds must be further treated to render them safe [17]. Many other solutions have been examined to treat wastewater, including direct oxidation [12], adsorption [57], electro-coagulation [61], anion exchange resins [62], and perhaps the most promising, Advanced Oxidation Processes (AOPs) [63-69].

### 2.2.1 Advanced Oxidation Processes

Advanced Oxidation Processes are defined as a broad class of treatments that operate primarily through the generation of hydroxyl radicals (HO•)[70]. The hydroxyl radical is a potent oxidant – as shown in Table 2.2, it is only second to fluorine in oxidation potential, and can provide almost total degradation of organic pollutants in wastewater [71]. AOPs were first defined in 1987 [71], and have since become a widely studied technique. AOPs are an especially attractive method [64-69] as they operate at or near ambient temperatures and pressures [72], and are able to degrade recalcitrant compounds that other methods cannot easily remove or degrade [73], while leaving little or no secondary waste [17].

Table 2.2 – Oxidation potentials of common oxidants [74].

| Oxidant | Oxidation potential (V) |
|---|---|
| Fluorine ($F_2$) | 3.03 |
| Hydroxyl radical (HO•) | 2.80 |
| Atomic oxygen ($O_1$) | 2.42 |
| Ozone ($O_3$) | 2.07 |
| Hydrogen peroxide ($H_2O_2$) | 1.77 |
| Potassium permanganate ($KMnO_4$) | 1.67 |
| Chlorine dioxide ($ClO_2$) | 1.5 |
| Hypochlorous acid (HClO) | 1.49 |
| Chlorine ($Cl_2$) | 1.36 |
| Oxygen ($O_2$) | 1.23 |
| Bromine ($Br_2$) | 1.09 |

While AOPs have not been put into commercial use on a large scale, due primarily to cost[75], the oxidative capability and efficiency have been established for a large number of recalcitrant organic wastewater contaminants; such as formaldehyde [76], aniline [77], textile dyes[78, 79], pesticides[80], and TNT [73]. In recent years, AOPs have also been applied to other reactions such as oxidative desulfurization of organosulfur compounds from liquid fuels [81-83].

One of the first AOPs described is the UV/$H_2O_2$ system, where UV light is used to cleave the O-O bond in $H_2O_2$, leading to the formation of two hydroxyl radicals:

$$H_2O_2 + h\nu \rightarrow 2HO\bullet \qquad 2.4$$

However, the molar extinction coefficient at 254 nm is only 19.6 $M^{-1}s^{-1}$ [84], which is exceptionally low for primary absorber in a photochemical process. Hydrogen peroxide also does not absorb significantly above 300 nm [85]. This means that using only the UV/$H_2O_2$ gives low reaction rates and poor conversion.

### 2.2.1 The Fenton reactions

As mentioned in Chapter 1 the Fenton reactions are a widely studied AOP based on the electron transfer between hydrogen peroxide and iron ions [75] to generate hydroxyl (HO• ) radicals. First described in detail 1894 by Henry J. Fenton [86], the traditional homogenous Fenton reaction is shown in Equations 1.1 and 2.6 below. The iron(II) ion is oxidized by hydrogen peroxide to iron(III) (Equation 1.1), and subsequently the iron(III) ion is reduced back to iron(II) (Equation 2.6), with the net effect being a disproportionation of hydrogen peroxide to form two oxygen radical species (hydroxyl HO• and hydroperoxyl HOO•) and water (in the form of $OH^- + H^+$) [87]:

$$Fe^{2+} + H_2O_2 \rightarrow Fe^{3+} + HO\bullet + OH^- \qquad 2.5$$

$$Fe^{3+} + H_2O_2 \rightarrow Fe^{2+} + HO_2\bullet + H^+ \qquad 2.6$$

While the overall theoretical reaction scheme for homogeneous Fenton reactions produces no net change in both iron ion oxidation states, or pH, in practice there is a build-up of ferric hydroxide sludge, as the rate constant of reaction 1.1, $k_{2.5}$, is ≈ 70 $M^{-1}$ $s^{-1}$ [88], while the rate constant of reaction 2.6, $k_{2.6}$ is 0.001-0.01 $M^{-1}$ $s^{-1}$ [89]. As ferric hydroxide precipitates from solution [90], the iron ions can no longer participate in the reaction cycle, and rate of generation of radicals drops [49].

In addition to this, homogeneous Fenton reactions are not suitable for industrial processes due to the potential threat of secondary contamination caused by the soluble metal catalyst. None the less, homogeneous Fenton catalysis have been used to treat many recalcitrant organic contaminants such as pesticides [91], pharmaceutical waste [92], and textile dyes [93]. Heterogenous Fenton catalysts – where the iron ions are immobilized by a support material rather than in solution, have been developed to overcome some of the inherent disadvantages of the homogeneous Fenton reactions.

Heterogeneous Fenton catalysts have many advantages over traditional homogenous Fenton catalysis and have been widely studied in recent years [94], with materials such as clay [95], silicate [96, 97], and zeolites[21] used as supports. In heterogeneous Fenton catalysis, the iron cation is immobilized within the structure of the catalyst/support [21], this allows the catalyst to maintain its

ability to generate hydroxyl radicals from $H_2O_2$ [98], and iron hydroxide precipitation can be prevented [94]. The solid catalysts can also be recovered from the treated solution by simple physical means and can be readily reused after treatment [98, 99].

Fenton reactions are significantly accelerated by UV irradiation [100], which is commonly called the photo-Fenton reaction. The photo-Fenton reaction gives faster rates and a higher degree of mineralization than the "dark" reaction [100], as it utilizes the photochemical reduction of $Fe^{3+}$ to $Fe^{2+}$, shown in Equation 2.7.

$$Fe^{3+} + H_2O + h\nu \rightarrow Fe^{2+} + HO\bullet \qquad 2.7$$

The introduction of UV light also provides additional channels to produce hydroxyl radicals or increase the production rate of hydroxyl:

$$H_2O_2 + h\nu \rightarrow 2HO\bullet \qquad 2.8$$

$$Fe(OH)^{2+} \rightarrow Fe^{2+} + HO\bullet \qquad 2.9$$

Although reactions 2.8 and 2.9 can be important in pollutant degradation, the photochemical cycling of $Fe^{3+}$ back to $Fe^{2+}$ is the most crucial in photo-Fenton process, considering the orders of magnitude difference in the rates of reactions 2.5 and 2.6. The photo-Fenton system has been applied to the degradation of a wide range of contaminants [93, 101-104], predominantly persistent organic pollutants such as pesticides, dyes, and pharmaceuticals [91, 92, 105, 106].

Both homogeneous and heterogeneous photo-Fenton catalysts are found to be functional only at low pH (around pH 3 [107]) as elevated pH causes iron hydroxides and oxides to form and precipitate for the homogeneous and iron hydroxide complexes to form for the heterogenous catalysts. Iron solubility can be a significant problem [90, 108] in photo-Fenton oxidation at high pH conditions because of the formation of iron hydroxides, oxides or oxyhydroxide (FeOOH), causing a significant decrease in hydroxyl radical formation rate which is directly proportional to the availability of immobilized $Fe^{3+}$.

The use of copper (or other transition metals) in the place of iron has also been studied, and is known as Fenton-like reactions or catalysts [109]. These reactions are substantially similar to the Fenton reactions, with copper (I) being oxidized to Cu(II) by hydrogen peroxide (Equation 2.10), generating a hydroxyl radical, while Cu (II) is reduced by hydrogen peroxide to Cu (I) producing a hydroperoxyl radical (Equation 2.11):

$$Cu^{+} + H_2O_2 \rightarrow Cu^{2+} + HO\bullet + OH^{-} \quad 2.10$$

$$Cu^{2+} + H_2O_2 \rightarrow Cu^{+} + HO_2\bullet + H^{+} \quad 2.11$$

Similarly to iron Fenton, UV irradiation has also been shown to enhance the copper Fenton-like reactions [98]. Heterogeneous Fenton-like catalysts have been developed, including Cu/MCM-41[85, 110], and Cu-zeolite Y[111].

Various methods have been proposed to widen the working pH range of heterogeneous photo-Fenton catalysts [95, 96, 98, 112, 113]. For instance, Lam et al. proposed the use of MCM-41 supported Cu catalyst to promote an analogous photo-Fenton reaction that showed promising Orange II degradation at neutral pH without formation of copper hydroxides or oxides [107]. Based on this observation, bimetallic catalyst systems, such as Fe-Cu/MCM-41 [97, 114] and Fe-Cu/Bentonite [95] were further developed to degrade organic pollutants at acidic and near neutral pH effectively. The exact mechanisms that enables the so-called bimetallic effect have not been fully elucidated yet[115], however one theory that has been put forward [111] is that the copper-iron interaction allows $Fe^{3+}$ to be reduced to $Fe^{2+}$ by the copper species:

$$Fe^{3+} + Cu^{+} \rightarrow Fe^{2+} + Cu^{2+} \quad 2.12$$

### 2.2.2 Microporous materials as supports for Fenton catalysts

Microporous materials are a subclass of nanoporous materials that are defined as having a pore size between 0.2-2 nm. Related subclasses include mesoporous materials, with pores between 2-50 nm and macroporous materials, with pore sizes greater than 50 nm. A number of materials can be engineered to have micropores, these include; carbon and carbon nano tubes [116], oxidic glasses [117], polymers [118], crystalline [119] and amorphous oxides [120], zeolites [121], and metal-organic frameworks [122]. Microporous materials are widely used for a range of applications including, separations [123] , medical applications [124], adsorption [125], catalysis [126, 127], as well as emerging areas such as photonics , microelectronics and bioengineering [128].

The support material for heterogenous Fenton catalysts is very important, as the ability of the iron ion to react with hydrogen peroxide is affected by the size and structure of the catalyst [129]. Microporous materials are desirable as catalyst support materials due to their extremely high surface areas when compared to bulk materials. Metal-organic frameworks are a class of microporous materials that have been of extreme interest [130] in recent years, however they are relatively untested as platforms for AOPs. Zeolites are another microporous material that has been more extensively studied as supports for AOPs, however typical zeolite Fenton catalysts have a limited pH range [131], similar to traditional Fenton catalysts.

## 2.3 Metal organic frameworks

Metal-organic frameworks (MOFs), also known as porous coordination polymers, are a relatively new class of crystalline microporous materials that are composed of metal ion vertices and organic bridging ligands that form 3D crystal lattices [132, 133]. MOFs have received significant attention in recent years, primarily due to their ultrahigh porosity (up to 90% free volume) [134] and extremely high internal surface area (up to 6000 $m^2/g$) [135-137]. Additionally, the large number of possible combinations between metal ions and organic bridging ligands allows for MOFs to be synthesized with a variety of structures and chemistries, potentially allowing for the design of MOFs for specific, targeted applications.

The term “metal-organic framework” first appeared in literature over 20 years ago [122], with the most well-known, and studied metal-organic framework, MOF-5 ($Zn_4O(BDC)_3$ where $BDC^{2-}$ = 1,4-benzenedicarboxylate), being described over a decade ago [138]. Although widely studied, MOF-5 has been found to not be suitable for most applications as it has a relatively low thermal [139] and chemical [140] stability, a problem typical with first generation MOFs [140]. However, more recent MOFs have been shown to be highly stable, relative to the first generation MOFs. One such MOF is PCN-225, a $Zr^{IV}$ and porphyrinic carboxylate based MOF which is stable in both boiling water and aqueous solutions with pH ranging from 1 to 11 [141]. While not all later generation MOFs are as stable as PCN-225, several classes have been found to be significantly more stable than MOF-5, including; zeolitic imidazole frameworks (ZIF); and several in the MIL (Materials Institute Lavoisier) series.

The series of MOF known as the MIL- series, first synthesized by the research group of Gérard Férey, has attracted significant attention due to the high stability that some of the compounds display compared to earlier MOFs. In particular, MIL-53(M), or $M(III)(OH)[O_2C\text{-}C_6H_4\text{-}CO_2]$ (M=Al,Cr,Fe,Ga), has been extensively studied, primarily due to the large “breathing” effect observed upon hydration[142].

MIL-47 or $V(III)(OH)[O_2C\text{-}C_6H_4\text{-}CO_2]$, a structurally similar MOF made up of $V^{4+}O_6$ octahedra linked by dicarboxylate groups , which does not display the “breathing” effect [143] under normal conditions, has yet to be studied as thoroughly as MIL-53. However in the limited research that has been conducted, MIL-47 has been found to be an excellent adsorbent for some organic molecules, with a significantly better performance than MIL-53 for the adsorption of alkylaromatics [144], and remarkable performance for the adsorption of benzothiophene [145]. Additionally the adsorptive

ability of MIL-47 for benzothiophene has also been demonstrated to be enhanced by the loading of copper ions into the framework [146]. The use of MIL-47 as a low leaching catalyst has also been studied [147], and it has also been used as a catalyst for oxidative desulfurization [148]. Recently published results have shown that there may be stability issues with using MIL-47 as a catalyst [148]. MIL-47 was found to decay into vanadium oxide and BDC in the presence of TBHP at 100°C, however this effect was not observed when a reactant (DBT) was present, and the analogous MIL-53 was observed to be stable in aqueous oxidation reactions at room temperature [64]. It was also shown that the observed catalytic activity over MIL-47 was not due to decomposition as the self-oxidation products, vanadium oxide and terephthalic acid, were found to show almost no activity for the same reactions.

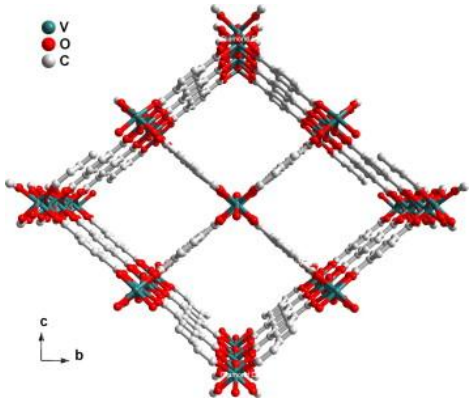


Figure 2.4 - Perspective view of structure of MIL-47 [147].

Heterogeneous catalysis was one of the earliest demonstrated applications for MOFs [149, 150], and has generated significant interest over the past decade[133]. Generally, there are four main ways MOFs have been used as heterogeneous catalysts. The first and most widely explored [151], is exchangeable coordination positions around the metal ion that act as active sites. Structural defects around the metal nodes have also recently been revealed to have an important role in catalysis [152]. The second approach is to use the ligands as active sites. This can be achieved by substituting some or all of a commonly used ligand, such as terephthalates or benzene tricarboxylates with a derivative that contains an additional acidic or basic group that can be used as an active site [151]. The third method is the post synthetic modification of the ligand [153, 154], which allows function groups to be added without interfering with synthesis. The fourth method is to use the large pore volume to incorporate a guest species [155]. Several recent reviews provide excellent coverage of the wide variety of reactions MOFs have been used to catalyse [149, 156].

The use of metal-organic frameworks as heterogeneous photocatalysts has also been reported [157-159], however it remains a relatively under developed area [64]. It has been reported that

MOF-5 has higher oxidation reaction efficiency than P25 $TiO_2$ under certain conditions [160], and has also been used as a catalyst for the photo-degradation of phenol[158], however as MOF-5 is unstable in water[140], it is of limited use as a catalyst. However other MOFs have also been found to be active in the photo-degradation of textile dyes [64, 66], and for visible light reduction of $CO_2$[161], however this later catalyst had a low activity and used a sacrificial electron donor, so cannot be considered a sustainable. It has also been observed that the photocatalytic activity did not change for different metal ions (Fe, Al, Cr) in MIL-53 [64], an interesting result that will require further investigation to determine the exact mechanism of photocatalysis.

In addition to catalysis, MOFs have also been used in a wide range of other applications, these include; as non-linear optics[162], as molecular sensors[155], gas separation[163-166], drug delivery[167] and as adsorbents for a range of compounds [23, 60, 144, 145, 168-171]. Another significant application for MOFs is in gas storage, particularly hydrogen and methane[137]. MOFs are excellent for gas storage because of their high porosity and surface area[172].

The inclusion of metal particles into MOFs, sometimes stylized as metal@MOF, is another area of MOF research that has been receiving considerable attention. Applications of metal@MOF that have been investigated include; gas storage [155, 173] chemical sensing[174] and heterogeneous catalysis[175-178]. Various loading methods have been demonstrated, including; incipient wetness method [179, 180], solid grinding [175, 181], microwave-assisted methods and gas phase loading via volatile organo-metallic precursors [182, 183]. Despite the recent attention, the exact nature of the metal-MOF interaction has yet to be elucidated [176]. Early attempts at characterization were complicated by destructive interactions between the imaging equipment and the nano particles[136]. However recent improvements to characterization techniques, such as electron tomography [155], may help to determine the precise location of metal particles inside frameworks.

While there have been numerous recent developments, the field of MOF catalysis is still underdeveloped, when compared to that of zeolitic catalysis [149]. While there are many similarities between MOFs and zeolites, MOFs are not likely to challenge zeolites as catalysts for reactions requiring forcing conditions (>500°C) as most MOFs begin to decompose at temperatures higher than 400°C [184]. This suggests that the true value in MOF catalysis may lie in high value reactions under mild conditions, such as homochiral catalysis [185-188].

## 2.4 Zeolites

Zeolites were first discovered in 1756 by Swedish scientist Axel Cronstedt, with the mineral stilbite, who named them *zeolites* (literally “boiling stone”), due to the visible water loss observed when zeolite powder is rapidly heated [189]. The next major milestone in zeolite science was in 1956 when the first zeolite without a natural counterpart was synthesized [190]. Since then, many more synthetic zeolites have been discovered, with 206 framework types recognized by the International Zeolite Agency [191]. Currently worldwide production of zeolites is over 3 million tonnes per year, with the majority of this derived from natural zeolites [191]. The main industrial uses for zeolites are; as catalysts in the petrochemical industry, agricultural applications, and the single largest use, laundry detergent.

Despite the recent development of advanced nanostructured materials, such as metal organic frameworks and carbon nanotubes, zeolites are still recognized as the most versatile, chemically and thermally stable catalysts or catalyst supports for many important reactions [137, 192, 193]. Their nanostructure, which is on the same scale as the molecules that react within their pores [194], often gives high product selectivity through the size exclusion process or stabilizing the transition state such as in the methanol-to-gasoline reaction [195].

Zeolites are now defined as microporous, crystalline aluminosilicates. The structure consists of an extended framework of corner sharing $TO_4$ tetrahedra, where T is an aluminium or silicon atom. The arrangement of these tetrahedra determines the overall topography of the zeolite, with four common zeolites shown in Figure 2.5 [196].The presence of $Al^{3+}$ atoms together with $Si^{4+}$ in the framework offers unique cation-exchange properties to zeolites due to imbalance in charge, allowing introduction of a wide range of foreign metal cations as catalytic sites. When the charge-balancing cations are protons, brønsted acid sites as strong as 85-90% sulfuric acid are readily available inside the cavity of the zeolites [197]. A commonly used measure of the number of these charge imbalance sites is the Si/Al ratio. Structurally analogous zeolites with different Si/Al ratios are given different names, e.g. zeolite Y and zeolite X, which both feature sodalite structure, with an overall structure analogous to naturally occurring faujasite, but have Si/Al ratios of 2-3 for zeolite X and >3 for zeolite Y [198].

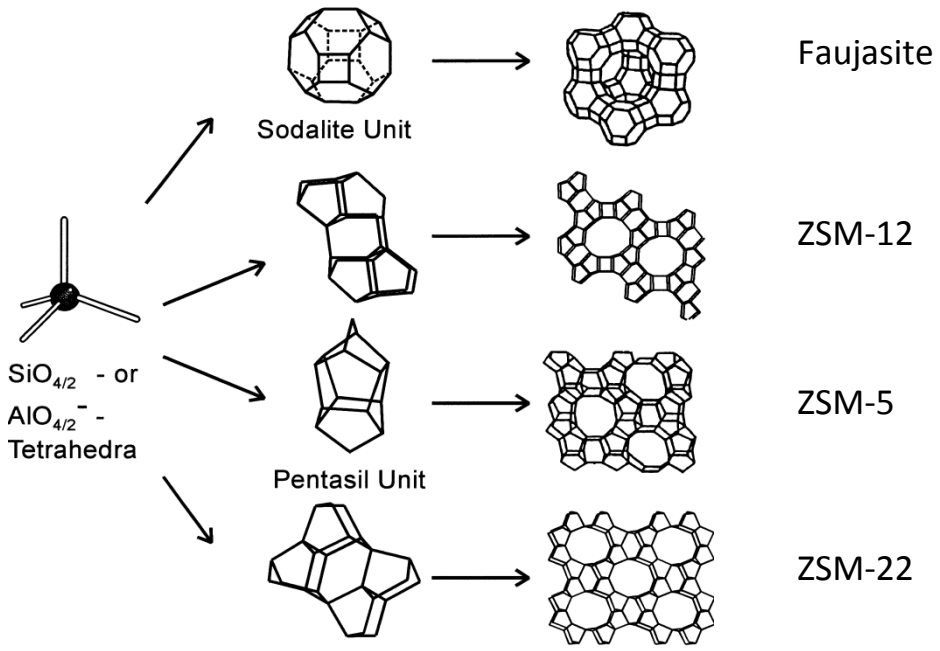


Figure 2.5 - Structure of four zeolites, showing ,left to right; tetrahedral TO4 units, unit cell structure, and overall structure[196].

The ability to introduce foreign metal ions allows use of zeolites as heterogeneous Fenton or photo-Fenton catalysts through the introduction of ionic Fe species. Studies have used various zeolites, such as MFI[16], BEA [199] and zeolite Y[21], to produce heterogeneous photo-Fenton catalysts, with the efficiency of zeolite based catalysts found to exceed that of homogeneous photo-Fenton catalysis[200]. Additionally it has been found that transition metal ions (Fe, Cu, etc) are bound to the exchange sites within the pore structure and are not likely to leach or precipitate out [194]. The field of metal deposition is also well developed for zeolites with commonly used techniques including; aqueous ion exchange, solid state ion exchange, and chemical vapour deposition [201, 202]. Therefore, the introduction of Fe to zeolites presents an attractive alternative to homogenous Fenton/photo-Fenton catalysis, as it combines the numerous benefits of heterogeneous photo-Fenton catalysis with the excellent adsorption and stability of zeolites. Bimetallic catalyst systems, such as Fe-Cu/MCM-41 [22] and Fe-Cu/Bentonite [19] that have been developed to effectively degrade organic pollutants at acidic and near neutral pH also suggest that similar bimetallic zeolite based systems have the potential to enhance the effective pH range of zeolite photo-Fenton catalysts.

## 2.5 Comparison of dye oxidation study conditions

The combined topics of dye degradation, AOPs, Fenton chemistry, and microporous supports for such catalysts represents a massive body of work. Several relatively comprehensive literature reviews exist among these fields, such as Soon et al (2010) [203] and Pouran et al (2015) [51]. The following table of dye oxidation conditions (Table 2.3) is not close to being as comprehensive as either of those two reviews, or many others, however for the comparison between catalysts there is a wide array of catalyst testing conditions, including; temperature, catalyst dosage, pH, irradiation type and intensity, dye concentration, and even dye type which often go unmentioned. Dye type is especially significant because different dyes have different characteristic chromophoric structures, and will therefore be degraded via different oxidative pathways, and possibly requiring different oxidation demands to achieve the same reduction in colour intensity. As dyes have a variety of molecular masses, the colour intensity per mass will also change. The carbon content of dyes can also vary, which makes it difficult to quickly compare the TOC removal using only the dye concentration (either mol $L^{-1}$ or g $L^{-1}$: which is usually all that is given). Therefore, summarised findings on prior studies on dye oxidation reported with standard measures, with a focus on Fenton reactions, zeolites and MOFs are presented below in Table 2.3. A more extensive comparison of conditions, such as carbon to catalyst ratio, and dye to hydrogen peroxide ratio is included in Appendix 2.

Table 2.3 - Comparison of dye oxidation conditions

| Author | | Irradiation | Catalyst | Catalyst Conc. [g $L^{-1}$] | Dye | Dye Conc. [mg $L^{-1}$] | Carbon Conc. [mg $L^{-1}$] | Colour Removal | TOC Removal |
|---|---|---|---|---|---|---|---|---|---|
| Du | [64] | UV | MIL-53 | 10 | MB | 32 | 19 | 99% / 20 min | - |
| Dükkancı | [204, 205] | | CuFe-ZSM-5 | 1000 | Rhodamine 6G | 100 | 70 | 100% / 45 min | 51.8% / 2h |
| Flores | [206] | | Fe-fly ash | 11300 | Reactive Black 5 | 60 | 19 | 100% / 2h | 80% / 2h [COD] |
| Hassan | [21] | | Fe-Y | 2500 | Acid Red 1 | 50 | 21 | 99% / 60 min | - |
| Height | [207] | UV | AgZnO | 300 | MB | 10 | 6 | 57% / 60 min | - |
| Houas | [18] | UV | P25 $TiO_2$ | 2500 | MB | 23 | 14 | 99% / 60 min | 80% / 6h |
| Jian-xiao | [65] | UV | UV/$H_2O_2$ | 0 | MB | 30 | 18 | 80% /160 min | - |
| Jing | [208] | UV | ZIF-8 | 50 | MB | 10 | 6 | 82.3% / 2h | 70% / 60 min |
| Kasiri | [209] | UV | Fe-ZSM-5 | 250 | Acid Red 14 | 40 | 19 | 90% / 30 min | 76% / 2h |
| Kasiri | [16] | UV | Fe-ZSM-5 | 500 | Acid Blue 74 | 46 | 21 | 99% / 10 min | 57.14% / 2h |
| Kondru | [210] | | Fe-Y | 1000 | Congo Red | 0 | 0 | 100% 4h | 69% / 4h |
| Kozlova | [211] | UV | MIL-47 | 50 | MB | *Not given | * | - | - |
| Lam | [112] | UV | FeCu/MCM-41 | 1000 | Orange II | 105 | 58 | - | 92% / 2h |
| Liang | [212] | Visible | MIL-53 | 1000 | Rhodamine B | 20 | 14 | 45.2% / 40 min | 22.3% / 40 min |
| Neamtu | [213] | | Fe-Y | 1000 | Procion Marine | 100 | 37 | 99% / 60 min | 40% / 60 min |
| Neamtu | [213] | | $Fe^{3+}$ (as iron nitrate) | 17 | Procion Marine | 100 | 37 | 80% / 60 min | - |
| Ramirez | [214] | | Fe/C | 300 | Orange II | 35 | 19 | 100% /4h | 90% / 4h |
| Singh | [215] | | Cu-Y | 1000 | Congo Red | 100 | 55 | 95.34% / 2h | 79.52% /4h |
| Xiao | [216] | Visible | $Co_3O4/Bi_2WO_6$ | 1000 | MB | 10 | 6 | 100% / 80 min | - |
| Yaman | [217] | | Fe-ZSM-5 | 1000 | CI Reactive Red | 100 | 35 | 97% / 2h | 52% / 2h |
| Zhou | [218] | Visible | Co-$BiVO_4$ | 1000 | MB | 10 | 6 | 85% / 330 min | - |

## 2.6 References


1. Caselli, G., J. Vallin, and G. Wunsch, *Demography: Analysis and Synthesis, Four Volume Set: A Treatise in Population*. 2005: Academic press.
2. Kundzewicz, Z.W., et al., *The implications of projected climate change for freshwater resources and their management.* Hydrological Sciences Journal, 2008. **53**(1): p. 3-10.
3. Schewe, J., et al., *Multimodel assessment of water scarcity under climate change.* Proceedings of the National Academy of Sciences, 2014. **111**(9): p. 3245-3250.
4. Kendy, E., et al., *Groundwater recharge from irrigated cropland in the North China Plain: case study of Luancheng County, Hebei Province, 1949–2000.* Hydrological Processes, 2004. **18**(12): p. 2289-2302.
5. Xiong, W., et al. *The Bimetallic Synergistic Effect in Heterogeneous UV/Fenton System for the Treatment of Refractory 6-Nitryl Wastewater*. in *Advanced Materials Research*. 2014. Trans Tech Publ.
6. Geng, Y., et al., *Spatial-temporal patterns and driving factors for industrial wastewater emission in China.* Journal of Cleaner Production, 2014. **76**: p. 116-124.
7. Kanagaraj, J., et al., *Eco-friendly waste management strategies for greener environment towards sustainable development in leather industry: a comprehensive review.* Journal of Cleaner Production, 2015. **89**: p. 1-17.
8. Council, C.C., *Trade Waste Bylaw 2015*. 2015, Christchurch City Council: New Zealand.
9. Oaks, J.L., et al., *Diclofenac residues as the cause of vulture population decline in Pakistan.* Nature, 2004. **427**(6975): p. 630-633.
10. Kolpin, D.W., et al., *Pharmaceuticals, hormones, and other organic wastewater contaminants in US streams, 1999− 2000: A national reconnaissance.* Environmental science & technology, 2002. **36**(6): p. 1202-1211.
11. Ternes, T.A., A. Joss, and H. Siegrist, *Peer reviewed: scrutinizing pharmaceuticals and personal care products in wastewater treatment*. 2004, ACS Publications.
12. Oyama, T., et al., *Remediation of aquatic environments contaminated with hydrophilic and lipophilic pharmaceuticals by TiO2-photoassisted ozonation.* Journal of Environmental Chemical Engineering, 2014. **2**(1): p. 84-89.
13. Pang, Y.L. and A.Z. Abdullah, *Current Status of Textile Industry Wastewater Management and Research Progress in Malaysia: A Review.* CLEAN – Soil, Air, Water, 2013. **41**(8): p. 751-764.
14. Textile, O., *The fibre year 2009/10: A world survey on textile and non-woven industry*. 2010.
15. Al-Qodah, Z., et al., *Adsorption of methylene blue by acid and heat treated diatomaceous silica.* Desalination, 2007. **217**(1–3): p. 212-224.
16. Kasiri, M.B., H. Aleboyeh, and A. Aleboyeh, *Degradation of Acid Blue 74 using Fe-ZSM5 zeolite as a heterogeneous photo-Fenton catalyst.* Applied Catalysis B: Environmental, 2008. **84**(1–2): p. 9-15.
17. El-Sharkawy, E.A., A.Y. Soliman, and K.M. Al-Amer, *Comparative study for the removal of methylene blue via adsorption and photocatalytic degradation.* Journal of Colloid and Interface Science, 2007. **310**(2): p. 498-508.
18. Houas, A., et al., *Photocatalytic degradation pathway of methylene blue in water.* Applied Catalysis B: Environmental, 2001. **31**(2): p. 145-157.
19. Sauer, T., et al., *Kinetics of photocatalytic degradation of reactive dyes in a TiO 2 slurry reactor.* Journal of Photochemistry and Photobiology A: Chemistry, 2002. **149**(1): p. 147-154.
20. Galindo, C., P. Jacques, and A. Kalt, *Photooxidation of the phenylazonaphthol AO20 on TiO 2: kinetic and mechanistic investigations.* Chemosphere, 2001. **45**(6): p. 997-1005.
21. Hassan, H. and B.H. Hameed, *Oxidative decolorization of Acid Red 1 solutions by Fe–zeolite Y type catalyst.* Desalination, 2011. **276**(1–3): p. 45-52.
22. Zollinger, H., *Color Chemistry, VCH.* Inc., New York, 1987: p. 25-41.
23. Haque, E., J.W. Jun, and S.H. Jhung, *Adsorptive removal of methyl orange and methylene blue from aqueous solution with a metal-organic framework material, iron terephthalate (MOF-235).* Journal of Hazardous Materials, 2011. **185**(1): p. 507-511.
24. Gupta, V.K., et al., *Removal of Rhodamine B, Fast Green, and Methylene Blue from Wastewater Using Red Mud, an Aluminum Industry Waste.* Industrial & Engineering Chemistry Research, 2004. **43**(7): p. 1740-1747.
25. Schirmer, R.H., et al., *Lest we forget you—methylene blue….* Neurobiology of aging, 2011. **32**(12): p. 2325. e7-2325. e16.
26. Salem, I.A. and M.S. El-Maazawi, *Kinetics and mechanism of color removal of methylene blue with hydrogen peroxide catalyzed by some supported alumina surfaces.* Chemosphere, 2000. **41**(8): p. 1173-1180.
27. Ghosh, D. and K.G. Bhattacharyya, *Adsorption of methylene blue on kaolinite.* Applied Clay Science, 2002. **20**(6): p. 295-300.

28. Wu, C.-H. and J.-M. Chern, *Kinetics of Photocatalytic Decomposition of Methylene Blue.* Industrial & Engineering Chemistry Research, 2006. **45**(19): p. 6450-6457.
29. Wang, Q., et al., *Use of Fe(II)Fe(III)-LDHs prepared by co-precipitation method in a heterogeneous-Fenton process for degradation of Methylene Blue.* Catalysis Today, 2014. **224**: p. 41-48.
30. Macedo, J.d.S., et al., *Kinetic and calorimetric study of the adsorption of dyes on mesoporous activated carbon prepared from coconut coir dust.* Journal of Colloid and Interface Science, 2006. **298**(2): p. 515-522.
31. Cenens, J. and R. Schoonheydt, *Visible spectroscopy of methylene blue on hectorite, laponite B, and barasym in aqueous suspension.* Clays and Clay Minerals, 1988. **36**(3): p. 214-224.
32. Fornili, S.L., G. Sgroi, and V. Izzo, *Solvent isotope effect in the monomer–dimer equilibrium of methylene blue.* Journal of the Chemical Society, Faraday Transactions 1: Physical Chemistry in Condensed Phases, 1981. **77**(12): p. 3049-3053.
33. Yu, Z. and S.S.C. Chuang, *The effect of Pt on the photocatalytic degradation pathway of methylene blue over TiO2 under ambient conditions.* Applied Catalysis B: Environmental, 2008. **83**(3–4): p. 277-285.
34. IARC, *IARC monographs on the evaluation of carcinogenic risks to human: Methylene Blue.* IARC Monographs, 2012. **108-06**.
35. Tan, I.A.W., B.H. Hameed, and A.L. Ahmad, *Equilibrium and kinetic studies on basic dye adsorption by oil palm fibre activated carbon.* Chemical Engineering Journal, 2007. **127**(1–3): p. 111-119.
36. Albert, M., M.S. Lessin, and B.F. Gilchrist, *Methylene blue: dangerous dye for neonates.* Journal of Pediatric Surgery, 2003. **38**(8): p. 1244-1245.
37. Tang, X., et al., *Formaldehyde in China: Production, consumption, exposure levels, and health effects.* Environment International, 2009. **35**(8): p. 1210-1224.
38. Kajitvichyanukul, P., M.-C. Lu, and A. Jamroensan, *Formaldehyde degradation in the presence of methanol by photo-Fenton process.* Journal of Environmental Management, 2008. **86**(3): p. 545-553.
39. IARC, *IARC monographs on the evaluation of carcinogenic risks to human: Formaldehyde.* IARC Monographs, 2012. **100F-29**.
40. Grafstrom, R.C., et al., *Genotoxicity of formaldehyde in cultured human bronchial fibroblasts.* Science, 1985. **228**(4695): p. 89-91.
41. Salman, M., et al., *Removal of formaldehyde from aqueous solution by adsorption on kaolin and bentonite: a comparative study.* Turkish Journal of Engineering and Environmental Sciences, 2012. **36**(3): p. 263-270.
42. Boonamnuayvitaya, V., S. Sae-ung, and W. Tanthapanichakoon, *Preparation of activated carbons from coffee residue for the adsorption of formaldehyde.* Separation and Purification Technology, 2005. **42**(2): p. 159-168.
43. Guimarães, J.R., et al., *Degradation of formaldehyde by advanced oxidation processes.* Journal of Environmental Management, 2012. **107**: p. 96-101.
44. Ghaly, M.Y., et al., *Photochemical oxidation of¡ i¿ p¡/i¿-chlorophenol by UV/H¡ sub¿ 2¡/sub¿ O¡ sub¿ 2¡/sub¿ and photo-Fenton process. A comparative study.* Waste Management, 2001. **21**(1): p. 41-47.
45. Kajitvichyanukul, P. and N. Suntronvipart, *Evaluation of biodegradability and oxidation degree of hospital wastewater using photo-Fenton process as the pretreatment method.* Journal of Hazardous Materials, 2006. **138**(2): p. 384-391.
46. Liou, M.-J., M.-C. Lu, and J.-N. Chen, *Oxidation of explosives by Fenton and photo-Fenton processes.* Water research, 2003. **37**(13): p. 3172-3179.
47. Tang, X., et al., *MnOx–CeO2 mixed oxide catalysts for complete oxidation of formaldehyde: Effect of preparation method and calcination temperature.* Applied Catalysis B: Environmental, 2006. **62**(3): p. 265-273.
48. Zhang, Y., et al., *Preparation of titania-based catalysts for formaldehyde photocatalytic oxidation from TiCl¡ sub¿ 4¡/sub¿ by the sol–gel method.* Catalysis Today, 2001. **68**(1): p. 89-95.
49. Umar, M., H.A. Aziz, and M.S. Yusoff, *Trends in the use of Fenton, electro-Fenton and photo-Fenton for the treatment of landfill leachate.* Waste Management, 2010. **30**(11): p. 2113-2121.
50. Dubber, D. and N.F. Gray, *Replacement of chemical oxygen demand (COD) with total organic carbon (TOC) for monitoring wastewater treatment performance to minimize disposal of toxic analytical waste.* Journal of Environmental Science and Health, Part A, 2010. **45**(12): p. 1595-1600.
51. Rahim Pouran, S., A.R. Abdul Aziz, and W.M.A. Wan Daud, *Review on the main advances in photo-Fenton oxidation system for recalcitrant wastewaters.* Journal of Industrial and Engineering Chemistry, 2015. **21**: p. 53-69.
52. Harrelkas, F., et al., *Photocatalytic and combined anaerobic–photocatalytic treatment of textile dyes.* Chemosphere, 2008. **72**(11): p. 1816-1822.

53. Baldrian, P., et al., *Decolorization of synthetic dyes by hydrogen peroxide with heterogeneous catalysis by mixed iron oxides.* Applied Catalysis B: Environmental, 2006. **66**(3–4): p. 258-264.
54. Yamazaki, T., W. Tsugawa, and K. Sode, *Biodegradation of formaldehyde by a formaldehyde-resistant bacterium isolated from seawater.* Applied Biochemistry and Biotechnology, 2001. **91**(1): p. 213.
55. Yoshida, K., et al., *Bioremediation Potential of Formaldehyde by the Marine Microalga Nannochloropsis oculata ST-3 Strain.* Applied Biochemistry and Biotechnology, 2009. **157**(2): p. 321-328.
56. El-Sersy, N.A., *Bioremediation of methylene blue by Bacillus thuringiensis 4 G 1: application of statistical designs and surface plots for optimization.* Biotechnology, 2007. **6**(1): p. 34-39.
57. Rafatullah, M., et al., *Adsorption of methylene blue on low-cost adsorbents: A review.* Journal of Hazardous Materials, 2010. **177**(1–3): p. 70-80.
58. El-Latif, M.M.A., A.M. Ibrahim, and M. El-Kady, *Adsorption Equilibrium, kinetics and thermodynamics of methylene blue from aqueous solutions using biopolymer oak sawdust composite.* Journal of American science, 2010. **6**(6).
59. Sohrabnezhad, S. and A. Pourahmad, *New Methylene Blue (NMB) Encapsulated in Mesoporous AlMCM-41 Material and Its Application for Amperometric Determination of Ascorbic Acid in Real Samples.* Electroanalysis, 2007. **19**(15): p. 1635-1641.
60. Halls, J.E., et al., *Redox Reactivity of Methylene Blue Bound in Pores of UMCM-1 Metal-Organic Frameworks.* Molecular Crystals and Liquid Crystals, 2012. **554**(1): p. 12-21.
61. Khandegar, V. and A.K. Saroha, *Electrocoagulation for the treatment of textile industry effluent – A review.* Journal of Environmental Management, 2013. **128**: p. 949-963.
62. Karcher, S., A. Kornmüller, and M. Jekel, *Anion exchange resins for removal of reactive dyes from textile wastewaters.* Water Research, 2002. **36**(19): p. 4717-4724.
63. Yang, S., et al., *Decolorization of methylene blue by heterogeneous Fenton reaction using Fe3−xTixO4 (0 ≤ x ≤ 0.78) at neutral pH values.* Applied Catalysis B: Environmental, 2009. **89**(3–4): p. 527-535.
64. Du, J.J., et al., *New photocatalysts based on MIL-53 metal-organic frameworks for the decolorization of methylene blue dye.* J Hazard Mater, 2011. **190**(1-3): p. 945-51.
65. Jian-xiao, L., et al., *Decoloration of methylene blue simulated wastewater using a UV-$H_2O_2$ combined system.* Journal of Water Reuse and Desalination, 2011. **1**(1): p. 45-51.
66. Mahata, P., G. Madras, and S. Natarajan, *Novel Photocatalysts for the Decomposition of Organic Dyes Based on Metal-Organic Framework Compounds.* The Journal of Physical Chemistry B, 2006. **110**(28): p. 13759-13768.
67. Arslan-Alaton, I., G. Tureli, and T. Olmez-Hanci, *Treatment of azo dye production wastewaters using Photo-Fenton-like advanced oxidation processes: Optimization by response surface methodology.* Journal of Photochemistry and Photobiology A: Chemistry, 2009. **202**(2–3): p. 142-153.
68. Carneiro, P.A., R.F.P. Nogueira, and M.V.B. Zanoni, *Homogeneous photodegradation of C.I. Reactive Blue 4 using a photo-Fenton process under artificial and solar irradiation.* Dyes and Pigments, 2007. **74**(1): p. 127-132.
69. Gemeay, A.H., et al., *Kinetics and mechanism of the heterogeneous catalyzed oxidative degradation of indigo carmine.* Journal of Molecular Catalysis A: Chemical, 2003. **193**(1–2): p. 109-120.
70. Munter, R., *Advanced oxidation processes–current status and prospects.* Proc. Estonian Acad. Sci. Chem, 2001. **50**(2): p. 59-80.
71. Glaze, W.H., J.-W. Kang, and D.H. Chapin, *The chemistry of water treatment processes involving ozone, hydrogen peroxide and ultraviolet radiation.* 1987.
72. Babuponnusami, A. and K. Muthukumar, *A review on Fenton and improvements to the Fenton process for wastewater treatment.* Journal of Environmental Chemical Engineering, 2014. **2**(1): p. 557-572.
73. Ayoub, K., et al., *Application of advanced oxidation processes for TNT removal: A review.* Journal of Hazardous Materials, 2010. **178**(1–3): p. 10-28.
74. Weast, R.C., M.J. Astle, and W.H. Beyer, *CRC handbook of chemistry and physics*. Vol. 69. 1988: CRC press Boca Raton, FL.
75. Pera-Titus, M., et al., *Degradation of chlorophenols by means of advanced oxidation processes: a general review.* Applied Catalysis B: Environmental, 2004. **47**(4): p. 219-256.
76. Liu, X., J. Liang, and X. Wang, *Kinetics and Reaction Pathways of Formaldehyde Degradation Using the UV-Fenton Method.* Water Environment Research, 2011. **83**(5): p. 418-426.
77. Brillas, E., et al., *Aniline mineralization by AOP's: anodic oxidation, photocatalysis, electro-Fenton and photoelectro-Fenton processes.* Applied Catalysis B: Environmental, 1998. **16**(1): p. 31-42.

78. Akpan, U.G. and B.H. Hameed, *Parameters affecting the photocatalytic degradation of dyes using TiO2-based photocatalysts: A review.* Journal of Hazardous Materials, 2009. **170**(2–3): p. 520-529.
79. Aleksić, M., et al., *Heterogeneous Fenton type processes for the degradation of organic dye pollutant in water — The application of zeolite assisted AOPs.* Desalination, 2010. **257**(1–3): p. 22-29.
80. Meijers, R., et al., *Degradation of pesticides by ozonation and advanced oxidation.* Ozone: science & engineering, 1995. **17**(6): p. 673-686.
81. Bunthid, D., P. Prasassarakich, and N. Hinchiranan, *Oxidative desulfurization of tire pyrolysis naphtha in formic acid/H2O2/pyrolysis char system.* Fuel, 2010. **89**(9): p. 2617-2622.
82. Campos-Martin, J.M., M.C. Capel-Sanchez, and J.L.G. Fierro, *Highly efficient deep desulfurization of fuels by chemical oxidation.* Green Chemistry, 2004. **6**(11): p. 557-562.
83. Campos-Martin, J.M., et al., *Oxidative processes of desulfurization of liquid fuels.* Journal of Chemical Technology & Biotechnology, 2010. **85**(7): p. 879-890.
84. Baxendale, J. and J. Wilson, *The photolysis of hydrogen peroxide at high light intensities.* Transactions of the Faraday Society, 1957. **53**: p. 344-356.
85. Lam, F.L.Y., A.C.K. Yip, and X. Hu, *Copper/MCM-41 as a Highly Stable and pH-insensitive Heterogeneous Photo-Fenton-like Catalytic Material for the Abatement of Organic Wastewater.* Industrial & Engineering Chemistry Research, 2007. **46**(10): p. 3328-3333.
86. Fenton, H., *On a new reaction of tartaric acid.* Chem News, 1876. **33**(190): p. 190.
87. Murale, D.P., et al., *Fluorescence probing of the ferric Fenton reaction via novel chelation.* Chemical Communications, 2014. **50**(3): p. 359-361.
88. Rigg, T., W. Taylor, and J. Weiss, *The rate constant of the reaction between hydrogen peroxide and ferrous ions.* The journal of chemical physics, 1954. **22**(4): p. 575-577.
89. Walling, C. and A. Goosen, *Mechanism of the ferric ion catalyzed decomposition of hydrogen peroxide. Effect of organic substrates.* Journal of the American Chemical Society, 1973. **95**(9): p. 2987-2991.
90. Huston, P.L. and J.J. Pignatello, *Degradation of selected pesticide active ingredients and commercial formulations in water by the photo-assisted Fenton reaction.* Water Research, 1999. **33**(5): p. 1238-1246.
91. Malato, S., et al., *Photocatalytic treatment of water-soluble pesticides by photo-Fenton and TiO2 using solar energy.* Catalysis Today, 2002. **76**(2–4): p. 209-220.
92. Rodríguez-Gil, J.L., et al., *Heterogeneous photo-Fenton treatment for the reduction of pharmaceutical contamination in Madrid rivers and ecotoxicological evaluation by a miniaturized fern spores bioassay.* Chemosphere, 2010. **80**(4): p. 381-388.
93. Sum, O.S.N., et al., *Photo-assisted fenton mineralization of an azo-dye acid black 1 using a modified laponite clay-based Fe nanocomposite as a heterogeneous catalyst.* Topics in Catalysis, 2005. **33**(1-4): p. 233-242.
94. Chen, J. and L. Zhu, *Heterogeneous UV-Fenton catalytic degradation of dyestuff in water with hydroxyl-Fe pillared bentonite.* Catalysis Today, 2007. **126**(3–4): p. 463-470.
95. Yip, A.C.-K., F. Leung-Yuk Lam, and X. Hu, *Novel bimetallic catalyst for the photo-assisted degradation of Acid Black 1 over a broad range of pH.* Chemical Engineering Science, 2007. **62**(18): p. 5150-5153.
96. Lam, F.L.Y. and X. Hu, *In situ oxidation for stabilization of Fe/MCM-41 catalyst prepared by metal organic chemical vapor deposition.* Catalysis Communications, 2007. **8**(11): p. 1719-1723.
97. Lam, F.L. and X. Hu, *A high performance bimetallic catalyst for photo-Fenton oxidation of Orange II over a wide pH range.* Catalysis Communications, 2007. **8**(12): p. 2125-2129.
98. Yip, A.C.-K., F.L.-Y. Lam, and X. Hu, *A novel heterogeneous acid-activated clay supported copper catalyst for the photobleaching and degradation of textile organic pollutant using photo-Fenton-like reaction.* Chemical communications, 2005(25): p. 3218-3220.
99. Feng, J., X. Hu, and P.L. Yue, *Effect of initial solution pH on the degradation of Orange II using clay-based Fe nanocomposites as heterogeneous photo-Fenton catalyst.* Water Research, 2006. **40**(4): p. 641-646.
100. Pignatello, J.J., E. Oliveros, and A. MacKay, *Advanced Oxidation Processes for Organic Contaminant Destruction Based on the Fenton Reaction and Related Chemistry.* Critical Reviews in Environmental Science and Technology, 2006. **36**(1): p. 1-84.
101. Walling, C., *Intermediates in the Reactions of Fenton Type Reagents.* Accounts of Chemical Research, 1998. **31**(4): p. 155-157.
102. Kitis, M., C.D. Adams, and G.T. Daigger, *The effects of Fenton's reagent pretreatment on the biodegradability of nonionic surfactants.* Water Research, 1999. **33**(11): p. 2561-2568.
103. Yoon, J., *Investigation of the reaction pathway of OH radicals produced by Fenton oxidation in the conditions of wastewater treatment.* Water science and technology, 2001. **44**(5): p. 15.
104. Lu, M., et al., *Influence of pH on the dewatering of activated sludge by Fenton's reagent.* Water Science & Technology, 2001. **44**(10): p. 327-332.
105. Trovó, A.G., S.A.S. Melo, and R.F.P. Nogueira, *Photodegradation of the pharmaceuticals amoxicillin, bezafibrate and paracetamol by the photo-Fenton process—Application to sewage*

*treatment plant effluent.* Journal of Photochemistry and Photobiology A: Chemistry, 2008. **198**(2–3): p. 215-220.
106. Micó, M.M., et al., *Enhancement of pesticide photo-Fenton oxidation at high salinities.* Applied Catalysis B: Environmental, 2013. **132–133**(0): p. 162-169.
107. Lam, F.L., A.C. Yip, and X. Hu, *Copper/MCM-41 as a highly stable and pH-insensitive heterogeneous photo-Fenton-like catalytic material for the abatement of organic wastewater.* Industrial & engineering chemistry research, 2007. **46**(10): p. 3328-3333.
108. Gogate, P.R. and A.B. Pandit, *A review of imperative technologies for wastewater treatment II: hybrid methods.* Advances in Environmental Research, 2004. **8**(3): p. 553-597.
109. Masarwa, M., et al., *Reactions of low-valent transition-metal complexes with hydrogen peroxide. Are they" Fenton-like" or not? 1. The case of Cu+ aq and Cr2+ aq.* Journal of the American Chemical Society, 1988. **110**(13): p. 4293-4297.
110. Wu, Q., et al., *Copper/MCM-41 as catalyst for the wet oxidation of phenol.* Applied Catalysis B: Environmental, 2001. **32**(3): p. 151-156.
111. Wang, Y., H. Zhao, and G. Zhao, *Iron-copper bimetallic nanoparticles embedded within ordered mesoporous carbon as effective and stable heterogeneous Fenton catalyst for the degradation of organic contaminants.* Applied Catalysis B: Environmental, 2015. **164**(0): p. 396-406.
112. Lam, F.L.Y. and X. Hu, *pH-Insensitive Bimetallic Catalyst for the Abatement of Dye Pollutants by Photo-Fenton Oxidation.* Industrial & Engineering Chemistry Research, 2013. **52**(20): p. 6639-6646.
113. Yip, A.C.-K., F.L.-Y. Lam, and X. Hu, *Chemical-vapor-deposited copper on acid-activated bentonite clay as an applicable heterogeneous catalyst for the photo-Fenton-like oxidation of textile organic pollutants.* Industrial & engineering chemistry research, 2005. **44**(21): p. 7983-7990.
114. Xia, M., et al., *A highly active bimetallic oxides catalyst supported on Al-containing MCM-41 for Fenton oxidation of phenol solution.* Applied Catalysis B: Environmental, 2011. **110**: p. 118-125.
115. Danish, M., et al., *Efficient transformation of trichloroethylene activated through sodium percarbonate using heterogeneous zeolite supported nano zero valent iron-copper bimetallic composite.* Chemical Engineering Journal, 2017. **308**: p. 396-407.
116. Rzepka, M., P. Lamp, and M. De la Casa-Lillo, *Physisorption of hydrogen on microporous carbon and carbon nanotubes.* The Journal of Physical Chemistry B, 1998. **102**(52): p. 10894-10898.
117. TAKAMORI, T., *Structural anisotropy and birefringence in microporous glasses.* Journal of the American Ceramic Society, 1978. **61**(9-10): p. 434-438.
118. Cooper, A.I., *Conjugated microporous polymers.* Advanced Materials, 2009. **21**(12): p. 1291-1295.
119. Lok, B.M., et al., *Silicoaluminophosphate molecular sieves: another new class of microporous crystalline inorganic solids.* Journal of the American Chemical Society, 1984. **106**(20): p. 6092-6093.
120. Axe, L. and P. Trivedi, *Intraparticle surface diffusion of metal contaminants and their attenuation in microporous amorphous Al, Fe, and Mn oxides.* Journal of colloid and interface science, 2002. **247**(2): p. 259-265.
121. Dong, J., et al., *Hydrogen storage in several microporous zeolites.* International Journal of Hydrogen Energy, 2007. **32**(18): p. 4998-5004.
122. Yaghi, O.M., G. Li, and H. Li, *Selective binding and removal of guests in a microporous metal-organic framework.* Nature, 1995. **378**(6558): p. 703-706.
123. Budd, P.M., et al., *Gas separation membranes from polymers of intrinsic microporosity.* Journal of Membrane Science, 2005. **251**(1): p. 263-269.
124. Groitzsch, D. and E. Fahrbach, *Microporous multilayer nonwoven material for medical applications*. 1986, Google Patents.
125. Akolekar, D., A. Hind, and S. Bhargava, *Synthesis of macro-, meso-, and microporous carbons from natural and synthetic sources, and their application as adsorbents for the removal of quaternary ammonium compounds from aqueous solution.* Journal of colloid and interface science, 1998. **199**(1): p. 92-98.
126. Sie, S., *Past, present and future role of microporous catalysts in the petroleum industry.* Studies in Surface Science and Catalysis, 1994. **85**: p. 587-631.
127. Garforth, A., et al., *Catalytic degradation of high density polyethylene: an evaluation of mesoporous and microporous catalysts using thermal analysis.* Thermochimica acta, 1997. **294**(1): p. 65-69.
128. Perez-Ramirez, J., et al., *Hierarchical zeolites: enhanced utilisation of microporous crystals in catalysis by advances in materials design.* Chemical Society Reviews, 2008. **37**(11): p. 2530-2542.
129. Navalon, S., M. Alvaro, and H. Garcia, *Heterogeneous Fenton catalysts based on clays, silicas and zeolites.* Applied Catalysis B: Environmental, 2010. **99**(1–2): p. 1-26.

130. Farrusseng, D., S. Aguado, and C. Pinel, *Metal–Organic Frameworks: Opportunities for Catalysis.* Angewandte Chemie International Edition, 2009. **48**(41): p. 7502-7513.
131. Rache, M.L., et al., *Azo-dye orange II degradation by the heterogeneous Fenton-like process using a zeolite Y-Fe catalyst—Kinetics with a model based on the Fermi's equation.* Applied Catalysis B: Environmental, 2014. **146**(0): p. 192-200.
132. Jiang, H.-L. and Q. Xu, *Porous metal-organic frameworks as platforms for functional applications.* Chemical Communications, 2011. **47**(12): p. 3351-3370.
133. Dhakshinamoorthy, A., et al., *Delineating similarities and dissimilarities in the use of metal organic frameworks and zeolites as heterogeneous catalysts for organic reactions.* Dalton Transactions, 2011. **40**(24): p. 6344-6360.
134. Zhou, H.-C., J.R. Long, and O.M. Yaghi, *Introduction to Metal–Organic Frameworks.* Chemical Reviews, 2012. **112**(2): p. 673-674.
135. Férey, G., et al., *Crystallized Frameworks with Giant Pores: Are There Limits to the Possible?* Accounts of Chemical Research, 2005. **38**(4): p. 217-225.
136. Turner, S., et al., *Direct Imaging of Loaded Metal−Organic Framework Materials (Metal@MOF-5).* Chemistry of Materials, 2008. **20**(17): p. 5622-5627.
137. Yilmaz, B., N. Trukhan, and U. MÜLler, *Industrial Outlook on Zeolites and Metal Organic Frameworks.* Chinese Journal of Catalysis, 2012. **33**(1): p. 3-10.
138. Li, H., et al., *Design and synthesis of an exceptionally stable and highly porous metal-organic framework.* 1999.
139. Zhang, L. and Y.H. Hu, *A Systematic Investigation of Decomposition of Nano Zn4O(C8H4O4)3 Metal−Organic Framework.* The Journal of Physical Chemistry C, 2010. **114**(6): p. 2566-2572.
140. Greathouse, J.A. and M.D. Allendorf, *The Interaction of Water with MOF-5 Simulated by Molecular Dynamics.* Journal of the American Chemical Society, 2006. **128**(33): p. 10678-10679.
141. Jiang, H.-L., et al., *An Exceptionally Stable, Porphyrinic Zr Metal−Organic Framework Exhibiting pH-Dependent Fluorescence.* Journal of the American Chemical Society, 2013. **135**(37): p. 13934-13938.
142. Loiseau, T., et al., *A rationale for the large breathing of the porous aluminum terephthalate (MIL-53) upon hydration.* Chemistry--A European Journal, 2004. **10**(6): p. 1373-82.
143. Yot, P.G., et al., *Large breathing of the MOF MIL-47(VIV) under mechanical pressure: a joint experimental-modelling exploration.* Chemical Science, 2012. **3**(4): p. 1100-1104.
144. Maes, M., et al., *Enthalpic effects in the adsorption of alkylaromatics on the metal-organic frameworks MIL-47 and MIL-53.* Microporous and Mesoporous Materials, 2011(0).
145. Khan, N.A., et al., *Remarkable adsorptive performance of a metal-organic framework, vanadium-benzenedicarboxylate (MIL-47), for benzothiophene.* Chemical Communications (Cambridge, United Kingdom), 2011. **47**(4): p. 1306-1308.
146. Khan, N.A. and S.H. Jhung, *Remarkable Adsorption Capacity of CuCl2-Loaded Porous Vanadium Benzenedicarboxylate for Benzothiophene.* Angewandte Chemie, International Edition, 2012. **51**(5): p. 1198-1201.
147. Leus, K., et al., *The coordinatively saturated vanadium MIL-47 as a low leaching heterogeneous catalyst in the oxidation of cyclohexene.* Journal of Catalysis, 2012. **285**(1): p. 196-207.
148. McNamara, N.D., et al., *Catalytic performance and stability of (V) MIL-47 and (Ti) MIL-125 in the oxidative desulfurization of heterocyclic aromatic sulfur compounds.* Journal of Catalysis, 2013. **305**(0): p. 217-226.
149. Lee, J., et al., *Metal-organic framework materials as catalysts.* Chemical Society Reviews, 2009. **38**(5): p. 1450-1459.
150. Czaja, A.U., N. Trukhan, and U. Muller, *Industrial applications of metal-organic frameworks.* Chemical Society Reviews, 2009. **38**(5): p. 1284-1293.
151. Dhakshinamoorthy, A. and H. Garcia, *Catalysis by metal nanoparticles embedded on metal-organic frameworks.* Chemical Society Reviews, 2012. **41**(15): p. 5262-5284.
152. Vermoortele, F., et al., *Tuning the catalytic performance of metal-organic frameworks in fine chemistry by active site engineering.* Journal of Materials Chemistry, 2012. **22**(20): p. 10313-10321.
153. Tanabe, K.K. and S.M. Cohen, *Engineering a Metal–Organic Framework Catalyst by Using Postsynthetic Modification.* Angewandte Chemie International Edition, 2009. **48**(40): p. 7424-7427.
154. Cohen, S.M., *Postsynthetic Methods for the Functionalization of Metal–Organic Frameworks.* Chemical Reviews, 2011. **112**(2): p. 970-1000.
155. Meilikhov, M., et al., *Metals@MOFs – Loading MOFs with Metal Nanoparticles for Hybrid Functions.* European Journal of Inorganic Chemistry, 2010. **2010**(24): p. 3701-3714.
156. Corma, A., H. Garci□a, and F.X. Llabre□s i Xamena, *Engineering Metal Organic Frameworks for Heterogeneous Catalysis.* Chemical Reviews, 2010. **110**(8): p. 4606-4655.

157. Llabrés i Xamena, F.X., A. Corma, and H. Garcia, *Applications for Metal−Organic Frameworks (MOFs) as Quantum Dot Semiconductors.* Journal of Physical Chemistry C, 2006. **111**(1): p. 80-85.
158. Silva, C.G., A. Corma, and H. Garcia, *Metal-organic frameworks as semiconductors.* Journal of Materials Chemistry, 2010. **20**(16): p. 3141-3156.
159. Gascon, J., et al., *Isoreticular MOFs as Efficient Photocatalysts with Tunable Band Gap: An Operando FTIR Study of the Photoinduced Oxidation of Propylene.* ChemSusChem, 2008. **1**(12): p. 981-983.
160. Tachikawa, T., et al., *Photoinduced Charge-Transfer Processes on MOF-5 Nanoparticles: Elucidating Differences between Metal-Organic Frameworks and Semiconductor Metal Oxides.* The Journal of Physical Chemistry C, 2008. **112**(36): p. 14090-14101.
161. Fu, Y., et al., *An Amine-Functionalized Titanium Metal−Organic Framework Photocatalyst with Visible-Light-Induced Activity for CO2 Reduction.* Angewandte Chemie, 2012. **124**(14): p. 3420-3423.
162. Evans, O.R. and W. Lin, *Crystal Engineering of NLO Materials Based on Metal−Organic Coordination Networks.* Accounts of Chemical Research, 2002. **35**(7): p. 511-522.
163. Phan, A., et al., *Synthesis, Structure, and Carbon Dioxide Capture Properties of Zeolitic Imidazolate Frameworks.* Accounts of Chemical Research, 2009. **43**(1): p. 58-67.
164. Li, K., et al., *Zeolitic Imidazolate Frameworks for Kinetic Separation of Propane and Propene.* Journal of the American Chemical Society, 2009. **131**(30): p. 10368-10369.
165. Hertäg, L., et al., *Diffusion of CH4 and H2 in ZIF-8.* Journal of Membrane Science, 2011. **377**(1–2): p. 36-41.
166. Pan, Y. and Z. Lai, *Sharp separation of C2/C3 hydrocarbon mixtures by zeolitic imidazolate framework-8 (ZIF-8) membranes synthesized in aqueous solutions.* Chemical Communications, 2011.
167. Liu, Y.-Y., et al., *New VIV-Based Metal−Organic Framework Having Framework Flexibility and High CO2 Adsorption Capacity.* Inorganic Chemistry, 2012. **52**(1): p. 113-120.
168. Achmann, S., et al., *Sulfur Removal from Low-Sulfur Gasoline and Diesel Fuel by Metal-Organic Frameworks.* Chemical Engineering & Technology, 2010. **33**(2): p. 275-280.
169. Blanco-Brieva, G., et al., *Effectiveness of metal–organic frameworks for removal of refractory organo-sulfur compound present in liquid fuels.* Fuel, 2011. **90**(1): p. 190-197.
170. Liu, B., et al., *Adsorption Equilibrium of Thiophenic Sulfur Compounds on the Cu-BTC Metal−Organic Framework.* Journal of Chemical & Engineering Data, 2012. **57**(4): p. 1326-1330.
171. Shi, F., M. Hammoud, and L.T. Thompson, *Selective adsorption of dibenzothiophene by functionalized metal organic framework sorbents.* Applied Catalysis B: Environmental, 2011. **103**(3–4): p. 261-265.
172. Mu, L., et al., *A novel method to improve the gas storage capacity of ZIF-8.* Journal of Materials Chemistry, 2012. **22**(24): p. 12246-12252.
173. Proch, S., et al., *Pt@MOF-177: Synthesis, Room-Temperature Hydrogen Storage and Oxidation Catalysis.* Chemistry--A European Journal, 2008. **14**(27): p. 8204-8212.
174. Hermes, S., et al., *Metal@MOF: Loading of Highly Porous Coordination Polymers Host Lattices by Metal Organic Chemical Vapor Deposition.* Angewandte Chemie, International Edition, 2005. **44**(38): p. 6237-6241.
175. Jiang, H.-L., et al., *Au@ZIF-8: CO Oxidation over Gold Nanoparticles Deposited to Metal−Organic Framework.* Journal of the American Chemical Society, 2009. **131**(32): p. 11302-11303.
176. Esken, D., et al., *Au@ZIFs: Stabilization and Encapsulation of Cavity-Size Matching Gold Clusters inside Functionalized Zeolite Imidazolate Frameworks, ZIFs.* Chemistry of Materials, 2010. **22**(23): p. 6393-6401.
177. Esken, D., et al., *GaN@ZIF-8: Selective Formation of Gallium Nitride Quantum Dots inside a Zinc Methylimidazolate Framework.* Journal of the American Chemical Society, 2011. **133**(41): p. 16370-16373.
178. Esken, D., et al., *ZnO@ZIF-8: stabilization of quantum confined ZnO nanoparticles by a zinc methylimidazolate framework and their surface structural characterization probed by CO2 adsorption.* Journal of Materials Chemistry, 2011. **21**(16): p. 5907-5915.
179. Sabo, M., et al., *Solution infiltration of palladium into MOF-5: synthesis, physisorption and catalytic properties.* Journal of Materials Chemistry, 2007. **17**(36): p. 3827-3832.
180. Leus, K., et al., *Ti-functionalized NH2-MIL-47: An effective and stable epoxidation catalyst.* Catalysis Today, (0).
181. Ishida, T., et al., *Deposition of Gold Clusters on Porous Coordination Polymers by Solid Grinding and Their Catalytic Activity in Aerobic Oxidation of Alcohols.* Chemistry – A European Journal, 2008. **14**(28): p. 8456-8460.
182. Meilikhov, M., et al., *Reduction of a Metal−Organic Framework by an Organometallic Complex: Magnetic Properties and Structure of the Inclusion Compound [(η5-*

*C5H5)2Co]0.5@MIL-47(V).* Angewandte Chemie International Edition, 2010. **49**(35): p. 6212-6215.
183. Schröder, F., et al., *Ruthenium Nanoparticles inside Porous [Zn4O(bdc)3] by Hydrogenolysis of Adsorbed [Ru(cod)(cot)]: A Solid-State Reference System for Surfactant-Stabilized Ruthenium Colloids.* Journal of the American Chemical Society, 2008. **130**(19): p. 6119-6130.
184. Isaeva, V. and L. Kustov, *The application of metal-organic frameworks in catalysis (Review).* Petroleum Chemistry, 2010. **50**(3): p. 167-180.
185. Seo, J.S., et al., *A homochiral metal-organic porous material for enantioselective separation and catalysis.* Nature, 2000. **404**(6781): p. 982-986.
186. Wenbin, L., *Homochiral porous metal-organic frameworks: Why and how?* Journal of Solid State Chemistry, 2005. **178**(8): p. 2486-2490.
187. Wu, C.-D., et al., *A Homochiral Porous Metal−Organic Framework for Highly Enantioselective Heterogeneous Asymmetric Catalysis.* Journal of the American Chemical Society, 2005. **127**(25): p. 8940-8941.
188. Jeong, K.S., et al., *Asymmetric catalytic reactions by NbO-type chiral metal-organic frameworks.* Chemical Science, 2011. **2**(5): p. 877-882.
189. Flanigen, E.M., *Zeolites and molecular sieves an historical perspective.* Studies in Surface Science and Catalysis, 1991. **58**: p. 13-34.
190. Cundy, C.S. and P.A. Cox, *The hydrothermal synthesis of zeolites: history and development from the earliest days to the present time.* Chemical Reviews, 2003. **103**(3): p. 663-702.
191. Rabo, J.A. and M.W. Schoonover, *Early discoveries in zeolite chemistry and catalysis at Union Carbide, and follow-up in industrial catalysis.* Applied Catalysis A: General, 2001. **222**(1): p. 261-275.
192. Corma, A., C. Martínez, and E. Doskocil, *Designing MFI-based catalysts with improved catalyst life for oligomerization to high-quality liquid fuels.* Journal of Catalysis, 2013. **300**: p. 183-196.
193. Starokon, E.V., et al., *Oxidation of methane to methanol on the surface of FeZSM-5 zeolite.* Journal of Catalysis, 2013. **300**: p. 47-54.
194. Neamţu, M., C. Catrinescu, and A. Kettrup, *Effect of dealumination of iron (III)—exchanged Y zeolites on oxidation of Reactive Yellow 84 azo dye in the presence of hydrogen peroxide.* Applied Catalysis B: Environmental, 2004. **51**(3): p. 149-157.
195. Hazari, N., et al., *Selective Homogeneous and Heterogeneous Catalytic Conversion of Methanol/Dimethyl Ether to Triptane.* Accounts of chemical research, 2012. **45**(4): p. 653-662.
196. Weitkamp, J., *Zeolites and catalysis.* Solid State Ionics, 2000. **131**(1–2): p. 175-188.
197. Haw, J.F., et al., *Physical organic chemistry of solid acids: Lessons from in situ NMR and theoretical chemistry.* Accounts of chemical research, 1996. **29**(6): p. 259-267.
198. Xu, Y. and C.H. Langford, *Photoactivity of titanium dioxide supported on MCM41, zeolite X, and zeolite Y.* The Journal of Physical Chemistry B, 1997. **101**(16): p. 3115-3121.
199. Gonzalez-Olmos, R., et al., *Fe-zeolites as heterogeneous catalysts in solar Fenton-like reactions at neutral pH.* Applied Catalysis B: Environmental, 2012. **125**: p. 51-58.
200. Noorjahan, M., et al., *Immobilized Fe(III)-HY: an efficient and stable photo-Fenton catalyst.* Applied Catalysis B: Environmental, 2005. **57**(4): p. 291-298.
201. Regalbuto, J.R., *Catalyst preparation: science and engineering*. 2007: CRC Press.
202. Battiston, A.A., et al., *Evolution of Fe species during the synthesis of over-exchanged Fe/ZSM5 obtained by chemical vapor deposition of FeCl3.* Journal of Catalysis, 2003. **213**(2): p. 251-271.
203. Soon, A.N. and B. Hameed, *Heterogeneous catalytic treatment of synthetic dyes in aqueous media using Fenton and photo-assisted Fenton process.* Desalination, 2011. **269**(1): p. 1-16.
204. Dükkancı, M., et al., *Heterogeneous Fenton-like degradation of Rhodamine 6G in water using CuFeZSM-5 zeolite catalyst prepared by hydrothermal synthesis.* Journal of Hazardous Materials, 2010. **181**(1–3): p. 343-350.
205. Dükkancı, M., et al., *Characterization and catalytic activity of CuFeZSM-5 catalysts for oxidative degradation of Rhodamine 6G in aqueous solutions.* Applied Catalysis B: Environmental, 2010. **95**(3–4): p. 270-278.
206. Flores, Y., R. Flores, and A.A. Gallegos, *Heterogeneous catalysis in the Fenton-type system reactive black 5/H2O2.* Journal of Molecular Catalysis A: Chemical, 2008. **281**(1–2): p. 184-191.
207. Height, M.J., et al., *Ag-ZnO catalysts for UV-photodegradation of methylene blue.* Applied Catalysis B: Environmental, 2006. **63**(3–4): p. 305-312.
208. Jing, H.-P., et al., *Photocatalytic degradation of methylene blue in ZIF-8.* RSC Advances, 2014. **4**(97): p. 54454-54462.
209. Kasiri, M.B., H. Aleboyeh, and A. Aleboyeh, *Mineralization of C.I. Acid Red 14 azo dye by UV/Fe-ZSM5/H2O2 process.* Environmental Technology, 2010. **31**(2): p. 165-173.

210. Kondru, A.K., P. Kumar, and S. Chand, *Catalytic wet peroxide oxidation of azo dye (Congo red) using modified Y zeolite as catalyst.* Journal of Hazardous Materials, 2009. **166**(1): p. 342-347.
211. Kozlova, E.A., et al., *Photoreactivity of metal-organic frameworks in the decolorization of methylene blue in aqueous solution.* Catalysis Today, 2016. **266**: p. 136-143.
212. Liang, R., et al., *MIL-53(Fe) as a highly efficient bifunctional photocatalyst for the simultaneous reduction of Cr(VI) and oxidation of dyes.* Journal of Hazardous Materials, 2015. **287**: p. 364-372.
213. Neamţu, M., et al., *Fe-exchanged Y zeolite as catalyst for wet peroxide oxidation of reactive azo dye Procion Marine H-EXL.* Applied Catalysis B: Environmental, 2004. **48**(4): p. 287-294.
214. Ramirez, J.H., et al., *Azo-dye Orange II degradation by heterogeneous Fenton-like reaction using carbon-Fe catalysts.* Applied Catalysis B: Environmental, 2007. **75**(3–4): p. 312-323.
215. Singh, L., P. Rekha, and S. Chand, *Cu-impregnated zeolite Y as highly active and stable heterogeneous Fenton-like catalyst for degradation of Congo red dye.* Separation and Purification Technology, 2016. **170**: p. 321-336.
216. Xiao, Q., et al., *Photocatalytic degradation of methylene blue over Co3O4/Bi2WO6 composite under visible light irradiation.* Catalysis Communications, 2008. **9**(6): p. 1247-1253.
217. Yaman, C. and G. Gündüz, *A parametric study on the decolorization and mineralization of CI Reactive Red 141 in water by heterogeneous Fenton-like oxidation over FeZSM-5 zeolite.* Journal of Environmental Health Science and Engineering, 2015. **13**(1): p. 7.
218. Zhou, B., et al., *Visible-light sensitive cobalt-doped BiVO4 (Co-BiVO4) photocatalytic composites for the degradation of methylene blue dye in dilute aqueous solutions.* Applied Catalysis B: Environmental, 2010. **99**(1–2): p. 214-221.

# 3 METAL-ORGANIC FRAMEWORK BASED PHOTOCATALYSTS FOR EFFICIENT OXIDATION OF METHYLENE BLUE

Partial results from this chapter were presented at WCCE9 as "*Decolourisation of Methylene Blue Aqueous Solution By Photo-Fenton Process Over Fe/MIL-47*"

## 3.1 Introduction

While methylene blue is not a human health risk at concentrations likely to result from industrial pollution, but it does still represent a significant visual environmental pollutant, and is frequently used as a model pollutant [1] in photo-catalytic research. In this section of work, MIL-47(V) and the structurally analogous MIL-53(Al) were synthesized and tested for the photo-decolourisation of methylene blue. A novel Fenton catalyst was also synthesized by the inclusion of iron ions into the MIL-47 framework. Similarly, a Fenton-like catalyst was also synthesized using copper in the place of iron. These Fe/MIL-47 and Cu/MIL-47 catalysts were also evaluated for the decolourisation and mineralization of methylene blue. A zeolite based Fenton catalyst was also synthesized and compared to the MIL-47 based catalyst.

## 3.2 Experimental

### 3.2.1 Chemicals used

All chemicals were used as received, except where indicated. The following chemicals were purchased from Sigma-Aldrich; aluminium nitrate nonahydrate 98%, copper (II) chloride 98%, iron (III) chloride 98%, iron (III) nitrate nonahydrate (>98%), methylene blue 99%, terepthalic acid 98%, vanadium (III) chloride 98%. Na-zeolite Y was obtained from Zeolyst International. Hydrogen peroxide (30% w/v) was purchased from Fisher Scientific. De-ionized water was obtained from a Millipore Milli-Q system.

### 3.2.2 Synthesis methods

MIL-47 was synthesised using a hydrothermal method described in literature [2]. Typically, $VCl_3$ and terephthalic acid were mixed together with deionised $H_2O$ at a molar ratio 1:0.25:100. The resulting mixture was transferred into a Teflon-lined stainless Parr Acid Digestion Vessel for 4 days at 200°C. The as-synthesized MIL-47 was then filtered, washed with acetone, and calcined for 21 hours at 300°C to remove free terephthalic acid from the pores. The iron- and copper-MIL-47 catalysts were synthesized by incipient wetness impregnation of $Fe^{3+}$ or $Cu^{2+}$ into MIL-47 using an ethanolic solution of $FeCl_3$ or $CuCl_2$ at a 0.05:1 (Fe or Cu):V molar ratio [3], followed by air drying overnight at 80°C, then calcination for 1 hour at 120°C. MIL-53(Al) was synthesized from literature methods described by Ferey et al [4]. Iron-zeolite Y was prepared by ion exchange of Na-Y in $Fe(NO_3)_3$ solution [5]. At the completion of ion exchange the zeolite was recovered through filtration, and dried at 80°C in a drying oven.

### 3.2.3 Catalyst characterisation

X-ray powder diffraction (XRD) data of the synthesized catalysts products was collected on a Philips PW1700 computer-controlled diffractometer with a graphite monochromator and Co Kα radiation. The surface topologies of the products were observed by field emission scanning electron microscopy (SEM) on a JEOL 7000F FE-SEM. High resolution transmission electron microscopy (TEM) images were obtained using a Philips CM200 high resolution analytical transmission electron microscope.

### 3.2.4 Photo-oxidation of methylene blue

The photocatalytic activities of MIL-47, Fe/MIL-47 and MIL-53(Al) were evaluated through the photo-degradation of methylene blue dye under 8W UVC irradiation at room temperature and in open air. The UVC lamp was placed in a quartz tube which was submerged in the centre of a 1L beaker. The catalyst was added to 800 mL of MB aqueous solution (typically $4\times10^{-4}$ mol $L^{-1}$). The solution was heated to 30°C and the pH was adjusted using 0.01M $H_2SO_4$ or 0.01M NaOH as needed. Hydrogen peroxide was added at a 1:26 MB:$H_2O_2$ molar ratio. Stirring was maintained throughout the reaction at a rate of 600 rpm.

The methylene blue concentration was examined by measuring the absorbance of sample at the maximum absorbance wavelength for methylene blue, 664 nm, using a VWR UV-1600 PC Spectrophotometer with a 1cm path length spectrometric glass cell. Samples were filtered and then diluted as necessary to ensure the concentration measured was within the linear relationship between absorbance and concentration for methylene blue. The total organic carbon of the solution was measured on a Shimadzu TOC-L total organic carbon analyser. Samples were filtered and centrifuged to removal any remaining catalyst particles.

The stability of the Fe/MIL-47 catalyst was also tested under simulated reaction conditions (30°C, pH 3, $H_2O_2$ concentration 0.01 M, 8W UVC irradiation), with no methylene blue present.

## 3.3 Results and discussion

### 3.3.1 Catalyst characterisation

The XRD results for the Fe-Y catalyst synthesized are presented in Chapter 4 and the XRD patterns for MIL-53(Al) are consistent with those in literature and are presented in Appendix 3. The XRD patterns of the synthesized catalysts presented in Figure 3.1 show that the crystalline structure of MIL-47 is maintained after the loading of Fe into the material. Furthermore, the XRD patterns obtained are consistent with those in literature for MIL-47 samples obtained under similar synthesis conditions.

It also can be seen from Figure 3.1 that at least some Fe/MIL-47 remains stable under reaction conditions, with no methylene blue present, for 24 hours. These conditions are analogous to those presented by McNarama et al [6], albeit at significantly lower temperature (30°C compared to 100°C). While this XRD result does not show the same behaviour observed by McNamara et al, this does not preclude the self-oxidation of some of the Fe/MIL-47 to vanadium/iron oxide and terephthalic acid, as those breakdown products could dissolve in the solution, and would therefore not show on XRD of the filtered solids. However, the XRD pattern for Fe/MIL-47 recovered after photo-oxidation of methylene blue does show a significant loss in crystallinity. This indicates that some form of structural degradation is likely.

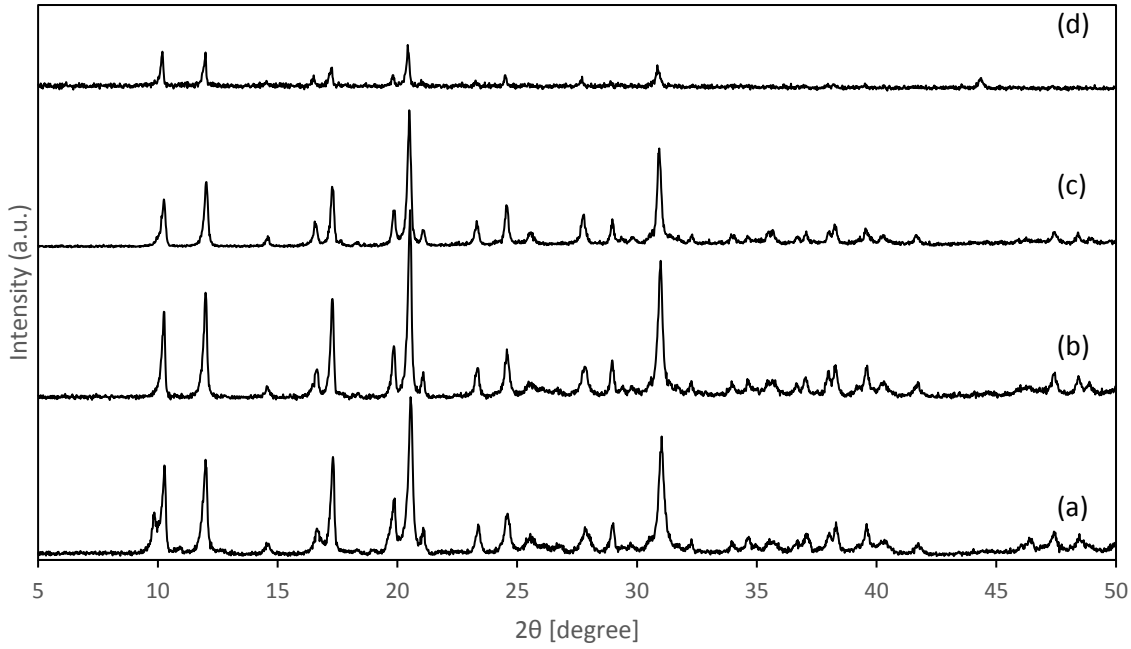


Figure 3.1 – XRD patterns of (a) MIL-47(as), (b) Fe/MIL-47, (c) Fe/MIL-47 after 24 hours at 30°C in the presence of $H_2O_2$, (d) Fe/MIL-47 after reaction with methylene blue.

Additionally, the SEM and TEM images shown in Figure 3.2 and Figure 3.3, respectively do not show the same vanadium oxide structures that McNamara et al found after oxidation reactions. However, some breakdown of the particle structure can be observed but this is likely due to mechanical stresses during the reaction, and filtration. The SEM and TEM results show that the MIL-47 structure is preserved after Fe loading. SEM images of the prepared Fe-zeolite Y, MIL-53(Al), and Cu/MIL-47 catalysts are included in the Appendix 3.

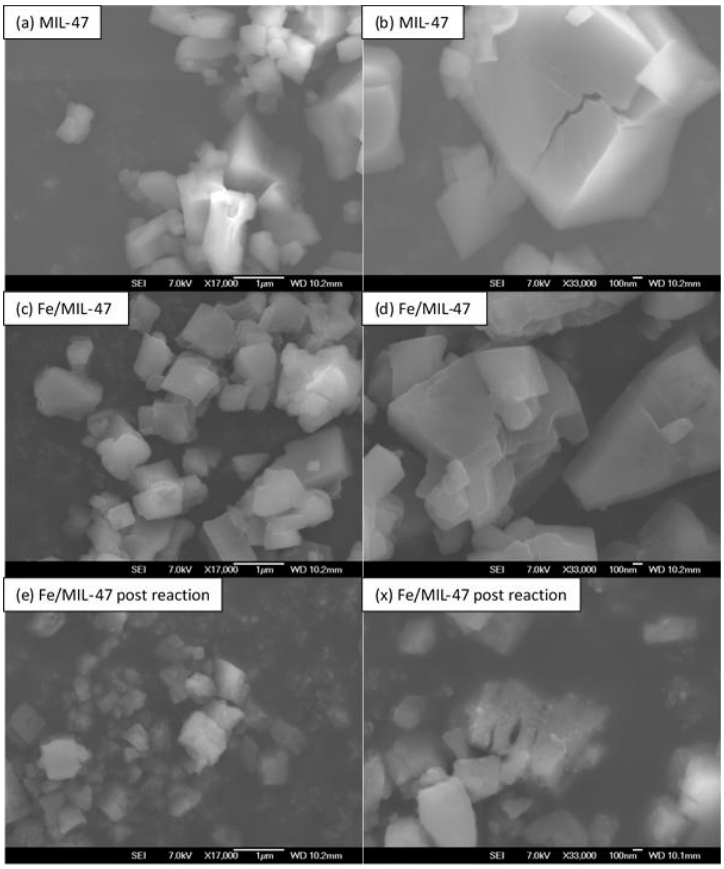


Figure 3.2 - SEM images of (a) MIL-47 as synthesized, (b) high magnification of MIL-47, (c) Fe/MIL-47 after loading of Fe onto MIL-47, (d) high magnification of Fe/MIL-47 showing no iron oxide species present on the surface, (e) Fe/MIL-47 after the reaction with methylene blue dye, (f) high magnification of Fe/MIL-47 after reaction with methylene blue dye, showing signs of degradation.

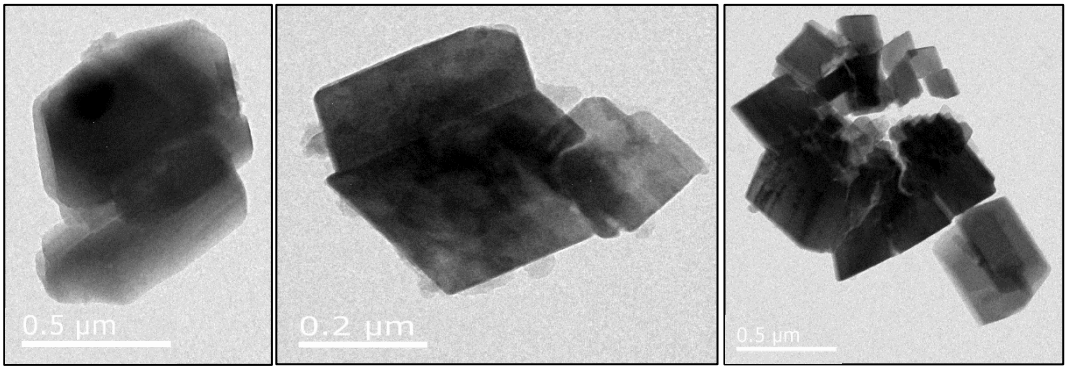


Figure 3.3 – TEM images of (a) MIL-47, (b) Fe/MIL-47, and (c) Fe/MIL-47 post reaction.

### 3.3.2 Photo-oxidation of methylene blue

The photocatalytic oxidation of methylene blue was conducted to evaluate the efficiency of the MIL-47 based photocatalysts. The photocatalysts MIL-53 and Fe/zeolite-Y were also investigated. The degradation of the methylene blue was quantified by the change in colour of the solution, by measuring the maximum absorbance intensity of the methylene blue chromophoric group, at 664 nm, and also the removal of total organic carbon from the solution. Colour removal in this Chapter specifically refers to the characteristic absorbance peak of methylene blue (at 664nm), as shown in Figure 3.4below.

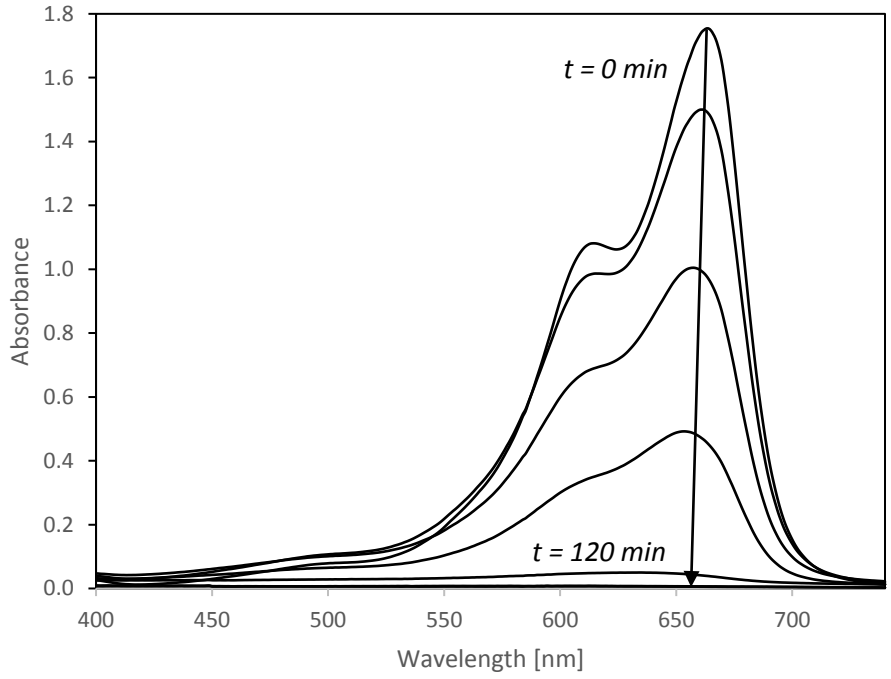


Figure 3.4 - Scan of methylene blue absorbance over visible range during oxidation reactions.

Control experiments with no UV irradiation were also carried out, with no significant change in the colour observed over the reaction period, after the initial adsorption. A control was also carried out in the absence of photocatalysts, utilizing the UV/$H_2O_2$ system.

The photo-degradation of methylene blue over these catalyst follows pseudo-first order kinetics, which can be modelled with Equation 3.1:

$$\ln\left(\frac{C_0}{C}\right) = Kt \qquad 3.1$$

where $C_0$ is the initial concentration of the methylene blue, $C$ is the concentration of the dye at the reaction time $t$, and $K$ is the kinetic rate constant [7]. Figure 3.5 shows that the catalytic activity for the photo-decolourisation of methylene blue are substantially similar for MIL-47 and the structurally analogous MIL-53(Al). This is in agreement with the findings of Du et al, who found that the metal ion used in MIL-53(M) (M=Fe,Al,or Cr) did not significantly affect the reaction rate [7]. The rate constant values are 0.0289 $min^{-1}$, 0.0385 $min^{-1}$, and 0.0229 $min^{-1}$ for MIL-47, MIL-53(Al), and UV/$H_2O_2$.

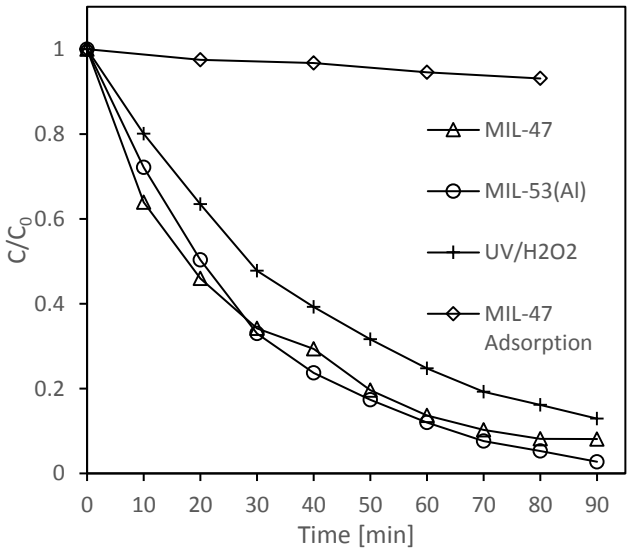


Figure 3.5 – Comparison of MIL-47 to MIL-53(Al), UV/$H_2O_2$, and dark adsorption over MIL-47. Lines are a guide for the eyes only. [MB concentration = $2\times10^{-5}$ mol $L^{-1}$, $H_2O_2$:MB = 26, 10 mg $L^{-1}$ catalyst loading (0 mg $L^{-1}$ catalyst for UV/$H_2O_2$), pH = 3.0, 30°C, 600 RPM stirring, 8W UVC irradiation (no irradiation for Adsorption)]

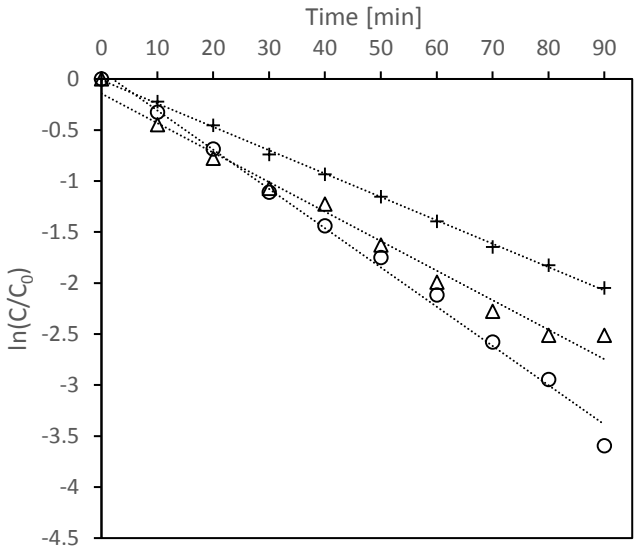


Figure 3.6 – Kinetics of decolourisation for (Δ) MIL-47, (○) MIL-53(Al), (+) UV/$H_2O_2$.

Figure 3.7 shows the degradation profile of methylene blue over the Fe/MIL-47 and bare MIL-47 photocatalyst under UVC irradiation. Almost complete decolourisation is achieved after 60 min with the Fe/MIL-47catalyst, while the MIL-47 photocatalyst could only decolourise around 85% of the methylene blue solution after 60 min. The rate constant values are 0.0685 $min^{-1}$ and 0.0289 $min^{-1}$ for Fe/MIL-47 and MIL-47, respectively (Figure 3.8). It should be noted that photolysis of methylene blue is significant at lower methylene blue concentrations, which, in addition to providing a higher signal to noise ratio for TOC measurements, is why a higher concentration ($4x10^{-4}$ mol $L^{-1}$) was used for subsequent oxidation tests.

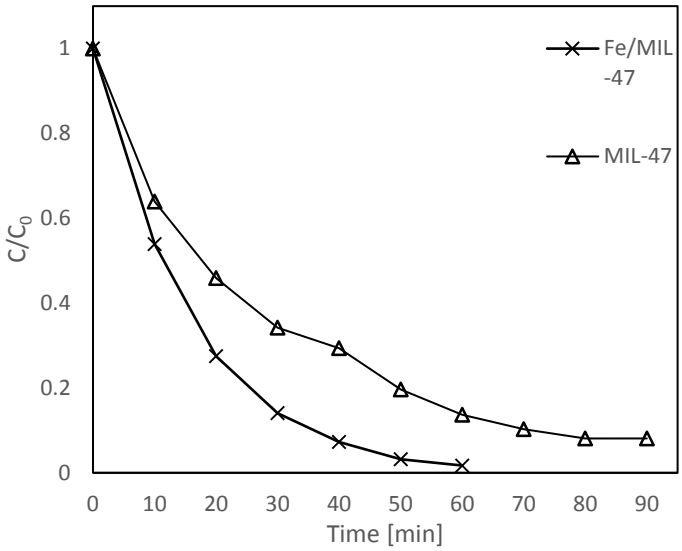


Figure 3.7 – Photocatalytic decolourisation of methylene blue by(X) Fe/MIL-47, and (Δ) MIL-47. Lines are a guide for the eyes only. [MB concentration = $2\times10^{-5}$ mol $L^{-1}$, H2O2:MB = 26, 10 mg $L^{-1}$ catalyst loading, pH = 3.0, 30°C, 600 RPM stirring, 8W UVC irradiation].

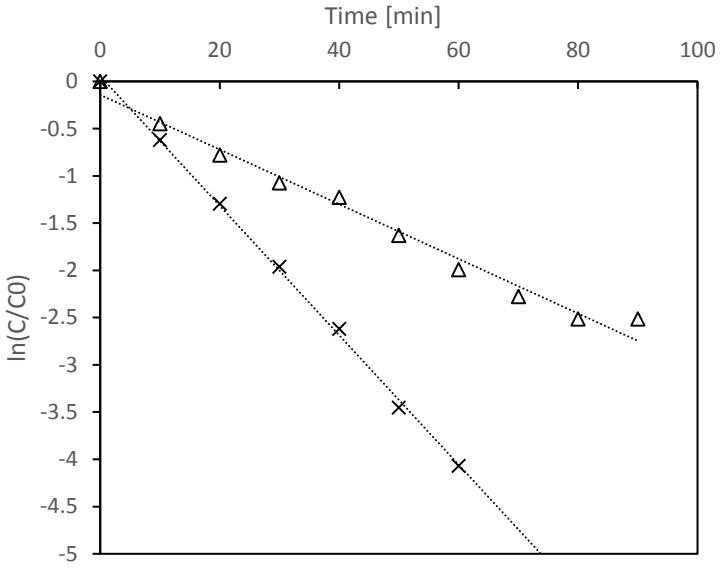


Figure 3.8 – Kinetics of decolourisation for (X) Fe/MIL-47, and (Δ) MIL-47.

The comparison of Fe/MIL-47 to Fe/zeolite-Y in the discoloration of methylene blue and TOC removal shows that Fe/MIL-47 is significantly faster for both discoloration and TOC removal, with both at similar weight-percent Fe (nominally 4%). The difference in TOC removal after 180 minutes is extremely large, with the Fe/MIL-47 achieving a TOC removal of 52%, compared to the Fe/zeolite-Y TOC removal of just 8%. This shows that the metal-organic framework catalyst is significantly more effective than the zeolite based catalyst at the catalyst dosages used. The rate constant for the

Fe/MIL-47 is 0.0167 $min^{-1}$ for the decolourisation and 0.0038 $min^{-1}$ for the TOC removal. These are significantly higher than those for the Fe/zeolite-Y, at 0.0068 $min^{-1}$ for decolourisation and 0.0004 $min^{-1}$ for the TOC removal. Typical dosages of zeolite catalysts for photo-Fenton dye degradation are usually at or higher than 1 g $L^{-1}$ [9], which explains why the TOC removal for the Fe/zeolite-Y catalyst is low compared with the results of Hassan et al, who reported 99% decolourisation of Acid Red 1 dye in 60 minutes with 2.5g $L^{-1}$ Fe/zeolite-Y [10]. This means that the effectiveness of Fe/MIL-47 at lower catalyst dosages is a significant advantage over these previous heterogeneous photo-Fenton catalysts.

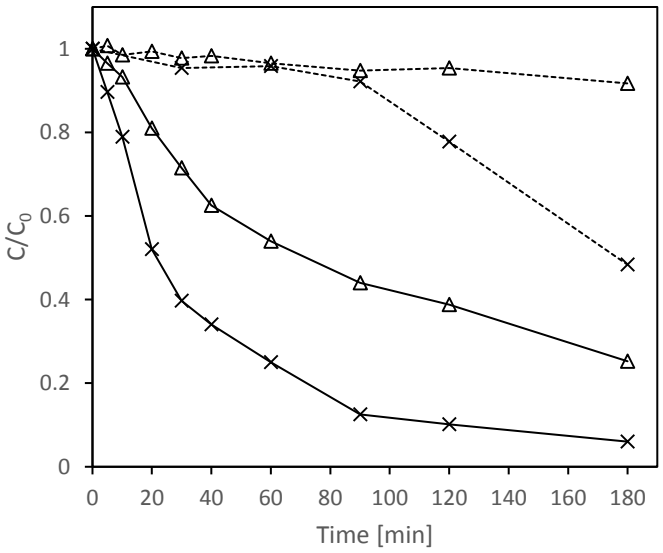


Figure 3.9 - Comparison of reactions in methylene blue solution; (X) Fe/MIL-47, (Δ) Fe/zeolite-Y, solid lines colour removal, dashed lines TOC removal. Lines are a guide for the eyes only. [MB concentration = $4x10^{-4}$ mol $L^{-1}$, $H_2O_2$:MB = 26, catalyst concentration = 50 mg $L^{-1}$, pH = 3.0, 30°C, 600 RPM stirring, 8W UVC irradiation].

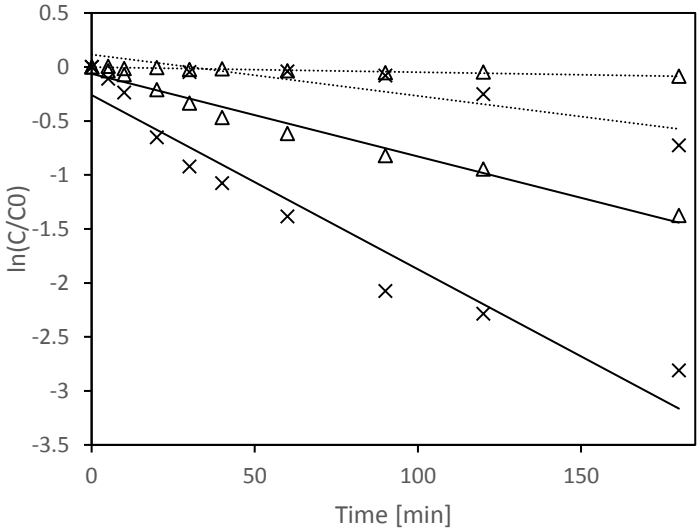


Figure 3.10 - Reaction kinetics for methylene blue colour and TOC degradation over (X) Fe/MIL-47 and (Δ) Fe/H-Y catalysts. Solid lines are colour, dotted are TOC. [MB concentration = $4x10^{-4}$ mol $L^{-1}$, $H_2O_2$:MB = 26, catalyst concentration = 50 mg $L^{-1}$, pH = 3.0, 30°C, 600 RPM stirring, 8W UVC irradiation].

The effect of temperature on the degradation of methylene blue shown in Figure 3.11 shows that the decolourisation rate improves with higher temperatures while the TOC removal rate slightly decreases. This effect is due to the increased reaction rate of hydrogen peroxide with the already generated hydroxyl radicals (Equation 3.2) at higher temperatures, limiting the availability of hydroxyl radicals for the multi-step TOC removal reactions.

C $$H_2O_2 + HO\bullet \rightarrow H_2O + HO_2\bullet$$ 3.2

The hydroperoxyl radicals generated through this reaction are less reactive than the hydroxyl radicals they replace, and they may also react with hydroxyl radicals themselves (Equation 3.3), further limiting the availability of hydroxyl radicals:

C $$HO_2\bullet + HO\bullet \rightarrow H_2O + O_2$$ 3.3

The initial decolourisation step (cleavage of the S-C bonds) requires comparably less oxidation, so the scavenging effect by hydrogen peroxide does not affect the decolourisation reaction, as there is a large excess of hydrogen peroxide above that needed for the decolourisation to be complete.

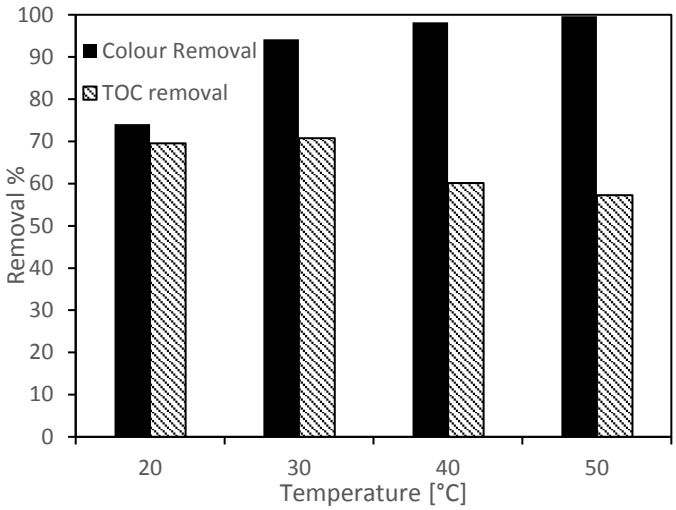


Figure 3.11 - Effect of temperature on removal of colour and TOC from methylene blue solution over Fe/MIL-47 catalyst. [MB concentration = $2x10^{-4}$ mol $L^{-1}$, $H_2O_2$:MB = 26, catalyst concentration = 60 mg $L^{-1}$, pH = 3.0, reaction time = 60 minutes, 600 RPM stirring, 8W UVC irradiation].

At concentrations above 60 mg $L^{-1}$ the colour removal only slightly improves with increasing concentration, while in contrast, the TOC removal is decreased. This is likely due to the increase in the rate of generation of hydroxyl radicals due to the higher iron concentration at higher catalyst concentrations. The TOC degradation of methylene blue is a multi-step process which has been shown to begin with the oxidation of the sulfur ion to sulfoxide, followed by the splitting of the methylene blue molecule into two separate single benzene ring based molecules [11], the ring opening of these single ring benzene molecules is likely to be a rate limiting step for the overall reaction, therefore an increase in the concentration of hydroxyl radicals will not benefit the TOC degradation reaction past a certain point.

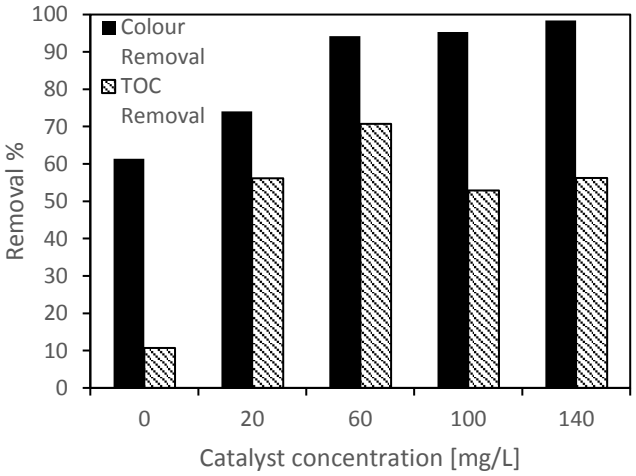


Figure 3.12 - Effect of catalyst concentration on removal of colour and TOC in methylene blue solution over Fe/MIL-47 catalyst. [MB concentration $2x10^{-4}$ mol $L^{-1}$, $H_2O_2$:MB = 26, pH = 3.0, 30°C, reaction time = 60 minutes, 600 RPM stirring, 8W UVC irradiation].

The scavenging effect of hydrogen peroxide on hydroxyl radicals can also be seen in Figure 3.13, where the fast colour removal is independent of the hydrogen peroxide concentration after a certain ratio, but the TOC removal begins to decrease at higher concentrations. This effect is well known [12], and is one of the reasons hydrogen peroxide concentration must be examined to create an efficient process. Another option would be to add a limited amount of hydrogen peroxide several times, to ensure the optimum ratio was maintained throughout the reaction.

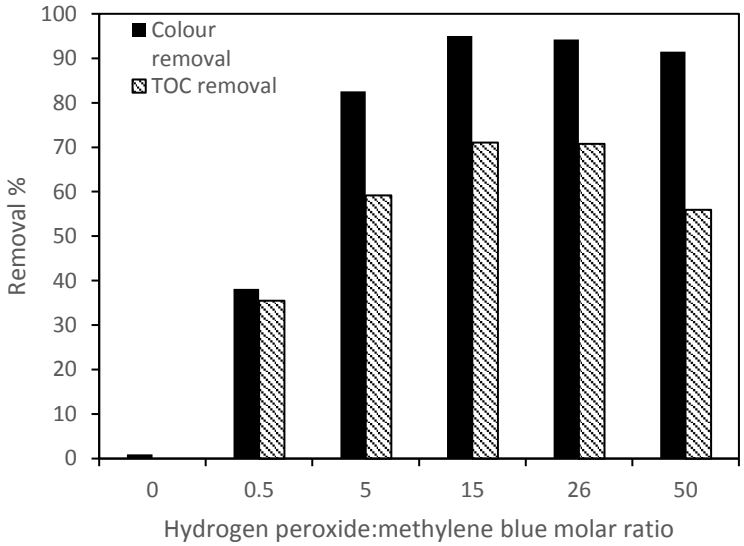


Figure 3.13 - Effect of hydrogen peroxide to methylene blue ratio on removal of colour and TOC in methylene blue solution over Fe/MIL-47 catalyst. [MB concentration $2x10^{-4}$ mol $L^{-1}$, catalyst concentration = 60 mg $L^{-1}$, pH = 3.0, 30°C, reaction time = 60 minutes, 600 RPM stirring, 8W UVC irradiation].

The discoloration of methylene blue and removal of TOC from the solution under different pH with Fe/MIL-47 catalyst is shown in Figure 3.14. This shows that the optimum pH for both colour and TOC removal is pH 3, which is in agreement with previous research which has shown that iron based Fenton reactions have maximum efficiency at this pH [13]. The low removal of TOC at pH 2 could potentially be due to partial framework destruction at such a low pH causing an increase in organic carbon in the solution due to the framework ligands dissolving.

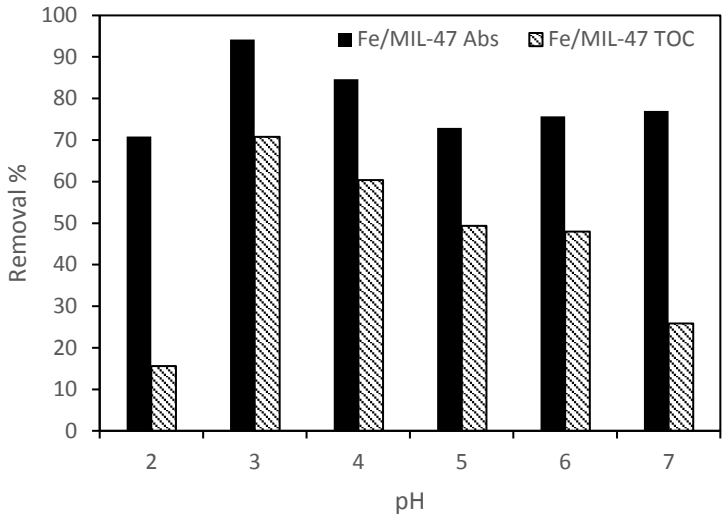


Figure 3.14 - Effect of pH on removal of colour and TOC in methylene blue solution over Fe/MIL-47 catalyst [MB concentration $2x10^{-4}$ mol $L^{-1}$, $H_2O_2$:MB = 26, catalyst concentration = 60 mg $L^{-1}$, 30°C, reaction time = 60 minutes, 600 RPM stirring, 8W UVC irradiation].

At pH higher than 4, iron hydroxide complexes can form [14], which precipitates the iron from the solution, removing it from the Fenton reaction cycle, which can degrade the ability of the Fenton catalysis. The addition of copper to the MIL-47 catalyst shows that the catalytic ability is retained at pH 7, as shown in Figure 3.15, where for the Fe/MIL-47 the decolourisation at these pH's was limited. Copper based photocatalysts are known to be most effective at higher pH, so the relatively good performance at low pH, specifically pH 4, is potentially due to the activity of the MIL-47 structure.

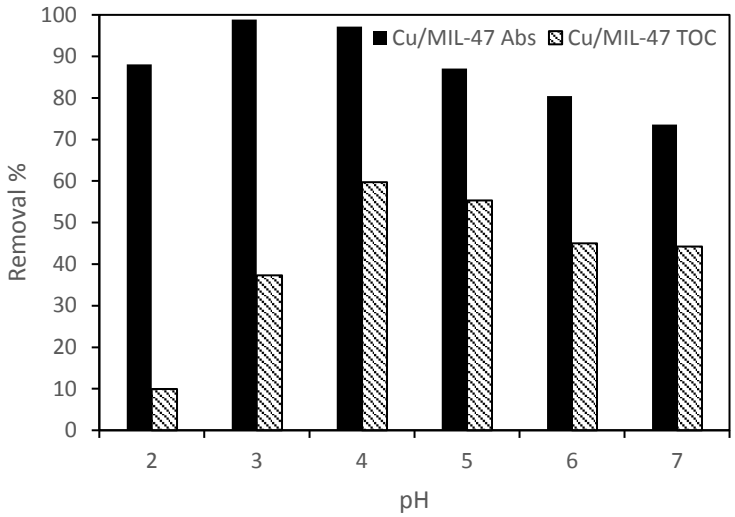


Figure 3.15 - Effect of pH on removal of colour and TOC in methylene blue solution over Cu/MIL-47 catalyst [MB concentration $2x10^{-4}$ mol $L^{-1}$, $H_2O_2$:MB = 26, catalyst concentration = 60 mg $L^{-1}$, 30°C, reaction time = 60 minutes, 600 RPM stirring, 8W UVC irradiation].

The recycle of Fe/MIL-47 is shown in Figure 3.16, which shows a drop in rate constant from 0.0167 $min^{-1}$ in the first 60 minutes to 0.0102 $min^{-1}$ in the second cycle. This indicates that there is some degradation happening to the catalyst during the reaction with hydrogen peroxide and methylene blue. This is further supported by the XRD results that show some loss in crystallinity of the recovered Fe/MIL-47 post-reaction. This suggests that degradation of the MIL-47 framework does occur during oxidation reactions.

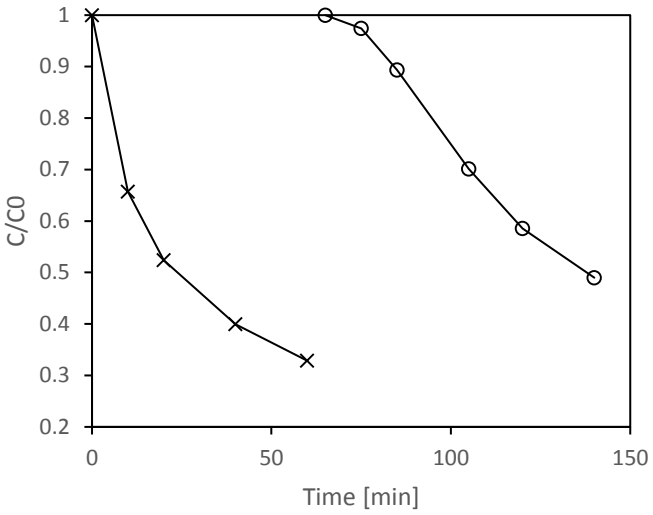


Figure 3.16 - Colour removal from methylene blue solution over Fe/MIL-47 catalyst with recycle. (X) First run, (○) Second run. Lines are a guide for the eyes only. [MB concentration = $4x10^{-4}$ mol $L^{-1}$, H2O2:MB = 26, catalyst concentration = 50 mg $L^{-1}$, pH = 3.0, 30°C, 600 RPM stirring, 8W UVC irradiation].

## 3.4 Conclusions

A new photo-Fenton catalyst based on the vanadium carboxylate MOF, MIL-47(V), was synthesised by incipient wetness ion impregnation of an ethanolic iron (III) chloride solution. The decolourisation of methylene blue was enhanced by the inclusion of Fe ions into the framework with the first order rate constant increasing from 0.0289 $min^{-1}$ for MIL-47 to 0.0685 $min^{-1}$ Fe/MIL-47. This work shows that Fe/MIL-47 is an effective photo-catalyst for the degradation of methylene blue dye, when compared with the base MIL-47 and similar MOFs. A copper catalyst was also synthesized and demonstrated better activity for the degradation of methylene blue at pH 7 than the iron based catalyst. The Fe/MIL-47 catalyst has also been shown to be more effective than Fe/zeolite-Y, removing 94% colour and 52% TOC in 180 minutes compared to just 74% colour and 8% TOC in 180 minutes for the zeolite based catalyst.

The catalyst was found to be stable under simulated reaction conditions with no methylene blue present (30°C, $5x10^{-3}$ mol $L^{-1}$ $H_2O_2$, 8W UVC irradiation), which other researchers [6] have found to cause auto-oxidation of the framework, and no vanadium oxide crystals were observed in SEM or TEM of the catalyst post reaction. Further muddying the water is the work of Nguyen et al [15], who explored using hydrogen peroxide as a method of purifying MIL-53(Fe) and found no damage to the structure at all. However, the decolourisation rate of methylene blue over Fe/MIL-47 was found to degrade with recycle, and the XRD results showing that there is loss of crystallinity after reaction with methylene blue. This suggests that there is degradation of the framework and therefore that other, more robust catalyst types should be utilized for future studies.

## 3.5 References


1. Kozlova, E.A., et al., *Photoreactivity of metal-organic frameworks in the decolorization of methylene blue in aqueous solution.* Catalysis Today, 2016. **266**: p. 136-143.
2. Barthelet, K., et al., *A Breathing Hybrid Organic-Inorganic Solid with Very Large Pores and High Magnetic Characteristics.* Angewandte Chemie, 2002. **114**(2): p. 291-294.
3. Khan, N.A. and S.H. Jhung, *Remarkable Adsorption Capacity of CuCl2-Loaded Porous Vanadium Benzenedicarboxylate for Benzothiophene.* Angewandte Chemie, International Edition, 2012. **51**(5): p. 1198-1201.
4. Loiseau, T., et al., *A rationale for the large breathing of the porous aluminum terephthalate (MIL-53) upon hydration.* Chemistry--A European Journal, 2004. **10**(6): p. 1373-82.
5. Roque-Malherbe, R., J. Oñ ate-Martinez, and E. Navarro, *Furfural oligomerization within H-Fe-FAU zeolite.* Journal of Materials Science Letters, 1993. **12**(13): p. 1037-1038.
6. McNamara, N.D., et al., *Catalytic performance and stability of (V) MIL-47 and (Ti) MIL-125 in the oxidative desulfurization of heterocyclic aromatic sulfur compounds.* Journal of Catalysis, 2013. **305**(0): p. 217-226.
7. Du, J.J., et al., *New photocatalysts based on MIL-53 metal-organic frameworks for the decolorization of methylene blue dye.* J Hazard Mater, 2011. **190**(1-3): p. 945-51.
8. Singh, L., P. Rekha, and S. Chand, *Cu-impregnated zeolite Y as highly active and stable heterogeneous Fenton-like catalyst for degradation of Congo red dye.* Separation and Purification Technology, 2016. **170**: p. 321-336.
9. Soon, A.N. and B. Hameed, *Heterogeneous catalytic treatment of synthetic dyes in aqueous media using Fenton and photo-assisted Fenton process.* Desalination, 2011. **269**(1): p. 1-16.
10. Hassan, H. and B.H. Hameed, *Oxidative decolorization of Acid Red 1 solutions by Fe– zeolite Y type catalyst.* Desalination, 2011. **276**(1– 3): p. 45-52.
11. Houas, A., et al., *Photocatalytic degradation pathway of methylene blue in water.* Applied Catalysis B: Environmental, 2001. **31**(2): p. 145-157.
12. Dü kkancı , M., et al., *Heterogeneous Fenton-like degradation of Rhodamine 6G in water using CuFeZSM-5 zeolite catalyst prepared by hydrothermal synthesis.* Journal of Hazardous Materials, 2010. **181**(1– 3): p. 343-350.
13. Chen, X., et al., *Degradation of Dye Methylene Blue Wastewater by Photo-Fenton Reaction Using FeY Catalyst [J].* Environmental Science & Technology, 2012. **2**: p. 031.
14. Huston, P.L. and J.J. Pignatello, *Degradation of selected pesticide active ingredients and commercial formulations in water by the photo-assisted Fenton reaction.* Water Research, 1999. **33**(5): p. 1238-1246.
15. Nguyen, M.-T.H. and Q.-T. Nguyen, *Efficient refinement of a metal– organic framework MIL-53(Fe) by UV– vis irradiation in aqueous hydrogen peroxide solution.* Journal of Photochemistry and Photobiology A: Chemistry, 2014. **288**: p. 55-59.

# 4 INVESTIGATIONS INTO EFFECT OF CHARGE BALANCING CATIONS IN ZEOLITE Y DURING PHOTO-OXIDATION OF FORMALDEHYDE

The work in this chapter was published as "*Catalytic consequences of charge-balancing cations in zeolite during photo-Fenton oxidation of Formaldehyde in alkaline conditions".* Separation and Purification Technology, 125 (2014): 269-274. DOI: 10.1016/j.seppur.2014.02.005

## 4.1 Introduction

The MIL-47 based catalysts tested in Chapter 3 showed significantly higher activity than the zeolite-Y based catalyst for the photo-oxidation of methylene blue, however the framework showed signs of structural failure under testing conditions. Therefore, the zeolite based Fenton catalyst was selected for further testing.

While many studies have used various zeolites, such as MFI [15], BEA [29] and zeolite Y [16,30], to produce heterogeneous photo-Fenton catalysts, the potential effect of the Brønsted acid sites on the reaction rate has not been illustrated. In this chapter, the effect of $NH_4^+$, $Na^+$ and $H^+$ in zeolite Y on photo-Fenton oxidation of FA in a batch reactor was examined. The catalysts were prepared and studied by partial exchange of photo-Fenton reagent, $Fe^{3+}$, in the zeolite Y. As the pore size of the zeolite Y catalyst is 7.4 Å [197], methylene blue would not be able to easily diffuse inside (diameters 5.91 Å x 13.82 Å [1]). While the generated hydroxyl radicals can diffuse out into the bulk solution, and hydrogen peroxide (2.8 Å [2]) can diffuse in , fully external oxidation could mask any effect caused by the internal pore environment.

Therefore formaldehyde (FA) with a diameter of 2.43 Å [3] was chosen as a pollutant, to enable the full examination of the internal effect of the charge balancing cations on the photo-Fenton reaction. While it is commonly anticipated that complete ion exchange in zeolite would yield a catalyst with the best performance, this work investigated partial exchange of photo-Fenton reagent, $Fe^{3+}$, in the zeolite Y and explicitly elucidated that the presence of acidic and basic charge-balancing ions in zeolite have a significant effect on the performance of photo-Fenton process at different pH. While these findings may seem obvious in hindsight, as it has been long known that Fenton reactions are more effective in acidic environments than basic, the specific observation of this effect in the internal pore environment of zeolites is novel, and provides a new, alternative approach to iron loading of zeolites for use in photo-Fenton reactions.

## 4.2 Experimental

### 4.2.1 Chemicals used

Formaldehyde (37%) and $H_2O_2$ (30%) were purchased from Univar and Fisher Chemical, respectively. Iron (III) nitrate nonahydrate (>98%), acetic acid (99.7%), acetylacetone (>99%), ammonium acetate (>98%), sodium sulphate and sodium hydroxide (98%) were obtained from Sigma-Aldrich. Potassium hydrogen phosphate and potassium iodide were supplied by BDH Chemicals. All reagents were of

analytical reagent grade. All solutions were prepared using deionised water produced from an ultrapure water system (Arium® 611 UV, Sartorius Stedim Biotech). Ammonium-form and sodium-form Faujasite (FAU) zeolites Y were obtained from Zeolyst International.

### 4.2.2 Synthesis methods

Fe/H-Y and Fe/$NH_4$-Y were prepared by ion exchange of Na-Y (Si/Al = 2.6) and $NH_4$-Y (Si/Al = 2.6) in $Fe(NO_3)_3$ solution with desired concentration. In general, 0.5 g $L^{-1}$ zeolite was loaded to the $Fe(NO_3)_3$ solution in a beaker and was heated on a hot plate at 303 K with sufficient mixing for 24 h [4]. The maximum Fe loading was determined for Na-Y and NH4-Y from calculations using known molecular weights and compositions. Specific concentration of $Fe(NO_3)_3$ solution was then used to produce catalysts with 50% of maximum Fe loading (partially exchanged) and 100% of maximum Fe loading (completely exchanged). At the completion of ion exchange the zeolite was recovered through filtration, and dried at 343 K in a drying oven. Fe/$NH_4$-Y was converted to its acid form, i.e. Fe/H-Y, by heat treatment at 773 K for 10 h. The remaining exchangeable cations in the catalysts which were not exchanged with Fe were assumed to be $Na^+$, $NH_4^+$ and $H^+$ for Fe/Na-Y, Fe/NH4-Y and Fe/H-Y, respectively. The catalysts which were completely exchanged with Fe are designated as Fe/Na-Y-100%, Fe/$NH_4$-Y-100% and Fe/H-Y-100% to indicate that the Fe content is approximately equivalent to the total amount of exchangeable cations in the catalysts.

### 4.2.3 Catalyst characterisation

The surface morphology of the samples was determined by scanning electron microscopy (SEM), on a JEOL 7000F FE-SEM. The crystalline structure of the zeolites was analyzed by powder X-ray diffraction (XRD) on an Agilent Supernova system, using Cu Ka radiation (k = 1.5418 Å) at 50 kV and 0.80 mA with a measuring time of 300 s. The surface area of the catalyst was estimated using an automated $N_2$ physisorption analyzer (Gemini VI 2385C). The Fe content in the catalyst was determined by acid ($HNO_3$) digestion with the use of inductively-coupled plasma emission spectroscopy (ICP).

### 4.2.4 Photo-oxidation of formaldehyde

Photo-Fenton oxidation of FA was performed in a batch reactor with a quartz tube in the center position containing 1 8W UVC lamp. For each experiment, 500 ml of 25 ppm FA solution was heated

to 303 K with a stirring hot plate. The solution pH was adjusted by adding 0.1 M H2SO4 or 0.1 M NaOH solution drop-wise.

The pH of the solution was measured at all time using a calibrated pH meter (Eutech pH 510 pH/mV/C) and was verified by universal indicator paper. Required stoichiometric amount of $H_2O_2$ (0.047 ml of 30% w/v $H_2O_2$ solution) was then added into the reactor. The reaction was carried on for 120 min timed as soon as the catalyst (0.5 g $L^{-1}$) was added and the UVC lamp was switched on. Samples were taken every 5–10 min and were put through the syringe filter to the sample vials containing a stopping reagent, which consists of 0.1 M $Na_2SO_4$, 0.1 M $KH_2PO_4$, 0.1 M KI and 0.05 M NaOH, in order to cease the oxidation. Measurement of FA concentration was done using colorimetric analysis which involved the addition of Fluoral-P, producing a yellow coloured complex [32,33]. Fluoral-P was prepared by reacting 0.3 ml acetic acid with 0.2 ml acetylacetone and 15.4 g of ammonium acetate in 100 ml of deionised water. After the Fluoral-P solution was added, the samples were kept in the dark by wrapping sample tubes in tin foil. The Fluoral-P/FA Absorbance was then measured directly using a UV–vis spectrophotometer (VWR UV-16000PC) at 412 nm [32,33]. The concentration of FA was then obtained from the absorbance through the calibration curve. Experiments were duplicated where necessary and the uncertainty was calculated from the mean deviation from the average.

## 4.3 Results and Discussion

### 4.3.1 Catalyst characterisation

The XRD patterns of zeolite H–Y before and after partial or complete ion-exchange with $Fe^{3+}$ (Figure 4.1) show that they are in crystalline phase and that all nine samples have a typical zeolite Y type (faujusite) structure. As the ion-exchange did not alter the d-spacing on the lattice structure of H–Y, it is inferred that $Fe^{3+}$ present in the zeolite as surface cations. The XRD results also indicate that $Fe_2O_3$ particles were absent. In addition, no structural change was observed for $NH_4$–Y and Na–Y after ion exchange with $Fe^{3+}$. XRD patterns show no loss of crystallinity with both partial and full exchange with $Fe^{3+}$ ions for Na-zeolite-Y and $NH_4$-zeolite-Y as shown in Figure 4.1. The $N_2$ physisorption measurement suggests that the surface area of the zeolite Y after ion exchange is in the range of 880–900 $m^2/g$ regardless of the form of charge-balancing cations.

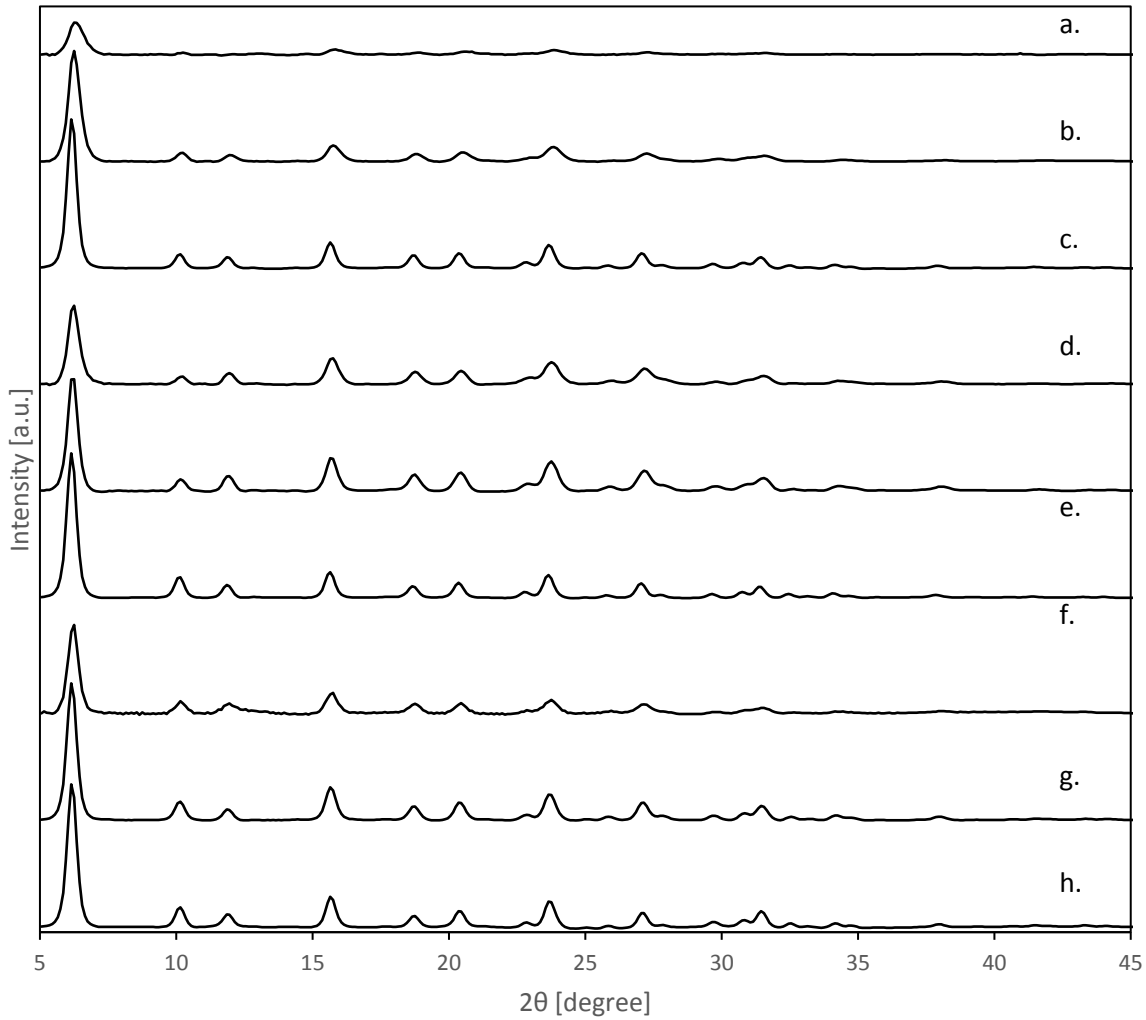


Figure 4.1 – XRD patterns of (a.) completely exchanged H–Y with $Fe^{3+}$, (b.) partially exchanged H–Y, (c.) the original zeolite H–Y, (d.) completely exchangd $NH_4$-Y, (e.) partially exchanged $NH_4$-Y, (f.) the original $NH_4$-Y, (g.) Fe/Na-Y-100%, (h.) partially exchanged Fe/Na-Y, and (i.) the original Na-Y

The SEM images of the original H–Y, partially exchanged Fe/H–Y and Fe/H–Y–100% (Figure 4.2) show that the observed surface morphologies are the same for all three samples. The surface is smooth with no observable deposits of iron particles in partially exchanged Fe/H–Y and Fe/H–Y–100%. This suggests further that Fe was dispersed into the micropores of the zeolite in the form of exchangeable cations. The same observation was made for partially exchanged Fe/Na–Y, Fe/Na–Y–100%, partially exchanged Fe/$NH_4$–Y and Fe/$NH_4$–Y–100% which show that there is no morphological change in the zeolites after partial or complete ion-exchange with $Fe^{3+}$. The samples only contain zeolite-Y without the presence of $Fe_2O_3$ particles in all cases. This gives evidence that $Fe^{3+}$ exist in the form of exchangeable surface cations in the zeolite.

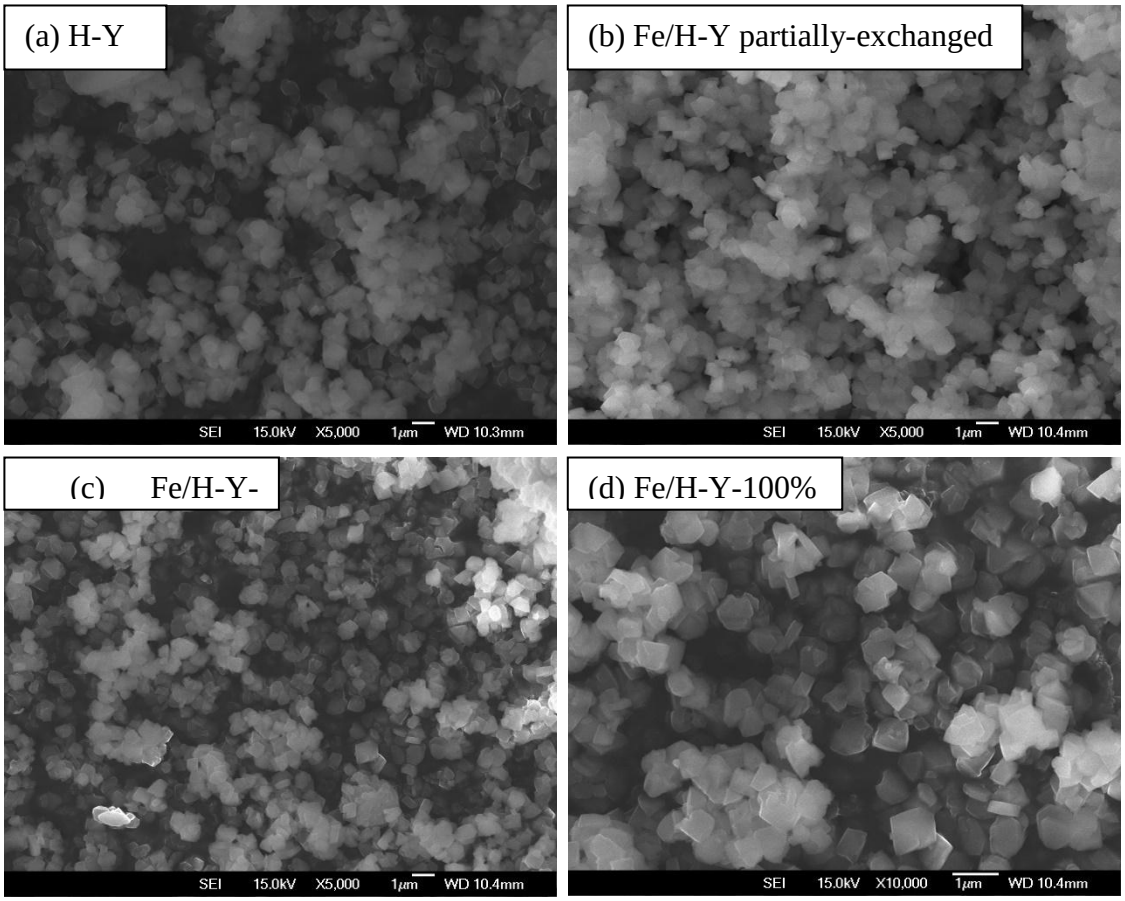


Figure 4.2 – SEM images of (a) H-Y before ion-exchange, (b) partially exchanged H-Y, and (c) completely exchanged H-Y with $Fe^{3+}$ show that there is no morphological change in zeolite. Image (d) shows the completely exchanged H-Y at high magnification (×10,000).

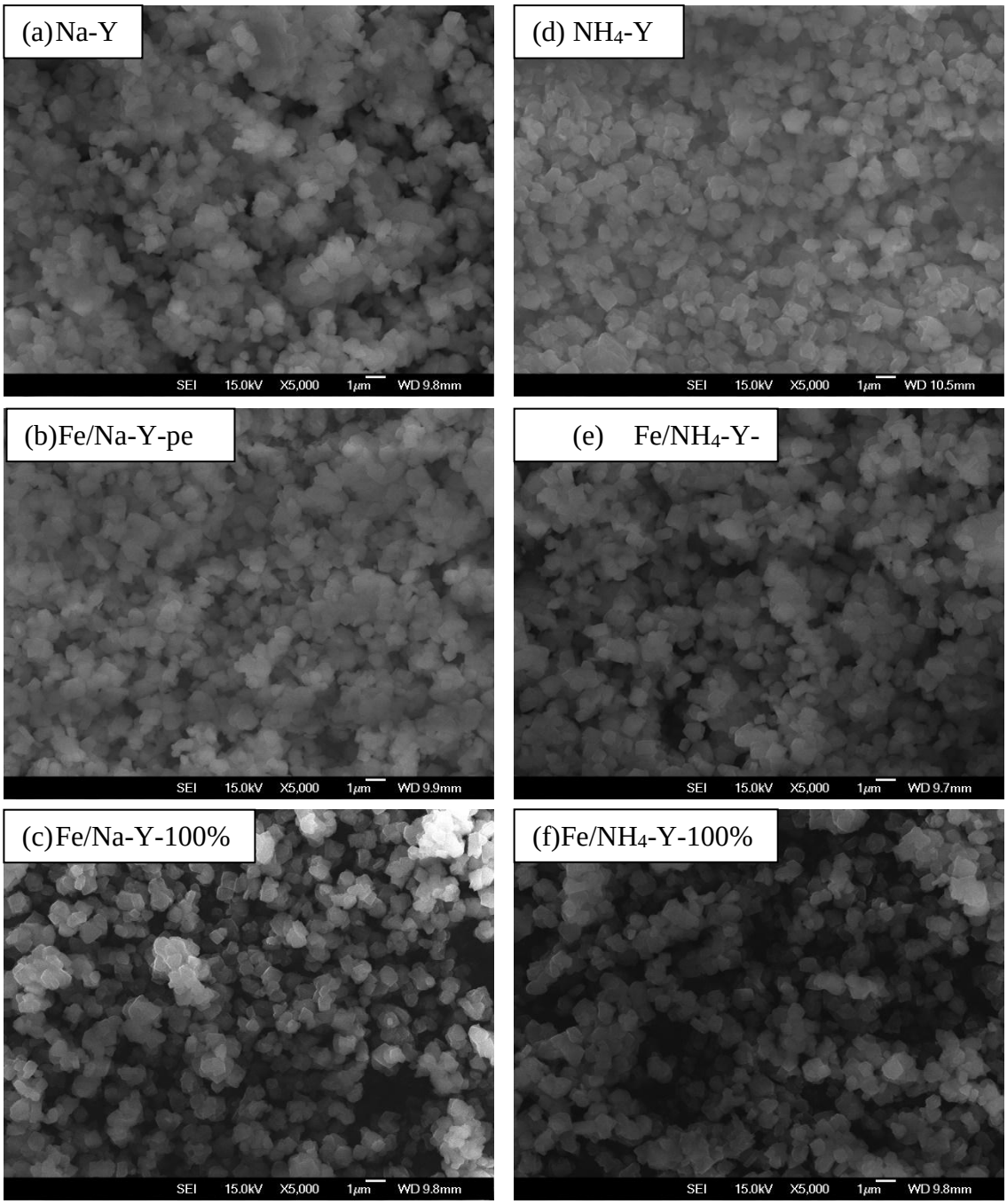


Figure 4.3 – SEM images of (a) Na-Y before ion-exchange, (b) partially exchanged Na-Y with $Fe^{3+}$, (c) completely exchanged Na-Y with $Fe^{3+}$, (d) $NH_4$-Y before ion-exchange, (e) partially exchanged $NH_4$-Y with $Fe^{3+}$, (f) completely exchanged $NH_4$-Y with $Fe^{3+}$.

The Fe content of the completely exchanged zeolite Y and the partially exchanged zeolite Y are reported in Table 4.1. The completely exchanged zeolite Y contain ca. 5.8 mmol of Fe per gram catalyst, which is almost 2 times higher than the Fe content in the partially exchanged zeolite Y (average: 2.9 mmol of Fe per gram catalyst). The measured Fe content was used to calculate the turnover frequency (TOF) of the Fe sites.

Table 4.1 - The Fe content of the zeolite Y containing different charge-balancing cations.

| | Mole of Fe per gram catalyst (mmol/g) | |
|---|---|---|
| Catalysts | Fully-exchanged | Partially exchanged |
| Fe/H-Y | 5.8 | 3.0 |
| Fe/$NH_4$-Y | 5.9 | 3.0 |
| Fe/Na-Y | 5.8 | 2.8 |

### 4.3.2 Photo-oxidation of formaldehyde

The FA conversion given by the completely exchanged zeolite Y catalysts (Figure 4.4) exhibited no significant difference at the same pH conditions, indicating $Fe^{3+}$ could be the only charge-balancing cation present in these catalysts and, therefore, they are identical in chemical nature regardless of the original cations ($H^+$, $NH_4^+$ and $Na^+$). The results clearly illustrate that FA conversion at pH 3 (28.6%) is almost 2 times higher than that obtained at pH 7 (14.5%). The low FA conversion at pH 7 could be attributed to the hydrolysis of ferric ions into iron oxyhydroxide (FeOOH) [5] which leached out from the zeolite and precipitated from the solution, resulting in loss of active Fe ions and the decrease in hydroxyl radical formation [6, 7]. Precipitation at the bottom of the reactor was readily observed from 60 min after the reaction began. This could also be inferred from the trend lines with the decreasing slope at both pH 3 and 7, suggesting the FA conversion rate decreased rapidly after 60 min with increasing iron precipitation in addition to the concentration effect on reaction rate. It is also clear that FA conversion at pH 7 reached a plateau earlier compared with the conversion at pH 3, which is consistent with the photo-Fenton oxidation of other organic pollutants at alkaline conditions reported in literature [8].

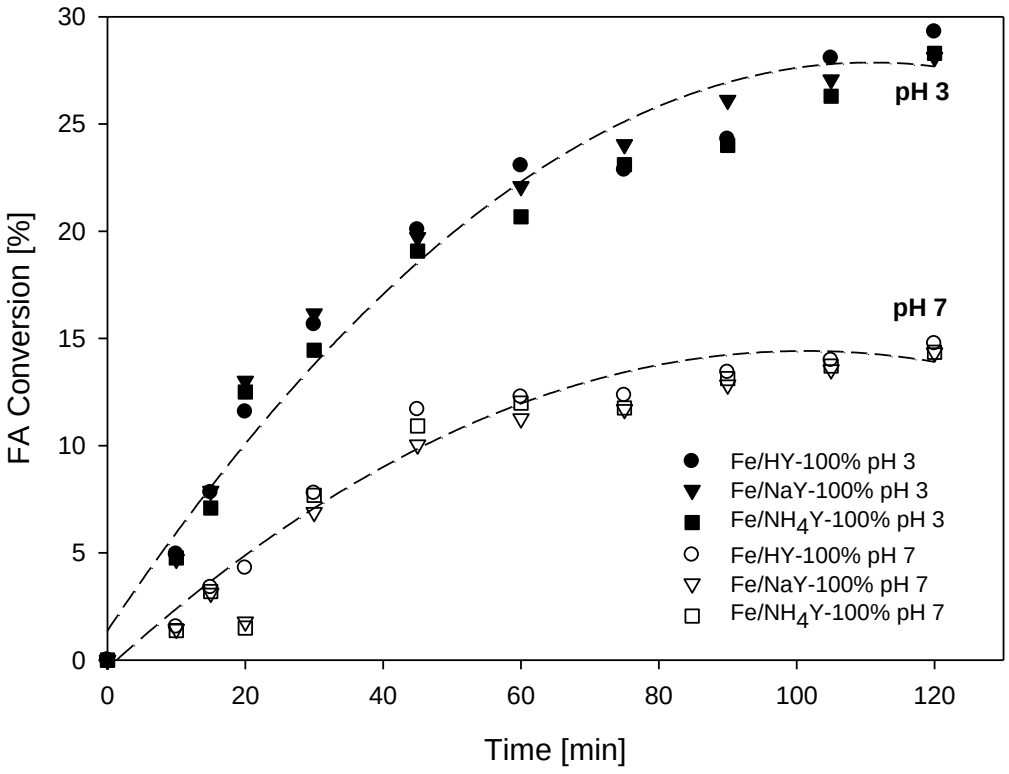


Figure 4.4 -The effect of solution pH on FA conversion catalysed by the fully-exchanged zeolite Y. [FA concentration = 25 ppm, 303 K, 1 × 8 W UVC, 0.5 g $L^{-1}$ catalyst loading].

To observe the effect of $H^+$, $NH_4^+$ and $Na^+$ on the photo-Fenton oxidation of FA, catalysts which were partially exchanged with $Fe^{3+}$ were prepared so that 50% of the original cations in the zeolite were replaced by $Fe^{3+}$ and the remaining cations were $H^+$, $NH_4^+$ or $Na^+$. The partially exchanged catalysts are denoted as Fe/H-Y-pe, Fe/$NH_4$-Y-pe and Fe/Na-Y-pe. The conversion of FA at pH 7 over the three forms of zeolite Y is shown in Figure 4.5. The results here point out explicitly that the performance of Fe/H-Y-pe is not limited by the alkaline reaction condition as much as $Na^+$ and $NH_4^+$ form of zeolite. The fast reaction rate given by Fe/H-Y-pe, and hence a much higher FA conversion at 120 min (26%), suggests that the presence of Brønsted acid sites ($H^+$) in the zeolite potentially provides a localized acidic reaction environment for the nearby $Fe^{3+}$. The spatial confinement inside the supercage of zeolite Y (diameter of 1.19 nm, 0.74 nm window of 12-ring) [9] ensures the surface $H^+$ and $Fe^{3+}$ are in close proximity at molecular scales. This condition mitigates the typical metal leaching/precipitation problem of supported $Fe^{3+}$ at pH 7. The catalytic cycle involving $Fe^{3+}/Fe^{2+}$ in the presence of UVC light thus maintains the facile generation of hydroxyl radicals from $H_2O_2$ for effective FA oxidation, even though the bulk solution is of pH 7. As the localized acidic environment depends on the steric effect as well as the proximity of the $H^+$ to $Fe^{3+}$, zeolites with a high Si/Al ratio (hence low acid site density) and large channels are unlikely to possess the effect of the surface $H^+$ on photo-Fenton reaction at alkaline pH.

In fact, Fe/ H–Y–pe achieved a higher FA conversion (26%) than catalytic ozonation with $TiO_2$ anatase) at a similar pH where only 18% decrease of FA was recorded after 120 min although with a much higher catalyst loading (5 g $L^{-1}$) [10]. The result in Figure 4.5 further shows that the completely exchanged catalyst (Fe/H–Y–100%) without any available $H^+$ only gave 14.8% FA conversion at pH 7, suggesting the difference in the environment of the two channels, i.e. Fe/H–Y–pe and Fe/H–Y–100%. The synergetic effect given by $Fe3^+$ and $H^+$ is also highlighted because the performance of Fe/$NH_4$–Y–pe and Fe/Na–Y–pe only gave 6.7% and 8.4% FA conversion, respectively, after 120 min. Clearly, the presence of NH4+ and Na+ in the zeolite channel does not offer the advantage of localized acidic environment for photo-Fenton reaction. While the present work focuses on the effect of the unique catalytic environment inside the microporous channel induced by $H^+$, the identity of the end products (humic acid or $CO_2/H_2O$) is not a particular concern, although our liquid chromatography analysis primarily showed that no humic acid was present in all cases.

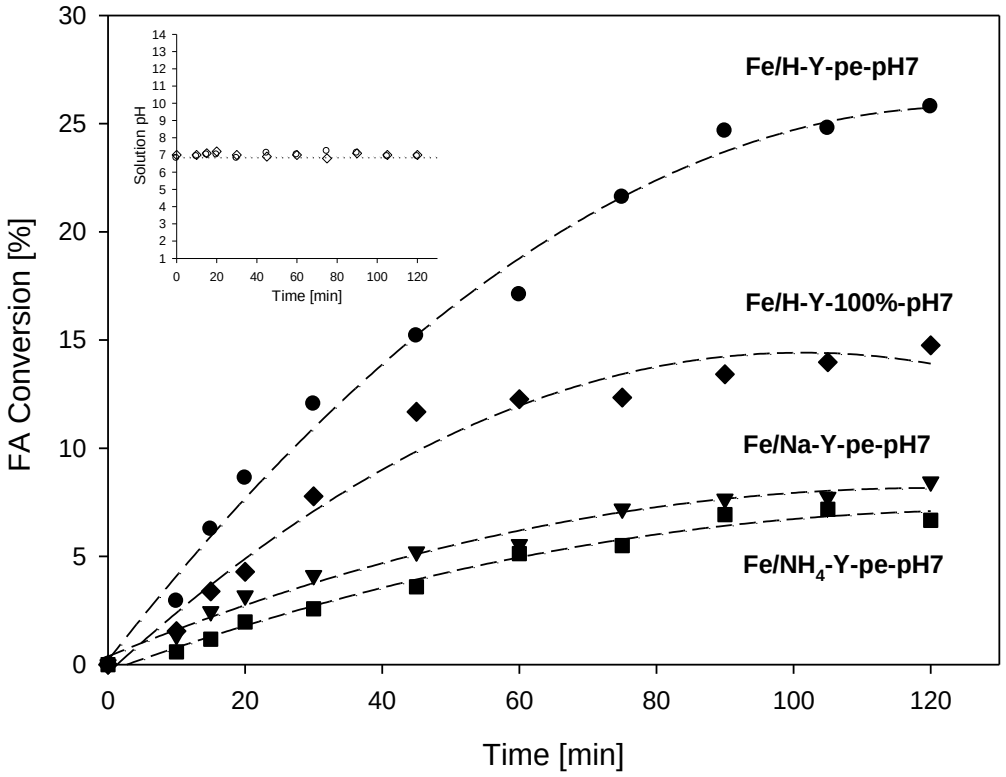


Figure 4.5 - FA conversion catalysed by the partially-exchanged zeolite Y at pH 7. Inset: solution pH during the course of reaction. [FA concentration = 25 ppm, 303 K, 1 × 8 W UVC, 0.5 g $L^{-1}$ catalyst loading].

The result further shows that the fully exchanged catalyst (Fe/H-Y-100%) without any available $H^+$ only gave 14.8% FA conversion at pH 7. The difference of the environment of the two channels, i.e. Fe/H-Y-pe and Fe/H-Y-100%, is depicted graphically by Figure 4.6. The synergetic effect given by $Fe^{3+}$ and $H^+$ is also highlighted because the performance of Fe/$NH_4$-Y-pe and Fe/Na-Y-pe only gave 6.7% and 8.4% FA conversion, respectively, after 120 min. Clearly, the presence of $NH_4^+$ and $Na^+$ in the zeolite channel does not offer the advantage of localized acidic environment for photo-Fenton reaction. While the present work focuses on the effect of the unique catalytic environment inside the microporous channel induced by $H^+$, the identity of the end products (humic acid or $CO_2$/$H_2O$) is not of particular concern although our liquid chromatography analysis primarily showed that no humic acid was present in all cases.

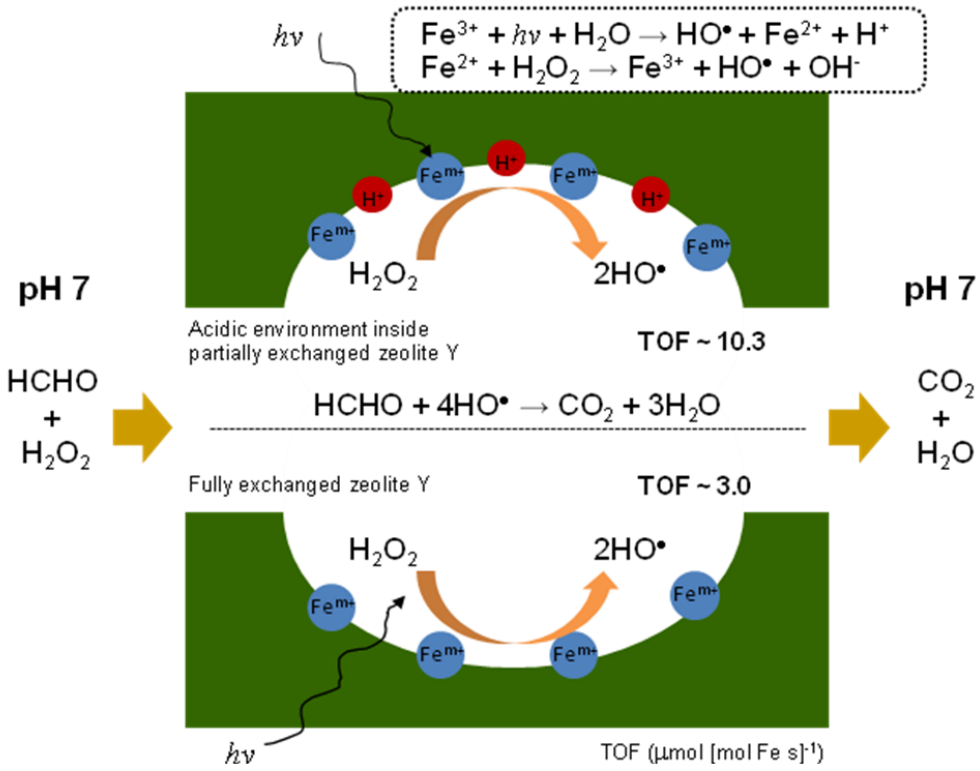


Figure 4.6 - The localized acidic environment available inside the supercage of the partially-exchanged zeolite Y (above the dotted line) and the supercage environment of the fully-exchanged zeolite Y (below the dotted line) .

It is worthwhile to point out that there were no significant changes in solution pH in the course of reaction catalysed by Fe/H-Y-pe and Fe/H-Y-100% as shown in the inset of Figure 4.5. The solution pH was kept almost constant at 7 for both cases, suggesting the given catalyst loading, i.e. 0.5 g $L^{-1}$, does not cause pH to decrease although the catalyst is slightly acidic in nature. Thus, the improvement of FA conversion given by Fe/H-Y-pe could be attributed to the presence of proton inside the microporous channel environment of the zeolite, instead of resulting from the pH effect that may be given directly by the addition of the catalyst. It is also important to note that such an increase in reaction rate at alkaline pHs specifically by the proton in the zeolite channel could only be manifested when the catalyst loading is low (~ 0.5 g $L^{-1}$). The FA conversion at initial pH 7 by Fe/H-Y-pe with different catalyst loading (Figure 4.7) suggests that 2.0 g $L^{-1}$ loading gave a significantly higher FA conversion than 0.5 g $L^{-1}$ (43% vs. 26% at 120 min) because more Fe active sites are available. With 2.0 g $L^{-1}$ loading, however, the solution pH decreased remarkably from its initial value of 7 to 3.5 as soon as the catalyst was added (inset of Figure 4.7). Therefore, the high FA conversion at higher catalyst loadings is more appropriately attributed to the solution pH effect rather than the proton effect within the zeolite channel. Moreover, the result may also indicate that the relationship between the solution pH and the amount of acid sites from the solid catalyst are not linear. The high

FA conversion (43%) achieved by 2.0 g $L^{-1}$ of Fe/H–Y–pe is comparable to the photo-Fenton process reported by Kajitvichyanukul et al. at pH 2.6 where 45% of FA was oxidized [11].

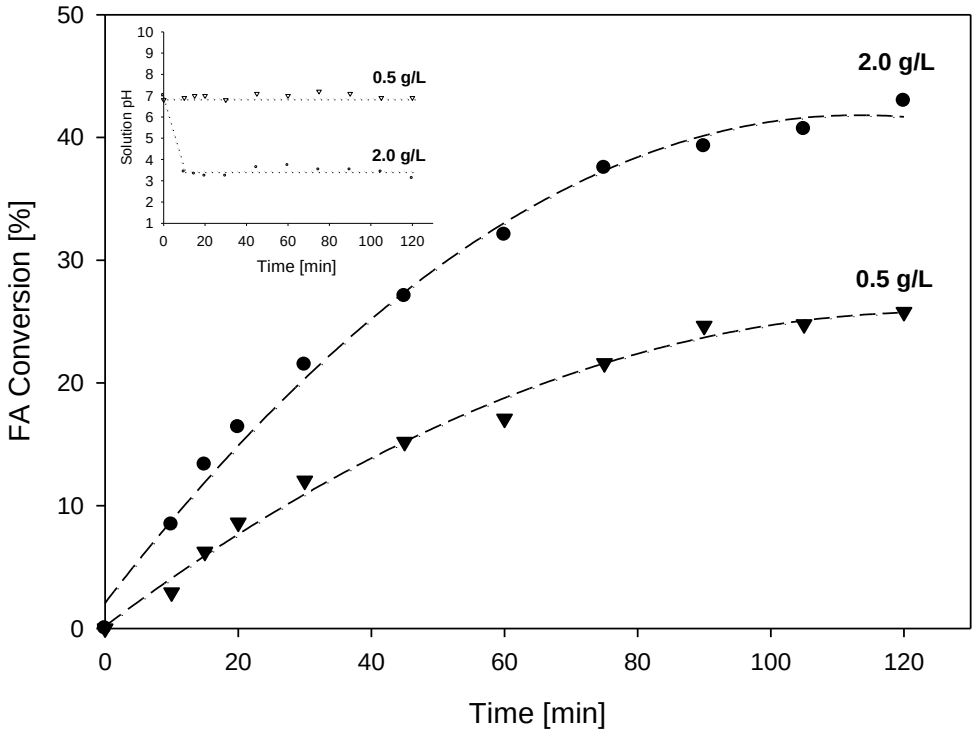


Figure 4.7. The effect of catalyst loading (Fe/H-Y-pe) on FA conversion. Inset: solution pH during the course of reaction. [FA concentration = 25 ppm, 303 K, 1 × 8 W UVC, initial solution pH = 7].

It is best to refer the reaction rate to the number of Fe active sites, i.e. turnover frequency (TOF), which is defined as the catalytic cycle turns over per unit time. Although the values of TOF are only approximate because of the approximations made in counting sites, it could reveal the influence of the $H^+$ present in the channel on the adjacent $Fe^{3+}$. The effect of $H^+$ sites in the zeolite on FA conversion at pH 7 is demonstrated by the TOF of Fe/H-Y, Fe/$NH_4$-Y and Fe/Na-Y Table 4.2.

Table 4.2 - TOF for FA conversion under photo-Fenton conditions with zeolite Y containing different charge-balancing cations at 303 K.

| | TOF (mmol [mol Fe s]$^{-1}$) at pH 7 | |
|---|---|---|
| Catalysts | Fully-exchanged | Partially exchanged |
| Fe/H-Y | 3 | 10.3 |
| Fe/$NH_4$-Y | 2.9 | 2.7 |
| Fe/Na-Y | 2.9 | 3.4 |

The TOF of the partially exchanged Fe/H-Y (10.3 µmol [mol Fe s]$^{-1}$) was more than 3 times higher than that of the partially exchanged Fe/NH-$_4$-Y (2.7 µmol [mol Fe s]$^{-1}$) and Fe/Na-Y (3.4 µmol [mol Fe s]$^{-1}$). This result gives further evidence to the role of $H^+$ in providing a localized acidic environment which promotes the photo-Fenton oxidation of FA. The TOF of Fe/$NH_4$-Y was slightly lower than that of Fe/Na-Y possibly because the channel environment of the zeolite Y was slightly alkaline in the presence of $NH_4^+$. This may have inhibited the generation of hydroxyl radicals and, to a certain extent, catalysed the conversion of $Fe^{3+}$ to less catalytically active iron species. This could be similar to the heterogeneous photo-Fenton reaction generally observed in the solution of high pH [8]. On the other hand, the TOF of the three catalysts which were fully-exchanged with $Fe^{3+}$ are considered the same (2.9 ~ 3.0 µmol [mol Fe s]$^{-1}$), suggesting that $H^+$, $NH_4^+$ and $Na^+$ were absent from the structure. Lastly, it is possible to prepare zeolite-supported catalysts with Brønsted acid sites with weaker acidity by incorporating Boron or Gallium atoms into the framework instead of Al [12]. It might be useful to investigate the effect of different acid strengths on the turnover rate to further understand the catalytic site requirement for photo-Fenton reaction at alkaline conditions.

## 4.4 Conclusions

The charge-balancing cations in zeolite play a vital role in photo-Fenton oxidation of formaldehyde. The Fe-zeolite Y with Brønsted acid sites ($H^+$) prepared by partial ion-exchange exhibited reaction rates and conversions that are significantly higher than that given by the same catalysts containing $NH_4^+$ or $Na^+$. The TOF given by Fe/H-Y, Fe/$NH_4$-Y and Fe/Na-Y at pH 7 are 10.3, 2.7 and 3.4 μmol [mol Fe s]$^{-1}$, respectively.

The remarkable performance of Fe/H-Y could be due to the localized acidic environment resulted from the $H^+$ inside the supercage of zeolite Y. The spatial confinement inside the zeolite ensures $H^+$ and $Fe^{3+}$ are in close proximity thus the photo-Fenton reaction could occur in an acid medium within the supercage, even though the bulk solution is alkaline (pH ~7). Increasing catalyst loading increases FA conversion but the solution pH is inevitably affected owing to the acidic nature of the catalyst.

The catalytic site requirement described in this Chapter can only be manifested at low catalyst loading and is rarely observed. It can be concluded that the results shown here could provide a simple solution to the fundamental pH problem in photo-Fenton catalysis, albeit with the trade offs of low catalyst concentrations and iron loading.

## 4.5 References


1. Macedo, J.d.S., et al., *Kinetic and calorimetric study of the adsorption of dyes on mesoporous activated carbon prepared from coconut coir dust.* Journal of Colloid and Interface Science, 2006. **298**(2): p. 515-522.
2. Bienert, G.P., J.K. Schjoerring, and T.P. Jahn, *Membrane transport of hydrogen peroxide.* Biochimica et Biophysica Acta (BBA) - Biomembranes, 2006. **1758**(8): p. 994-1003.
3. Pei, J. and J.S. Zhang, *Critical review of catalytic oxidization and chemisorption methods for indoor formaldehyde removal.* HVAC&R Research, 2011. **17**(4): p. 476-503.
4. Roque-Malherbe, R., J. Oñ ate-Martinez, and E. Navarro, *Furfural oligomerization within H-Fe-FAU zeolite.* Journal of Materials Science Letters, 1993. **12**(13): p. 1037-1038.
5. Huston, P.L. and J.J. Pignatello, *Degradation of selected pesticide active ingredients and commercial formulations in water by the photo-assisted Fenton reaction.* Water Research, 1999. **33**(5): p. 1238-1246.
6. Gogate, P.R. and A.B. Pandit, *A review of imperative technologies for wastewater treatment II: hybrid methods.* Advances in Environmental Research, 2004. **8**(3): p. 553-597.
7. Chen, Q., et al., *Heterogeneous photo-Fenton photodegradation of reactive brilliant orange X-GN over iron-pillared montmorillonite under visible irradiation.* Journal of hazardous materials, 2009. **168**(2): p. 901-908.
8. Soon, A.N. and B. Hameed, *Heterogeneous catalytic treatment of synthetic dyes in aqueous media using Fenton and photo-assisted Fenton process.* Desalination, 2011. **269**(1): p. 1-16.
9. Baerlocher, C., L.B. McCusker, and D.H. Olson, *Atlas of zeolite framework types*. 2007: Access Online via Elsevier.
10. Moussavi, G., A. Yazdanbakhsh, and M. Heidarizad, *The removal of formaldehyde from concentrated synthetic wastewater using O 3/MgO/H 2 O 2 process integrated with the biological treatment.* Journal of hazardous materials, 2009. **171**(1): p. 907-913.
11. Kajitvichyanukul, P., M.-C. Lu, and A. Jamroensan, *Formaldehyde degradation in the presence of methanol by photo-Fenton process.* Journal of Environmental Management, 2008. **86**(3): p. 545-553.
12. Beyer, H.K. and G. Borbely, *Transalkylation of Alkylaromatic Compounds on Silicates with ZSM-5 Structure Containing Al, B, and Ga*, in *Studies in Surface Science and Catalysis*, A.I. Y. Murakami and J.W. Ward, Editors. 1986, Elsevier. p. 867-874.

# 5 BIMETALLIC ZEOLITE Y PHOTOCATALYSTS FOR WIDE PH RANGE PHOTO-OXIDATION OF METHYLENE BLUE

## 5.1 Introduction

While the results of Chapter 4 present an effective catalyst for photo-Fenton reaction at alkaline conditions, it is only able to be used at low catalyst concentrations (~0.5 g/L), and with only partial iron loading on the catalyst. Therefore, it is desirable to create a catalyst that can be used at higher concentrations to enable better conversion per gram of catalyst used. One method to enhance the effective pH of an iron based Fenton catalyst is to add copper, to create a bimetallic catalyst[1, 2]. Copper-iron bimetallic catalysts have been shown to be more stable and effective over a wide range of pH [3] than iron by itself. Due to the difficulties arising from using wet ion exchange with two separate metal species, incipient wetness ion impregnation was used in this section, as it allows for better control of the metal content of the zeolites. Therefore, the work in this Chapter describes the synthesis and testing of an iron-copper zeolite-Y bimetallic photocatalyst for the oxidation of methylene blue.

## 5.2 Experimental

### 5.2.1 Chemicals used

All chemicals were used as received, except where indicated. The following chemicals were purchased from Sigma-Aldrich; copper (II) nitrate 98%, iron (III) chloride 98%, iron (III) nitrate nonahydrate (>98%), methylene blue 99%. $NH_4$-zeolite Y was obtained from Zeolyst International. Hydrogen peroxide (30% w/v) was purchased from Fisher Scientific. De-ionized water was obtained from a Millipore Milli-Q system.

### 5.2.2 Synthesis techniques

Incipient wetness ion impregnation (IWI) was used to prepare the catalysts. A specific concentration of iron/copper nitrate solution was made to contain the intended weight % iron or copper in a volume equal to that of the internal pores of the zeolite sample (1g $NH_4$-Y (Si/Al = 2.6) was typically used). For the bimetallic catalyst a solution containing both iron and copper nitrate at the desired concentrations was used. The specified volume of metal nitrate solution was then added dropwise to the dried zeolite sample, and vigorously stirred. No excess liquid was observed for any of the synthesises. The zeolite was then dried at 343 K in a drying oven before being calcined in a horizontal tube furnace at 773 K for 10 h under flowing air [1]. All catalysts were synthesised to have a nominal 4% weight metal (copper or iron). The catalyst referred to herein as FeCu-Y was

synthesised to have 4% weight of both copper and iron, with FeCu-Y-50% synthesised with 2% weight both copper and iron, for a total of 4% weight metal.

The calcined catalyst was then washed in dilute (pH 3) sulfuric acid at a catalyst loading of 1 g $L^{-1}$ for 30 minutes to remove any loosely attached metal oxide particles, then filtered and dried at 343 K.

### 5.2.3 Catalyst characterisation

Temperature Programmed Reduction (TPR) was carried out using the TCD within a gas chromatograph (Buck Scientific 910 GC), by bypassing the columns and inlet injector. The reduction was carried out in a vertical tubular furnace (MTI-GSL1100) with temperature monitored by thermocouple probe onto the reactor bed. 300 mg of catalyst was used for each reduction run. A 20°C $min^{-1}$ heating rate was used. Hydrogen concentration was 10% with Argon as the carrier gas (20 mL $min^{-1}$ total gas flow). A silica cooling trap was used to remove water from the outlet gases before entering the TCD.

X-ray powder diffraction (XRD) data of the synthesized catalysts products was collected on a Philips PW1700 computer-controlled diffractometer with a graphite monochromator and Co Kα radiation, weighted mean wavelength 1.79026 Angstroms.

The surface topologies of the catalysts were observed by field emission scanning electron microscopy (SEM) on a JEOL 7000F FE-SEM.

### 5.2.4 Photo-oxidation of methylene blue

The photo-oxidation of methylene blue was carried out under 8W UVC irradiation at room temperature and in open air. The UVC lamp was placed in a quartz tube which was submerged in the centre of a 500mL beaker. The catalyst was added to 200 mL of MB aqueous solution (typically 50 mg/L MB). The solution was heated to 30°C and the catalyst was added and given time to reach an adsorption equilibrium. The pH was adjusted using 0.01M $H_2SO_4$ or 0.01M NaOH as needed, after the catalyst was added, as the results from Chapter 4 show that high concentrations of certain zeolites can lower the solution pH. Hydrogen peroxide was added at a 1:26 MB:$H_2O_2$ molar ratio. Stirring was maintained throughout the reaction at a rate of 500 RPM.

The methylene blue concentration was examined by measuring the absorbance of sample at the maximum absorbance wavelength for methylene blue, 664 nm, using a VWR UV-1600 PC

Spectrophotometer with a 1cm path length spectrometric glass cell. Samples were filtered and then diluted as necessary to ensure the concentration measured was within the linear relationship between absorbance and concentration for methylene blue. The total organic carbon of the solution was measured on a Shimadzu TOC-L total organic carbon analyser. Samples were filtered and centrifuged to removal any remaining catalyst particles.

The reusability of the FeCu-Y catalyst was examined during three consecutive cycles. To limit losses of catalyst through TOC sample filtration, only the degradation of colour was monitored for the subsequent cycles. After each cycle the catalyst was filtered and washed with DI water, before being dried at 80°C and reused. As some catalyst was lost in the recovery step, each subsequent cycle was carried out at a volume that allowed the catalyst loading to be maintained.

## 5.3 Results and Discussion

### 5.3.1 Catalyst characterisation

The XRD patterns of zeolite H–Y before and after incipient wetness ion impregnation with $Cu^{2+}$, $Fe^{3+}$, or both $Cu^{2+}$ and $Fe^{3+}$ (Figure 5.1– XRD ) show that they are in crystalline phase and that all six samples have a typical zeolite Y type (faujusite) structure. As the ion impregnation did not alter the d-spacing on the lattice structure of H–Y, it is inferred that ions are present in the zeolite as surface cations. The XRD pattern of the FeCu-Y catalyst after recycle testing indicate that crystallinity has been maintained though-out the experiment.

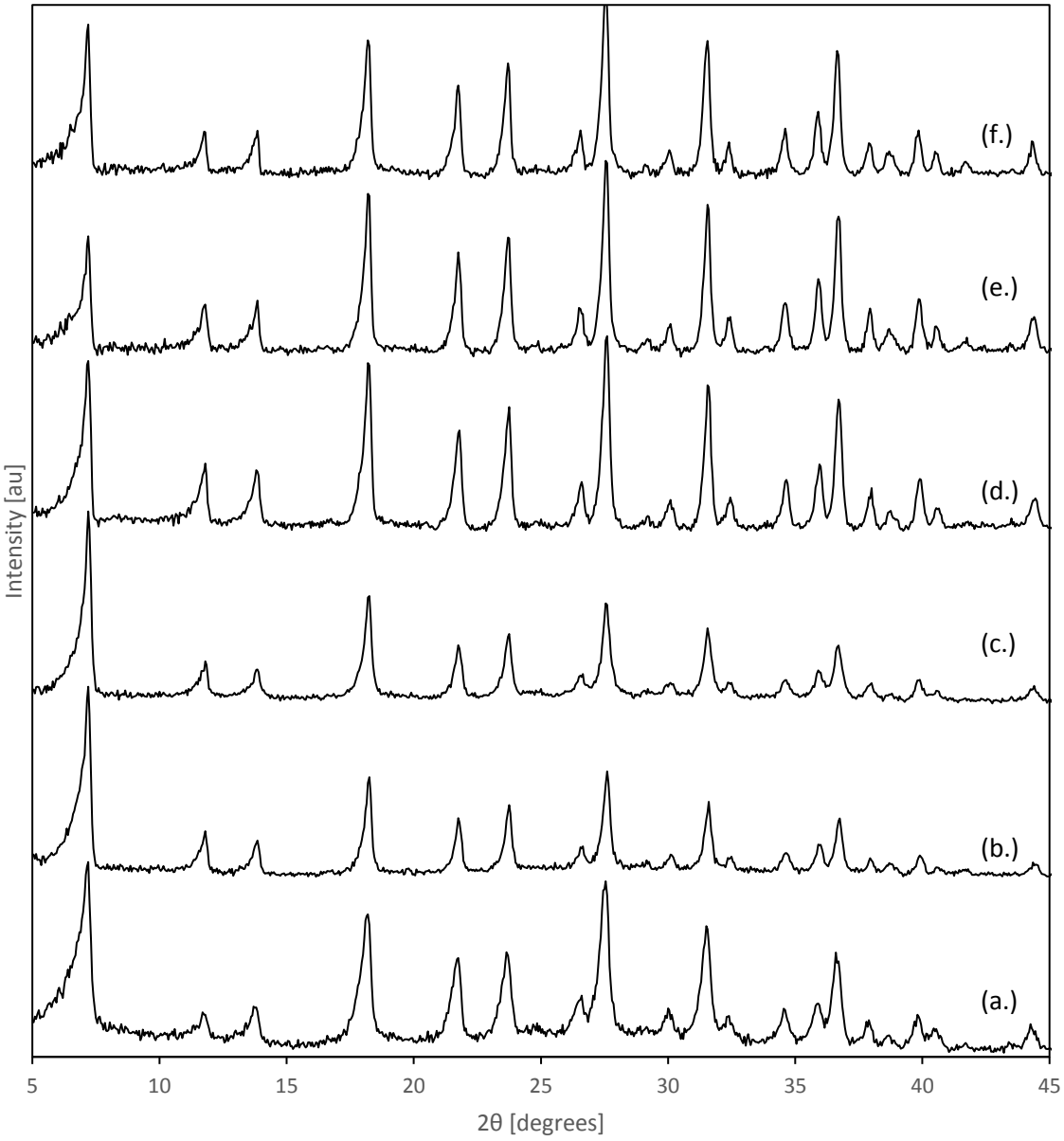


Figure 5.1– XRD patterns for (a.) H-Y, (b.) IWI Fe-Y, (c.) IWI Cu-Y, (d.) IWI-FeCu-Y-50%, (e.) IWI FeCu-Y, (f.) IWI FeCu-Y post recycle (3 runs).

Figure 5.2 shows the surface morphologies of the parent H-Y, and Fe-Y and FeCu-Y syunthesised by incipient wetness method. When comparing the SEM images of the parent H-Y with the two catalysts synthesised by incipient wetness method, it can be observed that no change has occurred in the surface morphology of the catalysts, with all remaining smooth, indicating there are no copper or iron particles deposited on the surface. This suggests that the iron and copper are dispersed homogeneously throughout the zeolite.

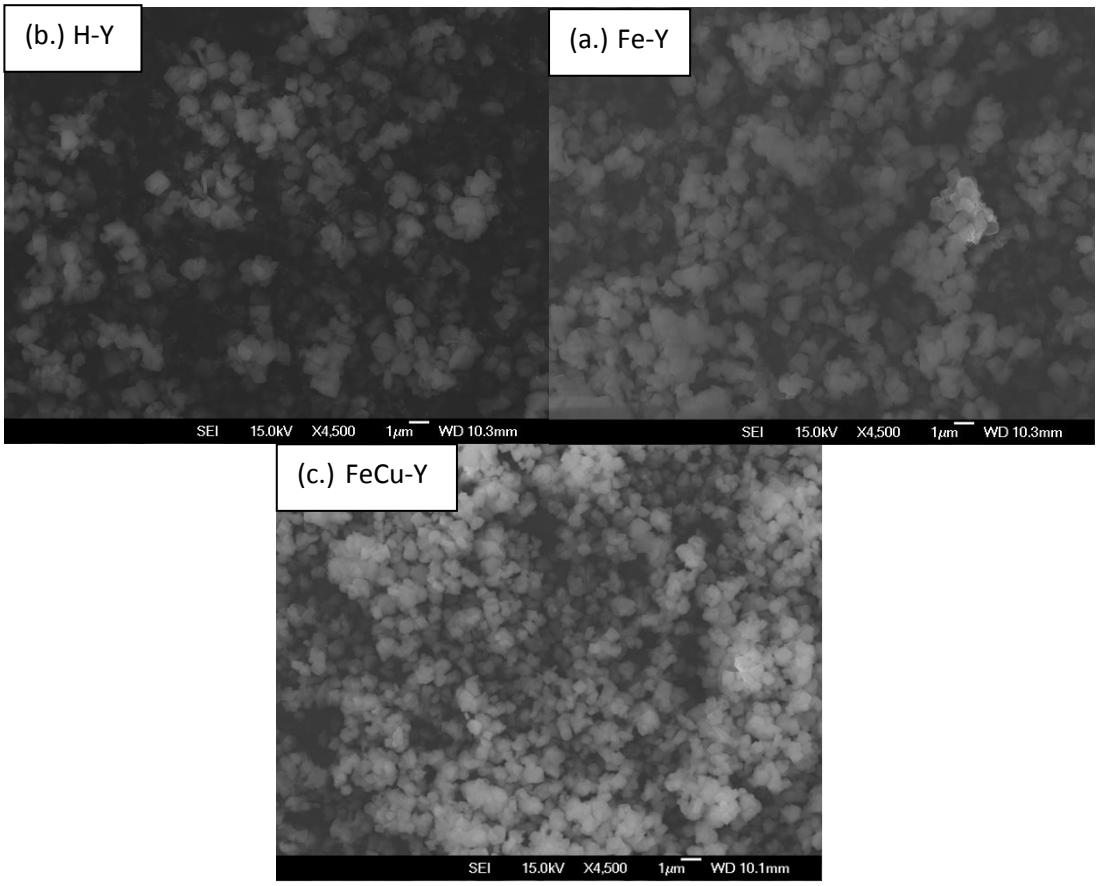


Figure 5.2 - SEM images of (a.) H-Y, (b.) Fe-Y prepared by incipient wetness method, (c.) FeCu-Y prepared by incipient wetness method.

Temperature Programmed Reduction (TPR) was carried out at a 20°C $min^{-1}$ heating with 20 mL $min^{-1}$ 10% $H_2$ in Ar. Due to limitations of the reactor used, a maximum temperature of 850°C was achieved for the reduction of the catalysts. This is a lower temperature than the reduction peak (>900°C) for some species of iron that have previously been found in iron zeolites [4], however the low temperature results can still be used to qualatatively reveal whether the two metals in the bimetallic catalyst are in contact or not, as once the metal with the lower reduction temperature

becomes metallic it will catalyse the reduction of any higher reduction temperature metal that it is in contact with [5].

Figure 5.3 shows no clear $H_2$ consumption peak was observed for H-Y. The peaks observed for Cu-Y and Fe-Y are typical for such materials [6], with another peak likely for Fe-Y if heating had continued past 900°C [5]. The reduction peak that should be around 630°C of the copper shifts to a lower temperature in the bimetallic catalyst, indicating that there is interaction between the iron and copper species present in the framework.

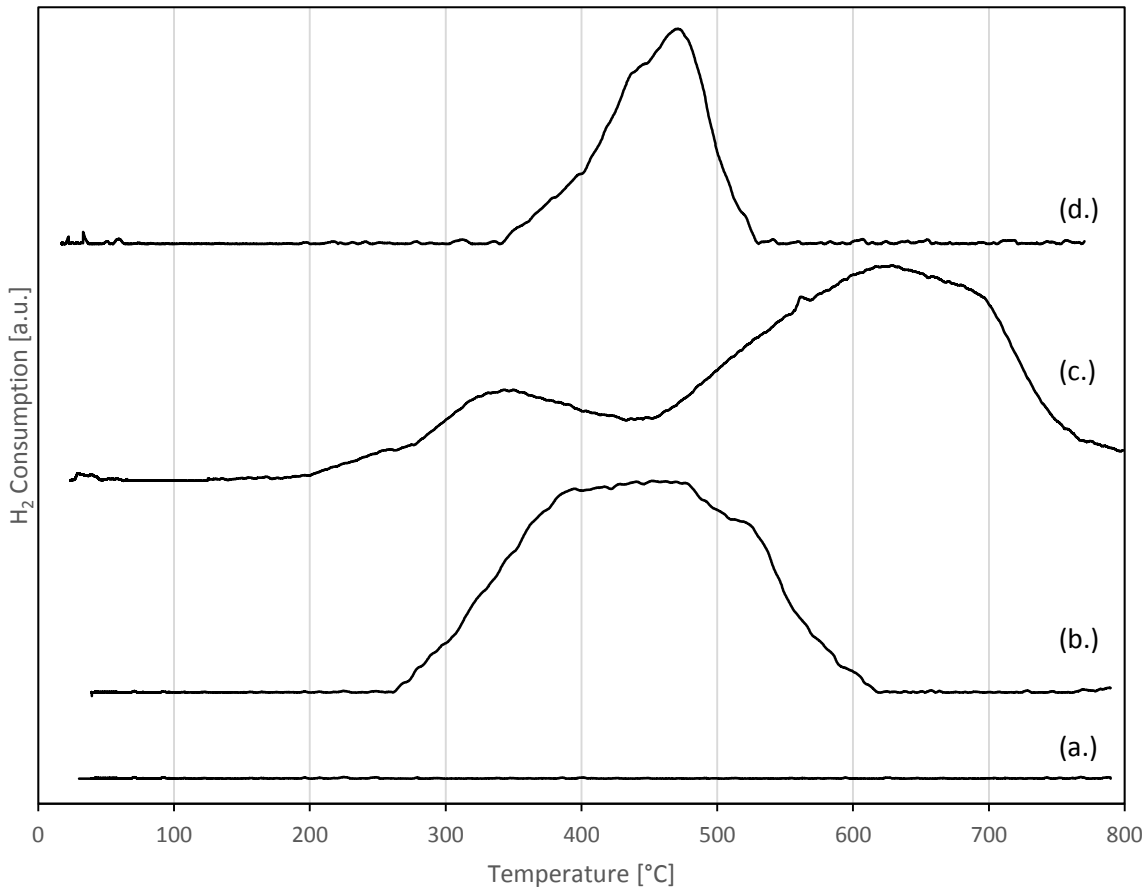


Figure 5.3 – TPR results for (a.) H-Y, (b.) FeCu-Y, (c.) Cu-Y, (d.) Fe-Y.

### 5.3.2 Photo-oxidation of methylene blue

To ensure that the catalyst synthesized by incipient wetness ion impregnation (IWI) was not inferior to that which was synthesized by wet ion exchange (IX), the degradation of methylene blue at pH 3 was assessed for Fe-Y catalysts synthesized by both methods (Figure 5.4). The experimental conditions are comparable to those for Figure 3.8, with the difference in the results for the ion

exchanged Fe-Y due to the catalyst loading in Figure 3.8 being 50 mg $L^{-1}$ compared to 1 g $L^{-1}$ for Figure 5.4. There were no significant differences observed between the two catalysts for the removal of TOC or of colour.

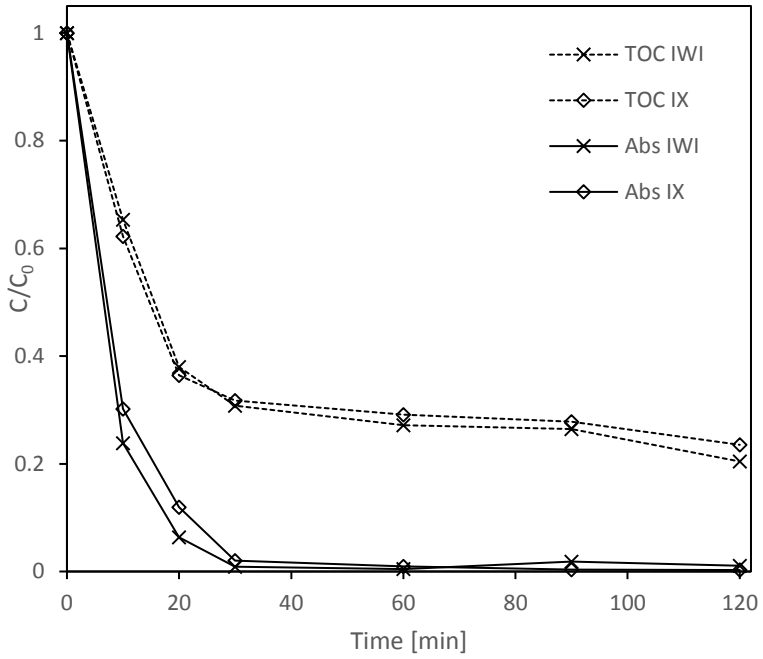


Figure 5.4 – Oxidation of methylene blue over Fe-Y prepared by (X) incipient wetness impregnation, (◊) ion exchange. Solid line is colour removal, dashed line is TOC. [50 mg/L MB, pH 3, 30°C, 1 g $L^{-1}$ catalyst , $H_2O_2$:MB = 26, 500RPM stirring, 8W UVC irradiation]

The catalytic activity of the incipient wetness synthesized catalysts was tested for the photo-oxidation of methylene blue at pH 3 (colour removal, Figure 5.5, TOC removal, Figure 5.6), pH 5 (colour removal, Figure 5.7, TOC removal, Figure 5.8), and pH 7 (colour removal, Figure 5.9, TOC removal, Figure 5.10). UV/$H_2O_2$ was tested under the same conditions as a control. The base zeolite H-Y was also tested, but showed no activity above the UV/$H_2O_2$ after the initial adsorption, so has not been shown on any of the following figures. The maximum TOC removal for Fe-Y was at pH 3, at 79.5% removal. The maximum TOC removal for FeCu-Y was also at pH 3, at 89.7% removal. The maximum TOC degradation for the Cu-Y catalyst was at pH 7, at 87.9% removal. This is comparable to the findings of Singh et al [7], who found that 1 g $L^{-1}$ Cu-Y degraded 80% of 0.143 mM Congo Red dye in 120 minutes. The congo red oxidation took place at 60°C in the presence of hydrogen peroxide, whereas the oxidation in this study on requires 30°C and UVC irradiation to achieve higher degradation. This demonstrates the advantages of the UV/copper Fenton-like reactions over the dark copper Fenton-like reactions.

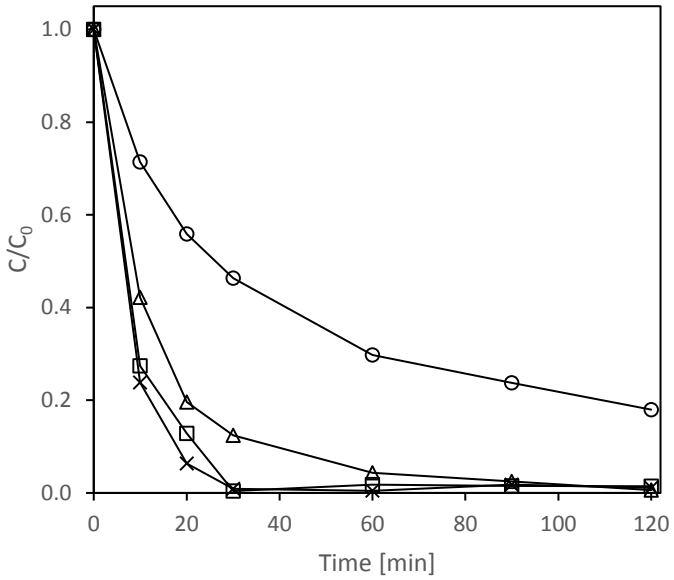


Figure 5.5 – Colour removal at pH 3 for (○) UV/$H_2O_2$, (Δ) Cu-Y, (X) Fe-Y, (□) FeCu-Y. [50 mg/L MB, 30°C, 1 g $L^{-1}$ catalyst (0 mg $L^{-1}$ catalyst for UV/$H_2O_2$), $H_2O_2$:MB = 26, 500RPM stirring, 8W UVC irradiation]

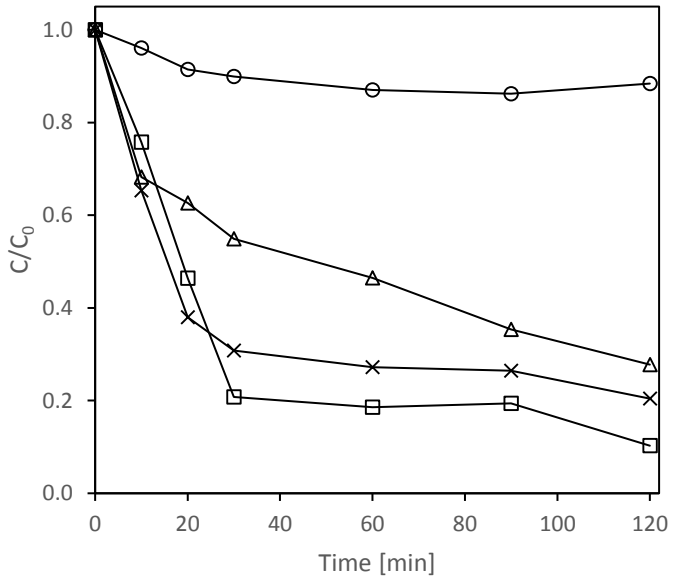


Figure 5.6 - TOC removal at pH 3 for (○) UV/$H_2O_2$, (Δ) Cu-Y, (X) Fe-Y, (□) FeCu-Y. [50 mg/L MB, 30°C, 1 g $L^{-1}$ catalyst (0 mg $L^{-1}$ catalyst for UV/$H_2O_2$), $H_2O_2$:MB = 26, 500RPM stirring, 8W UVC irradiation]

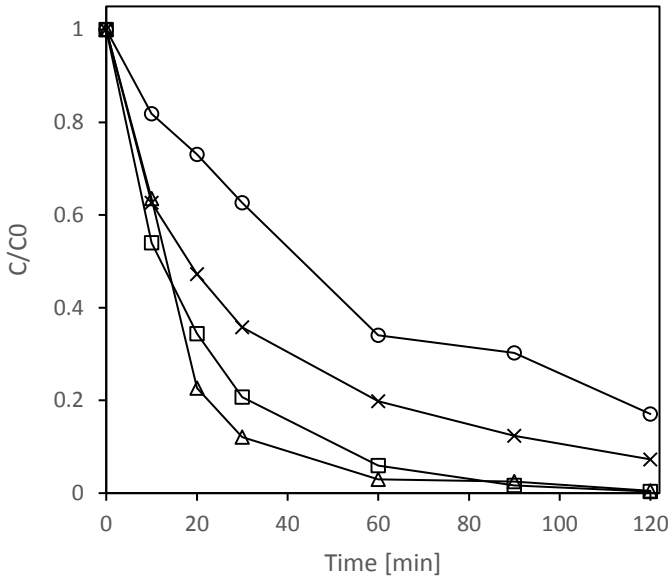


Figure 5.7 - Colour removal at pH 5 for (○) UV/$H_2O_2$, (Δ) Cu-Y, (X) Fe-Y, (□) FeCu-Y. [50 mg/L MB, 30°C, 1 g $L^{-1}$ catalyst (0 mg $L^{-1}$ catalyst for UV/$H_2O_2$), $H_2O_2$:MB = 26, 500RPM stirring, 8W UVC irradiation]

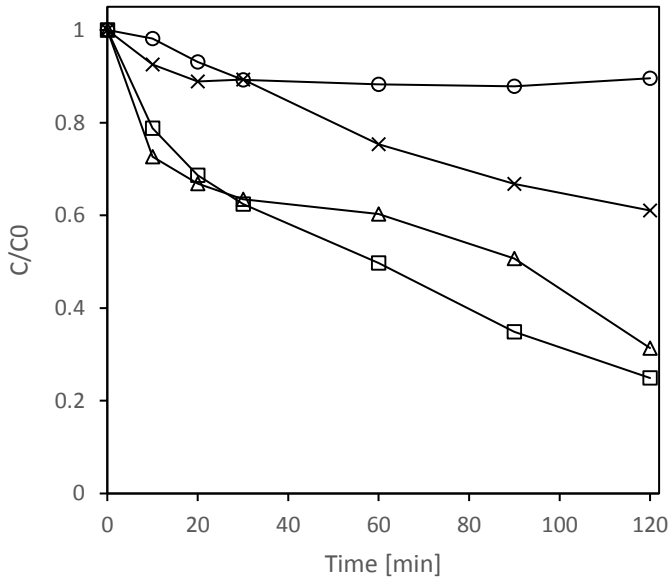


Figure 5.8 - TOC removal at pH 5 for (○) UV/$H_2O_2$, (Δ) Cu-Y, (X) Fe-Y, (□) FeCu-Y. [50 mg/L MB, 30°C, 1 g $L^{-1}$ catalyst (0 mg $L^{-1}$ catalyst for UV/$H_2O_2$), $H_2O_2$:MB = 26, 500RPM stirring, 8W UVC irradiation]

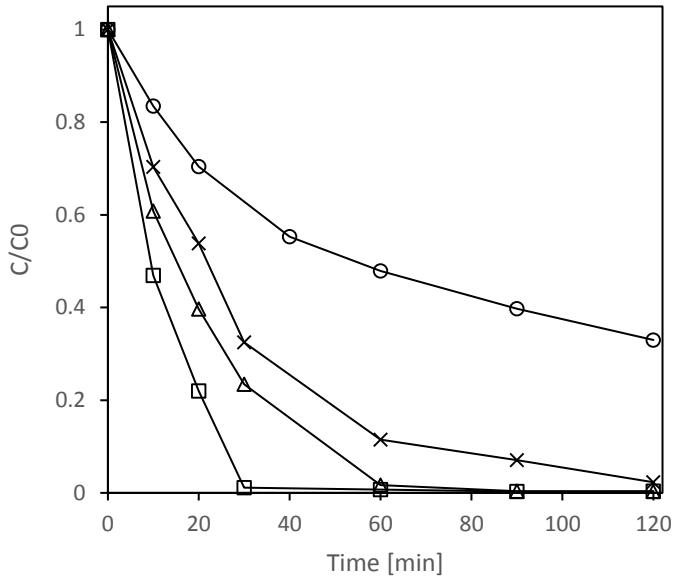


Figure 5.9 - Colour removal at pH 7 for (○) UV/$H_2O_2$, (Δ) Cu-Y, (X) Fe-Y, (□) FeCu-Y. [50 mg/L MB, 30°C, 1 g $L^{-1}$ catalyst (0 mg $L^{-1}$ catalyst for UV/$H_2O_2$), $H_2O_2$:MB = 26, 500RPM stirring, 8W UVC irradiation]

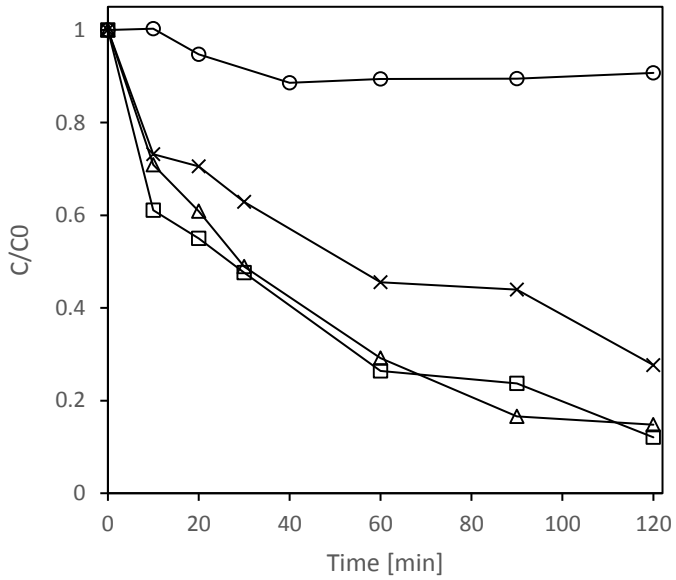


Figure 5.10 - TOC removal at pH 7 for (○) UV/$H_2O_2$, (Δ) Cu-Y, (X) Fe-Y, (□) FeCu-Y. [50 mg/L MB, 30°C, 1 g $L^{-1}$ catalyst (0 mg $L^{-1}$ catalyst for UV/$H_2O_2$), $H_2O_2$:MB = 26, 500RPM stirring, 8W UVC irradiation]

As the FeCu-Y catalyst has twice the total metal content of the Fe-Y and Cu-Y catalysts, there is the possibility that the increased oxidation rate for methylene blue is due to only the increase in metal active sites. Therefore, to test this theory, a catalyst (FeCu-Y-50%) with half the Fe and Cu

loading was synthesized using the same incipient wetness method. This catalyst was then compared with a physical mixture of the Fe-Y and Cu-Y catalysts. If there was no beneficial interaction between the iron and copper in the zeolite, then a physical mixture containing the same overall metal content, but with no possibility of interaction would show the same activity. Figure 5.11 shows the colour removal for the physical mixture, FeCu-Y-50% and FeCu-Y, at pH 5. Under these conditions, there is no significant difference between the three catalyst with colour removal rates of 97.0%, 96.7%, and 99.6% for the physical mixture, FeCu-Y-50% and FeCu-Y, respectively.

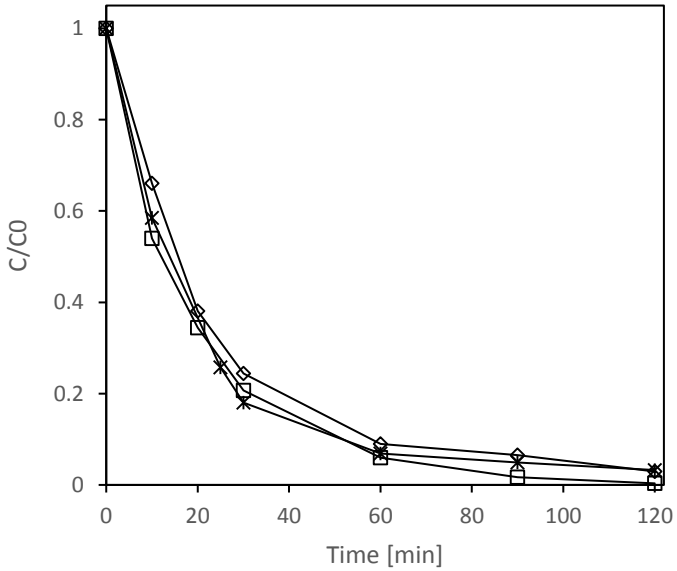


Figure 5.11 - Colour removal for (□) FeCu-Y, (*) FeCu-Y-50%, (◊) physical mixture of Fe-Y and Cu-Y. [50 mg/L MB, 30°C, 1 g $L^{-1}$ catalyst, pH 5, $H_2O_2$:MB = 26, 500RPM stirring, 8W UVC irradiation]

Figure 5.12 shows the TOC removal for the physical mixture, FeCu-Y-50% and FeCu-Y, at pH 5. This shows that the bimetallic catalyst FeCu-Y-50% has a better TOC removal, 69.6%, than the physical mixture of Fe-Y and Cu-Y, 57.7%. Therefore, it can be concluded that the catalytic ability of the bimetallic catalysts is not only due to the total metal content, but that there is a bimetallic synergistic effect.

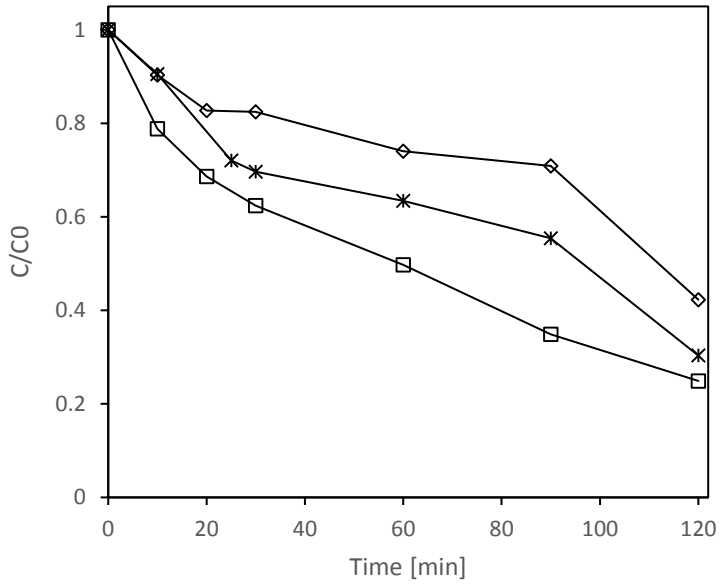


Figure 5.12 - TOC removal for (□) FeCu-Y, (*) FeCu-Y-50%, (◊) physical mixture of Fe-Y and Cu-Y. [50 mg/L MB, 30°C, 1 g $L^{-1}$ catalyst, pH 5, $H_2O_2$:MB = 26, 500RPM stirring, 8W UVC irradiation].

The reusability of the FeCu-Y catalyst was examined during three consecutive reaction cycles. While the colour removal over these cycles (Figure 5.13) remained the same, with 96% colour removal after 120 minutes for each run, the TOC removal over each run (not shown) decreased slightly with each run, going from 75% in the first run, to 72.4% in the second, and finally down to 71.6% in the third.

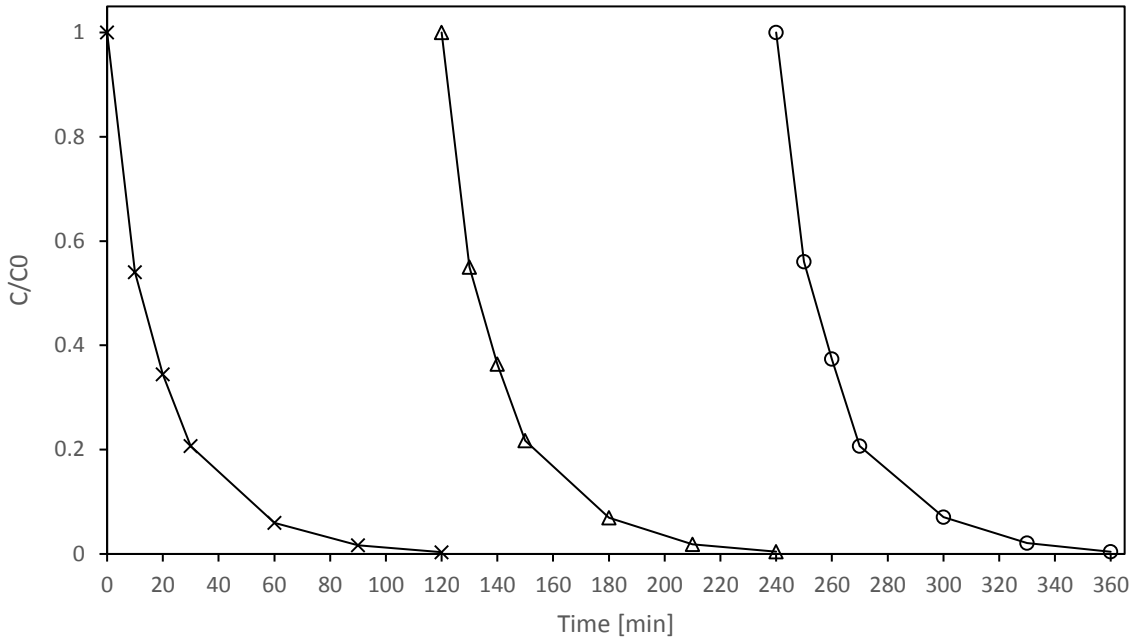


Figure 5.13 – Recycle for FeCu-Y [50 mg/L MB, 30°C, 1 g $L^{-1}$ catalyst, pH 5, $H_2O_2$:MB = 26, 500RPM stirring, 8W UVC irradiation].

The kinetics of colour removal (Figure 5.14) shows that the catalyst did not significantly degrade for the colour removal of methylene blue over the 3 catalytic runs. The pseudo-first order rate constants are 0.046 $min^{-1}$, 0.044 $min^{-1}$, and 0.044 $min^{-1}$ for the first, second and third run respectively. These results suggest that the bimetallic catalyst remains stable after these reaction runs, while being able to operate a significantly wider pH range than the iron-only Fe-Y catalyst. The XRD results also confirm that there is no loss in crystallinity after the third reaction cycle.

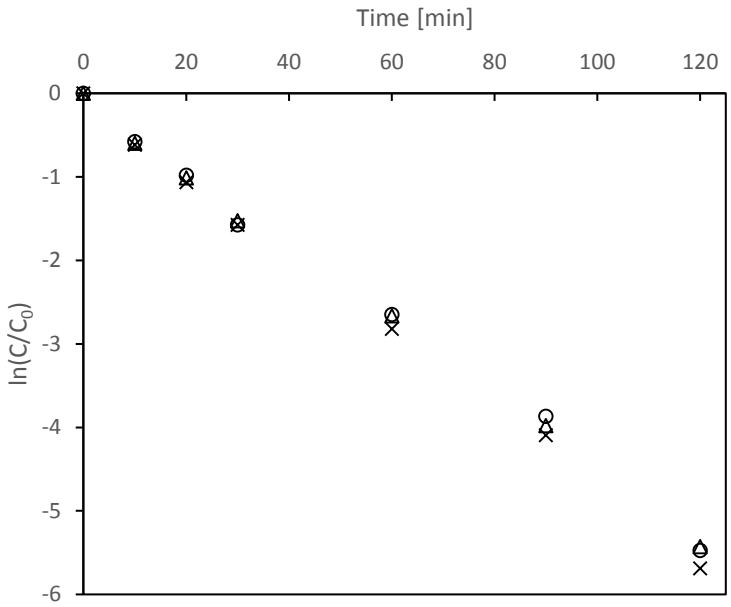


Figure 5.14 – Kinetics of recycle for FeCu-Y [50 mg/L MB, 30°C, 1 g $L^{-1}$ catalyst, pH 5, $H_2O_2$:MB = 26, 500RPM stirring, 8W UVC irradiation]

## 5.4 Conclusions

A bimetallic copper-iron catalyst was synthesized by incipient wetness ion impregnation of zeolite Y. This FeCu-zeolite Y catalyst was then tested for the photo-oxidation of methylene blue over a range of pHs. It was found to be effective at both low pH (pH3), with 98% colour removal and 89% TOC removal, and high pH (pH 7), with 99% colour removal and 79% TOC removal.

The bimetallic synergistic effect was revealed through the comparison of a physical mixture of Fe-Y and Cu-Y catalyst with the FeCu-Y-50% catalyst, which showed better catalytic ability for the TOC abatement at the same total metal weight. The bimetallic effect is likely due to the redox reactions between certain Fe and Cu species in the zeolite (Equation 2.12) providing additional avenues of regeneration of the primary hydroxyl generators ($Fe^{2+}$ and $Cu^{+}$).

Temperature programmed reduction of the bimetallic catalyst showed the iron and copper are well mixed inside the zeolite, and XRD and SEM showed that the zeolite structure remains unchanged after ion loading. The FeCu-zeolite Y catalyst was also tested under recycle and found to remain effective after 3 runs. The XRD results also showed no loss in crystallinity, indicating the catalyst support continued to be stable throughout the recycle.

## 5.6 References


1. Lam, F.L.Y. and X. Hu, *pH-Insensitive Bimetallic Catalyst for the Abatement of Dye Pollutants by Photo-Fenton Oxidation.* Industrial & Engineering Chemistry Research, 2013. **52**(20): p. 6639-6646.
2. Yip, A.C.-K., F. Leung-Yuk Lam, and X. Hu, *Novel bimetallic catalyst for the photo-assisted degradation of Acid Black 1 over a broad range of pH.* Chemical Engineering Science, 2007. **62**(18): p. 5150-5153.
3. Wang, Y., H. Zhao, and G. Zhao, *Iron-copper bimetallic nanoparticles embedded within ordered mesoporous carbon as effective and stable heterogeneous Fenton catalyst for the degradation of organic contaminants.* Applied Catalysis B: Environmental, 2015. **164**(0): p. 396-406.
4. Krishna, K., et al., *Selective Catalytic Reduction of NO with NH3 over Fe-ZSM-5 Catalysts Prepared by Sublimation of FeCl3 at Different Temperatures.* Catalysis Letters, 2002. **86**(1): p. 121-132.
5. Niemantsverdriet, J.W., *Temperature-Programmed Techniques*, in *Spectroscopy in Catalysis*. 2007, Wiley-VCH Verlag GmbH & Co. KGaA. p. 11-38.
6. Gentry, S.J., N.W. Hurst, and A. Jones, *Temperature programmed reduction of copper ions in zeolites.* Journal of the Chemical Society, Faraday Transactions 1: Physical Chemistry in Condensed Phases, 1979. **75**(0): p. 1688-1699.
7. Singh, L., P. Rekha, and S. Chand, *Cu-impregnated zeolite Y as highly active and stable heterogeneous Fenton-like catalyst for degradation of Congo red dye.* Separation and Purification Technology, 2016. **170**: p. 321-336.


1. Lam, F.L.Y. and X. Hu, *pH-Insensitive Bimetallic Catalyst for the Abatement of Dye Pollutants by Photo-Fenton Oxidation.* Industrial & Engineering Chemistry Research, 2013. **52**(20): p. 6639-6646.
2. Yip, A.C.-K., F. Leung-Yuk Lam, and X. Hu, *Novel bimetallic catalyst for the photo-assisted degradation of Acid Black 1 over a broad range of pH.* Chemical Engineering Science, 2007. **62**(18): p. 5150-5153.
3. Wang, Y., H. Zhao, and G. Zhao, *Iron-copper bimetallic nanoparticles embedded within ordered mesoporous carbon as effective and stable heterogeneous Fenton catalyst for the degradation of organic contaminants.* Applied Catalysis B: Environmental, 2015. **164**(0): p. 396-406.
4. Krishna, K., et al., *Selective Catalytic Reduction of NO with NH3 over Fe-ZSM-5 Catalysts Prepared by Sublimation of FeCl3 at Different Temperatures.* Catalysis Letters, 2002. **86**(1): p. 121-132.
5. Niemantsverdriet, J.W., *Temperature-Programmed Techniques*, in *Spectroscopy in Catalysis*. 2007, Wiley-VCH Verlag GmbH & Co. KGaA. p. 11-38.
6. Gentry, S.J., N.W. Hurst, and A. Jones, *Temperature programmed reduction of copper ions in zeolites.* Journal of the Chemical Society, Faraday Transactions 1: Physical Chemistry in Condensed Phases, 1979. **75**(0): p. 1688-1699.
7. Singh, L., P. Rekha, and S. Chand, *Cu-impregnated zeolite Y as highly active and stable heterogeneous Fenton-like catalyst for degradation of Congo red dye.* Separation and Purification Technology, 2016. **170**: p. 321-336.


8. Zhang, T., et al., *Selective catalytic reduction of NO with NH3 over HZSM-5-supported Fe–Cu nanocomposite catalysts: The Fe–Cu bimetallic effect.* Applied Catalysis B: Environmental, 2014. **148–149**(0): p. 520-531.


1. Lam, F.L.Y. and X. Hu, *pH-Insensitive Bimetallic Catalyst for the Abatement of Dye Pollutants by Photo-Fenton Oxidation.* Industrial & Engineering Chemistry Research, 2013. **52**(20): p. 6639-6646.
2. Yip, A.C.-K., F. Leung-Yuk Lam, and X. Hu, *Novel bimetallic catalyst for the photo-assisted degradation of Acid Black 1 over a broad range of pH.* Chemical Engineering Science, 2007. **62**(18): p. 5150-5153.
3. Wang, Y., H. Zhao, and G. Zhao, *Iron-copper bimetallic nanoparticles embedded within ordered mesoporous carbon as effective and stable heterogeneous Fenton catalyst for the degradation of organic contaminants.* Applied Catalysis B: Environmental, 2015. **164**(0): p. 396-406.
4. Krishna, K., et al., *Selective Catalytic Reduction of NO with NH3 over Fe-ZSM-5 Catalysts Prepared by Sublimation of FeCl3 at Different Temperatures.* Catalysis Letters, 2002. **86**(1): p. 121-132.
5. Niemantsverdriet, J.W., *Temperature-Programmed Techniques*, in *Spectroscopy in Catalysis*. 2007, Wiley-VCH Verlag GmbH & Co. KGaA. p. 11-38.
6. Gentry, S.J., N.W. Hurst, and A. Jones, *Temperature programmed reduction of copper ions in zeolites.* Journal of the Chemical Society, Faraday Transactions 1: Physical Chemistry in Condensed Phases, 1979. **75**(0): p. 1688-1699.
7. Singh, L., P. Rekha, and S. Chand, *Cu-impregnated zeolite Y as highly active and stable heterogeneous Fenton-like catalyst for degradation of Congo red dye.* Separation and Purification Technology, 2016. **170**: p. 321-336.

8. Zhang, T., et al., *Selective catalytic reduction of NO with NH3 over HZSM-5-supported Fe–Cu nanocomposite catalysts: The Fe–Cu bimetallic effect.* Applied Catalysis B: Environmental, 2014. **148–149**(0): p. 520-531.
1. Lam, F.L.Y. and X. Hu, *pH-Insensitive Bimetallic Catalyst for the Abatement of Dye Pollutants by Photo-Fenton Oxidation.* Industrial & Engineering Chemistry Research, 2013. **52**(20): p. 6639-6646.
2. Yip, A.C.-K., F. Leung-Yuk Lam, and X. Hu, *Novel bimetallic catalyst for the photo-assisted degradation of Acid Black 1 over a broad range of pH.* Chemical Engineering Science, 2007. **62**(18): p. 5150-5153.
3. Wang, Y., H. Zhao, and G. Zhao, *Iron-copper bimetallic nanoparticles embedded within ordered mesoporous carbon as effective and stable heterogeneous Fenton catalyst for the degradation of organic contaminants.* Applied Catalysis B: Environmental, 2015. **164**(0): p. 396-406.
4. Krishna, K., et al., *Selective Catalytic Reduction of NO with NH3 over Fe-ZSM-5 Catalysts Prepared by Sublimation of FeCl3 at Different Temperatures.* Catalysis Letters, 2002. **86**(1): p. 121-132.
5. Niemantsverdriet, J.W., *Temperature-Programmed Techniques*, in *Spectroscopy in Catalysis*. 2007, Wiley-VCH Verlag GmbH & Co. KGaA. p. 11-38.
6. Gentry, S.J., N.W. Hurst, and A. Jones, *Temperature programmed reduction of copper ions in zeolites.* Journal of the Chemical Society, Faraday Transactions 1: Physical Chemistry in Condensed Phases, 1979. **75**(0): p. 1688-1699.
7. Singh, L., P. Rekha, and S. Chand, *Cu-impregnated zeolite Y as highly active and stable heterogeneous Fenton-like catalyst for degradation of Congo red dye.* Separation and Purification Technology, 2016. **170**: p. 321-336.
8. Zhang, T., et al., *Selective catalytic reduction of NO with NH3 over HZSM-5-supported Fe–Cu nanocomposite catalysts: The Fe–Cu bimetallic effect.* Applied Catalysis B: Environmental, 2014. **148–149**(0): p. 520-531.
1. Lam, F.L.Y. and X. Hu, *pH-Insensitive Bimetallic Catalyst for the Abatement of Dye Pollutants by Photo-Fenton Oxidation.* Industrial & Engineering Chemistry Research, 2013. **52**(20): p. 6639-6646.
2. Yip, A.C.-K., F. Leung-Yuk Lam, and X. Hu, *Novel bimetallic catalyst for the photo-assisted degradation of Acid Black 1 over a broad range of pH.* Chemical Engineering Science, 2007. **62**(18): p. 5150-5153.
3. Wang, Y., H. Zhao, and G. Zhao, *Iron-copper bimetallic nanoparticles embedded within ordered mesoporous carbon as effective and stable heterogeneous Fenton catalyst for the degradation of organic contaminants.* Applied Catalysis B: Environmental, 2015. **164**(0): p. 396-406.
4. Krishna, K., et al., *Selective Catalytic Reduction of NO with NH3 over Fe-ZSM-5 Catalysts Prepared by Sublimation of FeCl3 at Different Temperatures.* Catalysis Letters, 2002. **86**(1): p. 121-132.
5. Niemantsverdriet, J.W., *Temperature-Programmed Techniques*, in *Spectroscopy in Catalysis*. 2007, Wiley-VCH Verlag GmbH & Co. KGaA. p. 11-38.
6. Gentry, S.J., N.W. Hurst, and A. Jones, *Temperature programmed reduction of copper ions in zeolites.* Journal of the Chemical Society, Faraday Transactions 1: Physical Chemistry in Condensed Phases, 1979. **75**(0): p. 1688-1699.
7. Singh, L., P. Rekha, and S. Chand, *Cu-impregnated zeolite Y as highly active and stable heterogeneous Fenton-like catalyst for degradation of Congo red dye.* Separation and Purification Technology, 2016. **170**: p. 321-336.
8. Zhang, T., et al., *Selective catalytic reduction of NO with NH3 over HZSM-5-supported Fe–Cu nanocomposite catalysts: The Fe–Cu bimetallic effect.* Applied Catalysis B: Environmental, 2014. **148–149**(0): p. 520-531.
1. Lam, F.L.Y. and X. Hu, *pH-Insensitive Bimetallic Catalyst for the Abatement of Dye Pollutants by Photo-Fenton Oxidation.* Industrial & Engineering Chemistry Research, 2013. **52**(20): p. 6639-6646.
2. Yip, A.C.-K., F. Leung-Yuk Lam, and X. Hu, *Novel bimetallic catalyst for the photo-assisted degradation of Acid Black 1 over a broad range of pH.* Chemical Engineering Science, 2007. **62**(18): p. 5150-5153.
3. Wang, Y., H. Zhao, and G. Zhao, *Iron-copper bimetallic nanoparticles embedded within ordered mesoporous carbon as effective and stable heterogeneous Fenton catalyst for the degradation of organic contaminants.* Applied Catalysis B: Environmental, 2015. **164**(0): p. 396-406.
4. Krishna, K., et al., *Selective Catalytic Reduction of NO with NH3 over Fe-ZSM-5 Catalysts Prepared by Sublimation of FeCl3 at Different Temperatures.* Catalysis Letters, 2002. **86**(1): p. 121-132.
5. Niemantsverdriet, J.W., *Temperature-Programmed Techniques*, in *Spectroscopy in Catalysis*. 2007, Wiley-VCH Verlag GmbH & Co. KGaA. p. 11-38.

6. Gentry, S.J., N.W. Hurst, and A. Jones, *Temperature programmed reduction of copper ions in zeolites.* Journal of the Chemical Society, Faraday Transactions 1: Physical Chemistry in Condensed Phases, 1979. **75**(0): p. 1688-1699.
7. Singh, L., P. Rekha, and S. Chand, *Cu-impregnated zeolite Y as highly active and stable heterogeneous Fenton-like catalyst for degradation of Congo red dye.* Separation and Purification Technology, 2016. **170**: p. 321-336.
8. Zhang, T., et al., *Selective catalytic reduction of NO with NH3 over HZSM-5-supported Fe–Cu nanocomposite catalysts: The Fe–Cu bimetallic effect.* Applied Catalysis B: Environmental, 2014. **148–149**(0): p. 520-531.

# 6 CONCLUSIONS AND RECOMMENDATIONS

## 6.1 Conclusions and recommendations

In this thesis, some significant findings were made within the field of Fenton chemistry. In the Chapter 3, a novel metal-organic framework photocatalyst was synthesized and tested for the oxidation of methylene blue. This catalyst Fe/MIL-47 was found to have remarkable activity for the decolourisation of methylene blue, with a first order rate constant of 0.0685 $min^{-1}$. The bare MIL-47 framework was also discovered to be photocatalytically active, with a first order rate constant of 0.0289 $min^{-1}$. The decolourisation rate of methylene blue over Fe/MIL-47 was found to degrade with recycle, and the XRD results showing that there is loss of crystallinity after reaction with methylene blue. This suggests that there is degradation of the framework during the reaction, a finding that is in agreement with the work of McNamara et al, who found that MIL-47 was not stable during oxidative desulfurization.

While it has become clear that MIL-47 is unsuitable as a catalyst support, it is unclear exactly how the degradation of the framework happens. Future studies should look into the exact degradation mechanisms of the framework, with a goal to modifying the MOF to inhibit this reaction, so that the excellent catalytic activity of the MIL-47 based catalyst can be utilized.

Moving on to the more robust iron zeolite Y catalyst, the charge-balancing cations were found to play a vital role in photo-Fenton oxidation of formaldehyde. The Fe/zeolite Y with Brønsted acid sites ($H^+$) prepared by partial ion-exchange exhibited reaction rates and conversions that were significantly higher than that given by the same catalysts containing $NH_4^+$ or $Na^+$. The TOF given by Fe/H-Y, Fe/$NH_4$-Y and Fe/Na-Y at pH 7 were 10.3, 2.7 and 3.4 μmol [mol Fe s]$^{-1}$, respectively. The remarkable performance of Fe/H-Y could be due to the localized acidic environment resulted from the $H^+$ inside the supercage of zeolite Y. The spatial confinement inside the zeolite ensures $H^+$ and $Fe^{3+}$ are in close proximity thus the photo-Fenton reaction could occur in an acid medium within the supercage, even though the bulk solution is alkaline (pH ~7). Increasing catalyst loading increases FA conversion but the solution pH is inevitably affected owing to the acidic nature of the catalyst.

The catalytic performance of Fe-zeolite Y was further enhanced by the addition of copper to form the bimetallic FeCu-zeolite Y catalyst. This bimetallic was tested for the photo-oxidation of methylene blue over a range of pHs. It was found to be effective at both low pH (pH3), with 98% colour removal and 89% TOC removal, and high pH (pH 7), with 99% colour removal and 79% TOC removal. The improved catalytic abilities of the bimetallic catalyst were shown to due to the interaction of iron and copper in the catalyst, by comparison with a physical mixture of iron and

copper catalyst. The FeCu-zeolite Y catalyst was also tested under recycle and found to remain effective after 3 runs with 96% colour removal after 120 minutes for each run. The XRD results also showed no loss in crystallinity, indicating the catalyst support continued to be stable throughout the recycle. Further studies on the bimetallic zeolite catalyst should consider the implantation of the catalyst for oxidation of other more harmful compounds, as it is unlikely that an advanced oxidation process will be implemented for dye wastewater at this point in time. Other synthesis methods that can potentially achieve higher metal loading, such as chemical vapor deposition could also be employed. Investigations should also be carried out to determine the optimum ratio of copper to iron in the catalyst, and whether a subsequent loading of either iron then copper, rather than both simultaneously, would confer any advantages to the catalyst with respect to catalytic activity.

# APPENDICES

Appendix 2

Table A2.1 – Further dye degradation conditions

| Author | | Catalyst | Dye | Dye Conc. [mg $L^{-1}$] | Carbon Conc. [mg $L^{-1}$] | Carbon:Catalyst Ratio | H2O2:Dye Ratio | TOC removal [mg $L^{-1}$] | TOC removal [mg TOC / g Cat.] |
|---|---|---|---|---|---|---|---|---|---|
| Du | [1] | MIL-53 | MB | 32 | 19 | 1920.0 | 0.1 | - | - |
| Dükkancı | [2, 3] | CuFe-ZSM-5 | Rhodamine 6G | 100 | 70 | 70.1 | | 36 | 36 |
| Flores | [4] | Fe-fly ash | Reactive Black 5 | 60 | 19 | 1.7 | 76.0 | 15 | 1 |
| Hassan | [5] | Fe-Y | Acid Red 1 | 50 | 21 | 8.5 | | - | - |
| Height | [6] | AgZnO | MB | 10 | 6 | 20.0 | | - | - |
| Houas | [7] | P25 TiO2 | MB | 23 | 14 | 5.5 | | 11 | 4 |
| Jian-xiao | [8] | UV/H2O2 | MB | 30 | 18 | 0.0 | 1174.0 | - | - |
| Jing | [9] | ZIF-8 | MB | 10 | 6 | 120.1 | | 4 | 84 |
| Kasiri | [10] | Fe-ZSM-5 | Acid Red 14 | 40 | 19 | 76.4 | | 15 | 58 |
| Kasiri | [11] | Fe-ZSM-5 | Acid Blue 74 | 46 | 21 | 41.1 | 250.0 | 12 | 23 |
| Kondru | [12] | Fe-Y | Congo Red | *Not given | | | | - | - |
| Kozlova | [13] | MIL-47 | MB | 0 | 38 | 768.0 | | - | - |
| Lam | [14] | FeCu/MCM-41 | Orange II | 105 | 58 | 57.6 | 47.3 | 53 | 53 |
| Liang | [15] | MIL-53 | Rhodamine B | 20 | 14 | 14.0 | | 3 | 3 |
| Neamtu | [16] | Fe-Y | Procion Marine | 100 | 37 | 37.2 | 350.0 | 15 | 15 |
| Neamtu | [16] | Fe3+ (as iron nitrate) | Procion Marine | 100 | 37 | 2205.7 | 350.0 | - | - |
| Ramirez | [17] | Fe/C | Orange II | 35 | 19 | 64.0 | | 17 | 58 |
| Singh | [18] | Cu-Y | Congo Red | 100 | 55 | 54.9 | 365.3 | 44 | 44 |
| Xiao | [19] | Co3O4/Bi2WO6 | MB | 10 | 6 | 6.0 | 6269.1 | - | - |
| Yaman | [20] | Fe-ZSM-5 | CI Reactive Red | 100 | 35 | 35.2 | 4736.6 | 18 | 18 |
| Zhou | [21] | Co-BiVO4 | MB | 10 | 6 | 6.0 | | - | - |

## Appendix 2 References


1. Du, J.J., et al., *New photocatalysts based on MIL-53 metal-organic frameworks for the decolorization of methylene blue dye.* J Hazard Mater, 2011. **190**(1-3): p. 945-51.
2. Dükkancı, M., et al., *Heterogeneous Fenton-like degradation of Rhodamine 6G in water using CuFeZSM-5 zeolite catalyst prepared by hydrothermal synthesis.* Journal of Hazardous Materials, 2010. **181**(1–3): p. 343-350.
3. Dükkancı, M., et al., *Characterization and catalytic activity of CuFeZSM-5 catalysts for oxidative degradation of Rhodamine 6G in aqueous solutions.* Applied Catalysis B: Environmental, 2010. **95**(3–4): p. 270-278.
4. Flores, Y., R. Flores, and A.A. Gallegos, *Heterogeneous catalysis in the Fenton-type system reactive black 5/H2O2.* Journal of Molecular Catalysis A: Chemical, 2008. **281**(1–2): p. 184-191.
5. Hassan, H. and B.H. Hameed, *Oxidative decolorization of Acid Red 1 solutions by Fe– zeolite Y type catalyst.* Desalination, 2011. **276**(1–3): p. 45-52.
6. Height, M.J., et al., *Ag-ZnO catalysts for UV-photodegradation of methylene blue.* Applied Catalysis B: Environmental, 2006. **63**(3–4): p. 305-312.
7. Houas, A., et al., *Photocatalytic degradation pathway of methylene blue in water.* Applied Catalysis B: Environmental, 2001. **31**(2): p. 145-157.
8. Jian-xiao, L., et al., *Decoloration of methylene blue simulated wastewater using a UV-$H_2O_2$ combined system.* Journal of Water Reuse and Desalination, 2011. **1**(1): p. 45-51.
9. Jing, H.-P., et al., *Photocatalytic degradation of methylene blue in ZIF-8.* RSC Advances, 2014. **4**(97): p. 54454-54462.
10. Kasiri, M.B., H. Aleboyeh, and A. Aleboyeh, *Mineralization of C.I. Acid Red 14 azo dye by UV/Fe-ZSM5/H2O2 process.* Environmental Technology, 2010. **31**(2): p. 165-173.
11. Kasiri, M.B., H. Aleboyeh, and A. Aleboyeh, *Degradation of Acid Blue 74 using Fe-ZSM5 zeolite as a heterogeneous photo-Fenton catalyst.* Applied Catalysis B: Environmental, 2008. **84**(1–2): p. 9-15.
12. Kondru, A.K., P. Kumar, and S. Chand, *Catalytic wet peroxide oxidation of azo dye (Congo red) using modified Y zeolite as catalyst.* Journal of Hazardous Materials, 2009. **166**(1): p. 342-347.
13. Kozlova, E.A., et al., *Photoreactivity of metal-organic frameworks in the decolorization of methylene blue in aqueous solution.* Catalysis Today, 2016. **266**: p. 136-143.
14. Lam, F.L.Y. and X. Hu, *pH-Insensitive Bimetallic Catalyst for the Abatement of Dye Pollutants by Photo-Fenton Oxidation.* Industrial & Engineering Chemistry Research, 2013. **52**(20): p. 6639-6646.
15. Liang, R., et al., *MIL-53(Fe) as a highly efficient bifunctional photocatalyst for the simultaneous reduction of Cr(VI) and oxidation of dyes.* Journal of Hazardous Materials, 2015. **287**: p. 364-372.
16. Neamt□u, M., et al., *Fe-exchanged Y zeolite as catalyst for wet peroxide oxidation of reactive azo dye Procion Marine H-EXL.* Applied Catalysis B: Environmental, 2004. **48**(4): p. 287-294.
17. Ramirez, J.H., et al., *Azo-dye Orange II degradation by heterogeneous Fenton-like reaction using carbon-Fe catalysts.* Applied Catalysis B: Environmental, 2007. **75**(3–4): p. 312-323.
18. Singh, L., P. Rekha, and S. Chand, *Cu-impregnated zeolite Y as highly active and stable heterogeneous Fenton-like catalyst for degradation of Congo red dye.* Separation and Purification Technology, 2016. **170**: p. 321-336.
19. Xiao, Q., et al., *Photocatalytic degradation of methylene blue over Co3O4/Bi2WO6 composite under visible light irradiation.* Catalysis Communications, 2008. **9**(6): p. 1247-1253.
20. Yaman, C. and G. Gündüz, *A parametric study on the decolorization and mineralization of CI Reactive Red 141 in water by heterogeneous Fenton-like oxidation over FeZSM-5 zeolite.* Journal of Environmental Health Science and Engineering, 2015. **13**(1): p. 7.
21. Zhou, B., et al., *Visible-light sensitive cobalt-doped BiVO4 (Co-BiVO4) photocatalytic composites for the degradation of methylene blue dye in dilute aqueous solutions.* Applied Catalysis B: Environmental, 2010. **99**(1–2): p. 214-221.

## Appendix 3

The XRD patterns presented in Figure A3.1 below are consistent with those reported in literature for MIL-53(Al) [1].

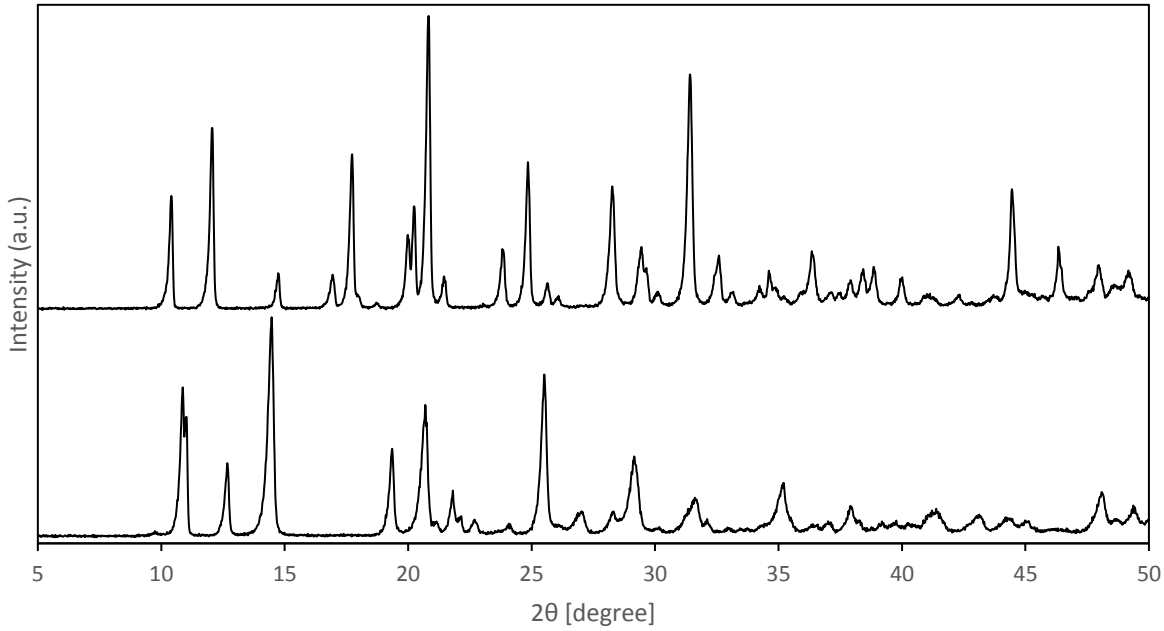


Figure A3.1 – XRD pattern of MIL-53(Al)-as (top), MIL-53(Al)-lt (below).

The SEM images below show a typical distribution of particles for MIL-53(Al), again comparable with those presented in prior studies [2-5]

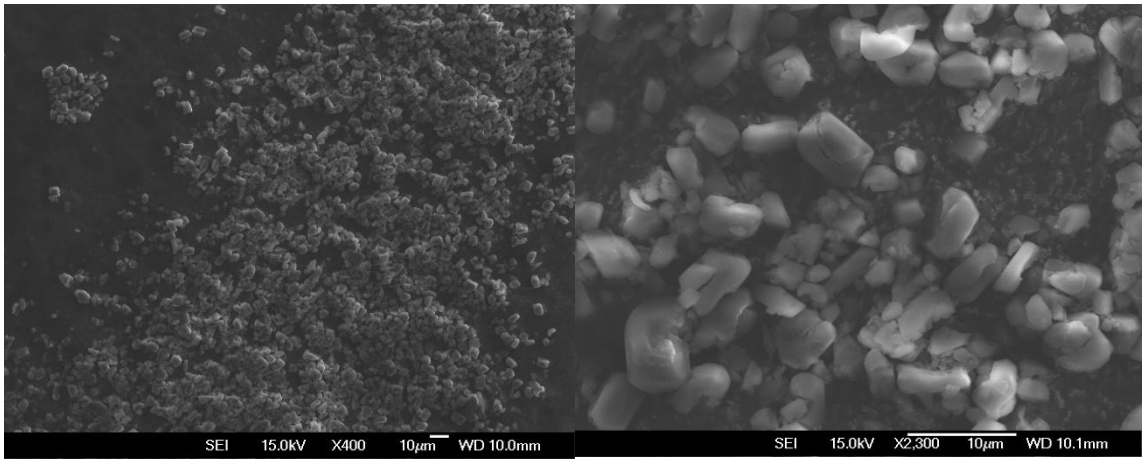


Figure A3.2 – SEM images of MIL-53(Al)-lt.

## Appendix 3 References


1. Trung, T.K., et al., *Hydrocarbon Adsorption in the Flexible Metal Organic Frameworks MIL-53(Al, Cr).* Journal of the American Chemical Society, 2008. **130**(50): p. 16926-16932.
2. Yang, C.-X., H.-B. Ren, and X.-P. Yan, *Fluorescent Metal-Organic Framework MIL-53(Al) for Highly Selective and Sensitive Detection of Fe3+ in Aqueous Solution.* Analytical Chemistry, 2013.
3. Remy, T., et al., *Vapor Phase Adsorption and Separation of Ethylbenzene and Styrene on the Metal-Organic Frameworks MIL-47 and MIL-53(Al).* Industrial & Engineering Chemistry Research, 2012.
4. Do, X.-D., V.-T. Hoang, and S. Kaliaguine, *MIL-53(Al) mesostructured metal-organic frameworks.* Microporous and Mesoporous Materials, 2011. **141**(1–3): p. 135-139.
5. Patil, D.V., et al., *MIL-53(Al): An Efficient Adsorbent for the Removal of Nitrobenzene from Aqueous Solutions.* Industrial & Engineering Chemistry Research, 2011. **50**(18): p. 10516-10524.